DISSERTATION

Computational Methods for the Prediction of Emergence and Growth of Delaminations in Laminated Composite Components

ausgeführt zum Zwecke der Erlangung des akademischen Grades eines

Doktors der technischen Wissenschaften unter der Leitung von

Univ.Doz. Dipl.-Ing. Dr.techn. Heinz Pettermann

E317

Institut für Leichtbau und Struktur–Biomechanik

eingereicht an der Technischen Universität Wien

Fakultät für Maschinenwesen und Betriebswissenschaften

von

Dipl.-Ing. Mag.rer.soc.oec. Gerald Wimmer

Matrikelnummer: 0026439

Herklotzgasse 13/9

A-1150 Wien

Wien, im Jänner 2009   Gerald Wimmer

KURZFASSUNG

Die vorliegende Arbeit beschäftigt sich mit der Simulation des Delaminationsprozesses in Laminaten aus faserverstärkten Polymeren, d.h. dem Versagen des Interfaces zwischen zwei Schichten. Der Delaminationsvorgang wird dazu als ein Prozess betrachtet, der in zwei Schritten abläuft: 1. Bildung einer Anfangsdelamination im intakten Interface und 2. Wachstum vorhandener Delaminationen. Ziel dieser Arbeit ist es, numerisch effiziente und robuste Methoden für die Vorhersage der Bildung von Anfangsdelaminationen und für die Vorhersage von Delaminationswachstum zu entwickeln und an Beispielen zu testen.

Für die Vorhersage der Bildung einer Anfangsdelamination wird eine Methode entwickelt, welche auf der Kombination eines Spannungskriteriums mit Prinzipien der linear elastischen Bruchmechanik beruht. Überbeanspruchte Bereiche im Interface werden mit einem Spannungskriterium vorhergesagt, und es wird angenommen, dass sich in diesen Bereichen Anfangsdelaminationen bilden. Der Beginn des Wachstums dieser Anfangsdelamination wird mit Hilfe linear elastischer Bruchmechanik berechnet. Diese Methode erlaubt es, die kritische Größe und Lage einer Anfangsdelamination vorherzusagen sowie die Traglast der Struktur zu bestimmen. Des weiteren können die Sensitivität der Traglast bezüglich Ungenauigkeiten und Änderungen in den Materialeigenschaften untersucht werden.

Für die Vorhersage des Wachstums von Delaminationen mit geraden Fronten wird eine semi–analytische Methode vorgeschlagen. Diese Methode basiert auf der Annahme, dass die bei Delaminationswachstum freigesetzte Energie aus der Änderung der Struktursteifigkeit berechnet werden kann. Zu diesem Zweck wird mit Hilfe der Finiten Elemente Meth-

ode die Struktursteifigkeit als Funktion der Delaminationsgröße bestimmt. Mit der semi–analytischen Methode können allgemeine Kombinationen von Verschiebungs– und Kraftrandbedingungen behandelt werden. Des weiteren können Beanspruchungen, welche durch Änderung der Temperatur oder durch Änderung der Feuchtigkeit im Laminat entstehen, berücksichtigt werden. Die vorgeschlagene Methode erlaubt es, sowohl quasi–statische Beanspruchungen als auch zyklische Beanspruchungen zu analysieren.

Um das Wachstum von Delaminationen mit gekrümmten Fronten vorherzusagen, wurde ein Kriterium entwickelt, welches die Energiebilanz entlang der gesamten Delaminationsfront beurteilt. Einige vereinfachende Annahmen bezüglich der Form der Delaminationsfront sind hier nötig. Das vorgeschlagene Kriterium beinhaltet allerdings ein Methode zur Abschätzung der Qualität dieser Annahmen und eine Anleitung zur systematischen Verbesserung derselben.

Zur Verifikation der Vorhersagen wird die Bildung von Anfangsdelaminationen und Delaminationswachstum in einem gekrümmten Laminat mit den vorgeschlagenen Methoden untersucht. Die Vorhersagen werden mit Ergebnissen von experimentellen Tests, welche am *Polymer Competence Center Leoben GmbH* (*PCCL*, Leoben, Österreich) durchgeführt wurden, verglichen. Die Probekörper für die Tests wurden von der *FACC AG* (Ried i. I., Österreich) hergestellt. Es werden Laminate ohne Anfangsdelamination und Laminate mit einer Anfangsdelamination von definierter Lage und Größe numerisch untersucht und mit den Experimenten verglichen. In beiden Fällen wird eine relativ gute Übereinstimmung zwischen Experiment und Vorhersage erzielt.

ABSTRACT

The present thesis is concerned with the computational simulation of delamination in fiber reinforced polymer laminates. The delamination process, from the pristine structure to the formation of large delaminated regions, is considered as a two–step process. In the first step an initial delamination emerges in an intact interface and in the second step the delamination grows. The objective of this work is to develop numerically efficient and robust tools for predicting the emergence and growth of delaminations. To demonstrate the application and the capability of the proposed approaches several examples are analyzed.

For the prediction of emergence of delaminations a combination of a strength criterion with an energy release rate criterion is developed. A stress based failure criterion is employed to predict overloaded interface regions and initial delaminations are assumed to emerge there. The propagation of delaminations is analyzed using linear elastic fracture mechanics. The *strength/energy approach* allows to predict the critical size and position of an initial delamination as well as the load carring capacity of the structure. Furthermore, the sensitivity of the predicted load carring capacity with respect to changes and uncertainties in the material properties is determined.

For the prediction of consecutive growth of delaminations with straight fronts a computationally efficient *semi–analytical approach* is implemented. It uses the fact that the energy released at delamination growth is proportional to the increase of the structural compliance caused by an increase of the delaminated area. The structural compliance is determined as a function of the delaminated area by an automated procedure employing the finite element

method. The semi–analytical approach can handle arbitrary combinations of mechanical, temperature, and moisture loads. A Griffith type growth criterion is used to predict consecutive growth caused by quasi–static loads. The stability of the growth process as well as the non–linear structural response are predicted. For the analysis of delamination growth caused by cyclic loading a Paris type growth law is employed.

For simulation of delaminations with curved fronts a *total delamination front criterion* is developed. Growth along the entire delamination front is assumed to take place if the growth criterion is satisfied. A set of smooth and continuous delamination fronts is defined and growth is predicted by selecting that shape for which the load required to caused delamination growth is smallest. For computation of the delamination growth load an automated finite element method is employed. A criterion is developed that allows to check whether or not the assumed shape of the delamination front is a good approximation. This criterion can also guide the way towards improvement of the shape.

For verification of the developed approaches emergence of delaminations and growth of existing delaminations in an L–shaped laminate is predicted numerically and compared to results from experimental tests. The test are performed at the *Polymer Competence Center Leoben GmbH* (*PCCL*, Leoben, Austria). The test specimens are produced by *FACC AG* (Ried i. I., Austria). Test specimens without initial delaminations and test specimens with defined initial delaminations are studied. For both test series reasonably good agreement between the numerical predictions and the experimental results is obtained.

Acknowledgements

Contents

Chapter 1

Introduction

1.1   Fiber Reinforced Polymer Laminates

Fiber Reinforced Polymer (FRP) laminates have become increasingly important over the past years due to their great potential for weight saving. They are successfully used in many structural applications where high stiffness, high strength, and low weight are required, such as spacecraft, aircraft, ship hulls, sports equipment, etc. A prominent example of increasing use of FRP laminates is the Airbus A380. In this modern aircraft interior components, fairings, as well as structural parts such as elevators, wings, or spoilers are made of FRP laminates [44]. In total more than 20% of the total structural weight is contributed by parts made of this material. For the next generation of aircrafts, like the Airbus A350XWB or the Boeing Dreamliner 787, more than 50% of the total structural weight will be contributed by FRP laminates.

In order to fully exploit the advantages of FRP laminates accurate and reliable methods are required to predict their response to service loads. The objective of this thesis is to improve and develop modeling tools that are adequate for the computational simulation of emergence and growth of delaminations in load carring aircraft structures made from FRP

laminates.

What are FRP Laminates?

An FRP is a composite material with a matrix–inclusion type topology made of two constituents, i.e. one of the constituents is topologically connected, the matrix, while the other is distributed in the matrix, the inclusions. The inclusions considered here are continuous fibers which can be unidirectional, woven, knitted, or braided. Typical fiber materials used in aircraft structures are carbon, glass, and aramid. These fibers have diameters of some micrometers and possess high stiffness and high strength in longitudinal direction. As matrix materials typically polymers (e.g. epoxy, polyester, or phenolic resins) are used for aircraft structures. These polymers show a rather brittle failure behavior and good adhesive properties [68]. Compared to the fibers the polymer matrix possess low stiffness and low strength.

Thin plies of FRP with a thickness of some hundred micrometers are formed. In the present work unidirectionally reinforced plies, called tapes, and plies reinforced in two directions by woven fibers, called fabrics, are considered. Tapes can be considered as transversely isotropic materials for which the plane perpendicular to the fibers is a plane of material isotropy. They have high stiffness and strength in fiber direction and low stiffness and strength in direction perpendicular to the fibers and in shear loading. Fabrics can be considered as orthotropic materials for which the ply–midplane is one plane of material symmetry. They have high stiffness and strength in both reinforcement directions. Several tapes or fabrics are grouped together to create a laminate, its stiffness and strength is controlled by the number, the material, and the orientation of the plies. Hence, one can tailor the mechanical properties of such multi– directional laminates.

Conventional laminates have a layered structure without any reinforcement in thickness direction. Hence, they possess low resistance against failure in the interface between the

plies. To circumvent this problem special techniques for reinforcement in thickness may be used, such as stitching, tufting, Z–pinning, or 3D braiding.

Where are FRP Laminates used?

FRP laminates are used wherever light weight paired with requirements of high load carrying capacity and high stiffness is an issue, i.e in applications where the strength–to–weight ratio and stiffness–to–weight ratio are important. In this respect, FRP laminates are superior to other engineering materials, such as steel, aluminum, or titanium. Another advantage of FRP laminates is the possibility of creating structures with tailored mechanical properties to meet specific design needs. On the one hand, one can select fiber and matrix materials to design ply properties, on the other hand one can select the ply number and orientation to tailor the laminate properties. FRP laminates are used to create thin or thick monolithic structures as well as sandwich structures, where typically a honeycomb core is embedded between face sheets made of FRP laminates. Traditional fields where FRP laminates have been used for years are aeronautics and astronautics. Nowadays they are also used for maritime vessels, road vehicles, wind turbines, fast rotating shafts, golf clubs, tennis rackets, frames for bikes, etc.

How do FRP Laminates fail?

Due to the layered structure of conventional FRP laminates two principle failure mechanisms are distinguished, failure of the ply and failure of the interface between plies. The microstructure of the plies allows to classify ply failure as failure of the fibers, the matrix, or the interface between fiber and matrix. The latter two are summarized as matrix dominated failure and occur in a plane parallel to the fibers. The failure behavior of a unidirectionally reinforced ply depends on the loading. If the ply is loaded by normal stresses in fiber direction or in a direction transverse to the fibers it fails in a brittle manner. A ply

loaded by in–plane shear stresses shows considerable plastic deformation before it fails. Failure of one ply within a laminate does not necessarily mean that the entire laminate fails. The stresses might be redistributed and carried by the remaining plies. Hence, one has to distinguish between the point at which the first ply within a laminate fails, called First Ply Failure (FPF), and the failure of the entire laminate (i.e. failure of all plies), called ultimate failure.

Failure of the interface between plies is referred to as delamination. It is caused by over-loading of the interface due to out–of–plane stresses attributed to, e.g. transverse loading, free edge effects, ply drop off, local load introduction, or impact loads. Delamination can be considered as a special case of matrix dominated failure as it is a failure of the matrix with a fracture plane parallel to the ply. The interface between the plies is typically weaker than the ply itself, consequently, delaminations will typically grow along the interface. Sometimes delamination is defined as the failure of primary bonds while debonding is defined as the failure of secondary bonds. Primary bonds are formed between the plies during production of the laminate, while secondary bonds are created by glueing compo-nents together (e.g. sublaminates, face sheet and core, etc.). As the failure mechanisms for delamination and debonding are the same, debonding is considered as a form of delamina-tion in this work.

1.2 Scope of the Present Work

The objective of the present work is the development of numerically efficient tools for the simulation of delamination in FRP laminates. The delamination process from the perfect, flaw free structure, up to final failure of the structure is considered as a two step process. In the first step an *initial delamination* is formed at an interface between plies, called *emer-gence of delaminations.* In the second step the delamination size increases, called *growth of delaminations.* The maximum load reached during the entire delamination process is called the *load carrying capacity* of the structure. Concerning step one the load at which initial

delaminations emerge and the position of the initial delamination will be predicted. Concerning step two the load at which delamination growth starts, the stability of the growth, the non–linear structural response, and the load carring capacity are predicted. For both steps numerically efficient approaches are proposed which allow for a systematic and general understanding of the delamination problem under consideration. For verification of the proposed methods a comparison between numerical predictions and experimental results is done. All experimental tests were carried out by the *Polymer Competence Center Leoben GmbH* (*PCCL*, Austria), the specimens used for testing were produced by *FACC AG* (Ried, Austria).

For all FEM computations the general purpose finite element program package *ABAQUS/-Standard/V6.6 (ABAQUS Inc., Pawtucket, RI, USA)* is used. For automated preprocessing of FEM models and for automated reading and preparation of results of the FEM analyses *Python 2.4* and the *ABAQUS* scripting interface are employed. For data processing *MATLAB R2007b (The MarthWork Inc.)* is used.

The approaches proposed within this thesis are based on the principles of linear elastic fracture mechanics. These principles are summarized in Chapter 2 and their applicability to delamination problems is discussed. In Chapter 3 a combination of a strength criterion with Linear Elastic Fracture Mechanics (LEFM) is proposed for the simulation of emergence of delaminations. In Chapter 4 a semi–analytical approach for the prediction of delamination growth in structures loaded by quasi–static and cyclic loads is presented. Only delaminations with straight fronts can be handled by the proposed semi–analytical approach. A criterion for the prediction of growth of delaminations with curved fronts is presented in Chapter 5. In Chapter 6 emergence and growth of delaminations in an L–shaped laminate is investigated with the proposed methods and tested experimentally. The test specimens were produced by *FACC AG* and the experimental testing was done at the *PCCL*.

1.3 Literature Review

The increase in use of FRP laminates in the past years has been accompanied by intensive research concerning the prediction of their failure behavior. In the following the literature most relevant for prediction of emergence and growth of delaminations is summarized.

One of the critical failure modes in FRP laminates is delamination, as it can change significantly the structural stiffness and the load carrying capacity of components. An overview of delamination and its effects is given in [22, 49], delamination related stability problems are discussed in [10].

For the prediction of the onset of interface damage, which can be considered as the onset of the formation of a delamination, methods based on the interface strength have been developed [22, 11, 41]. The normal and shear tractions acting on the interface are computed and assessed by a strength criterion. In laminated composites quadratic strength criteria are used successfully for this purpose [11, 27]. A general, strength based FPF criterion was developed by Puck [52, 65]. In this criterion delamination is considered as a special case of matrix dominated failure. A strength based analysis of delaminations emerging from free edges is presented in [50].

For the prediction of delamination growth fracture mechanics can be applied. It is a widely used assumption that conventional FRP laminates show brittle fracture behavior if they are loaded in a out–of–plane direction. Consequently, local material non–linearities in the vicinity of the delamination front are neglected and LEFM is used [30]. For the prediction of delamination growth stress intensity factors [32] or energy release rates [23] can be used. The latter are commonly used for FRP laminates, as they can be directly determined by experimental testing. Within the framework of the Finite Element Method (FEM) several methods for the computation of energy release rates have been developed, such as the J–integral [58], the Virtual Crack Extension Technique [28], Crack Tip Elements [17], and the Virtual Crack Closure Technique (VCCT) [62, 55, 35]. The VCCT is used successfully for the simulation of consecutive delamination growth in–plane problems loaded by quasi–

static [36] and cyclic loads [67]. A numerical more efficient semi–analytical approach is employed for the prediction of delamination growth in–plane problems loaded by quasi–static loads [78, 77] or by combinations of quasi–static and cyclic loads [79, 80, 81]. For the simulation of consecutive growth of delaminations with curved fronts moving mesh techniques [38, 85, 86] or methods that take some assumptions concerning the shape of the delamination front [82] can be used.

Strength criteria can be applied to predict the onset of interface damage, but, that does not necessarily mean that a delamination is formed. LEFM, on the other hand, can be used to predict the propagation of delaminations, but, an initial delamination must exist. Methods that combine strength criteria with LEFM have been proposed for the prediction of the formation of initial delaminations [72, 83, 84, 77].

An alternative approach for the prediction of delamination growth is to take into account the non–linear interface behavior at the delamination tip and to introduce a cohesive zone [19, 8]. Based on this idea, Cohesive Zone Elements (CZE) have been developed within the FEM [3, 14]. Due to their formulation CZE can be used to predict the formation of an initial delamination as well as to predict propagation of delaminations. CZE have been used successfully for the analysis of quasi–static [75, 18] and cyclic [74] loads. However, they are numerically expensive and the achievement of convergence can be a tricky task [75].

Another approach successfully used for the simulation of delamination is to consider delamination as a special case of ply damage. In [40] an extended ply damage model is proposed which can be used for the simulation of emergence of delaminations as well as for the simulation of consecutive delamination growth.

Chapter 2

Fracture Mechanics

For the prediction of delamination growth in an interface between plies of FRP laminates linear elastic fracture mechanics as well as elastic–plastic fracture mechanics are employed successfully, most widely used are the VCCT and CZE. The principles of LEFM and the formulation of the VCCT are summarized in the following, including remarks concerning their application to delamination problems. Bimaterial problems are also discussed briefly, as delaminations between plies with different orientation have to be considered as cracks in a bimaterial interface. Furthermore, elastic–plastic fracture mechanics is briefly reviewed and the principal idea of CZE is discussed. For a more detailed discussion of linear elastic and elastic–plastic fracture mechanics see e.g. [6, 24, 26]. FEM based methods for solving fracture mechanics problems are discussed in detail in e.g. [39].

2.1   Linear Elastic Fracture Mechanics

A crack in an isotropic linear elastic material with Young's modulus, E, and shear modulus, G, is considered. The crack is described by the two crack surfaces and is bordered by the crack front. The crack surfaces are assumed to be traction free and parallel to each other.

The crack area, A, is defined by the projection of the crack surfaces to a reference plane. Three different relative displacements of the crack surfaces with respect to each other are distinguished which leads to the definition of the basic fracture modes, shown in Fig. 2.1. The opening mode, for which the crack surfaces move in a direction normal to the crack plane (mode I), the sliding mode or in–plane shear mode, for which the crack surfaces slide in a direction perpendicular to the crack front (mode II), and the tearing or anti–plane shear mode, for which the crack surfaces slide in a direction parallel to the crack front (mode III). For mode I the displacements are symmetric with respect to the crack plane, for mode II and mode III they are antisymmetric.

2.1.1 Stress Intensity Factor

The two–dimensional problem of an infinite body made of a homogeneous and isotropic material containing a plane crack with straight crack fronts is considered. The crack possesses total length $2a$ and a polar coordinate system (r, θ) is centered at the crack tip, see Fig. 2.2. Note, that an interior crack of finite length within an infinite body is investigated. Hence, the crack does not interact with the applied boundary conditions. Plane models of the structure are investigated and plane strain assumptions and plane stress assumptions are considered.

It was shown in [69] that for such problems the stress field can be written by a series
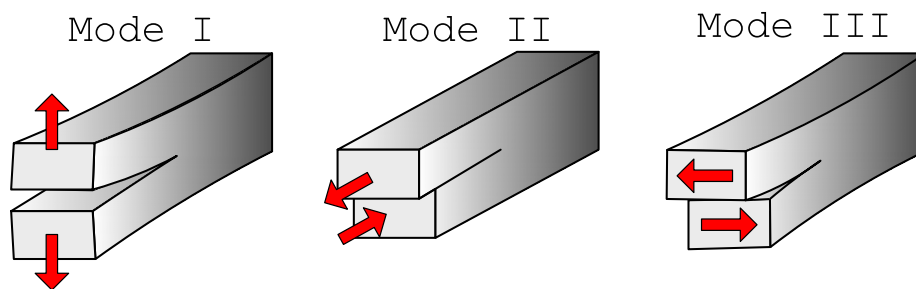
Figure 2.1: Definition of the fracture modes, opening mode I, sliding mode II, tearing mode III; Definition is based on the displacements of the crack surface relative to each other.

representation of the stress tensor,

$$\sigma_{ij}(r,\theta) = \frac{1}{\sqrt{2\pi r}} \left[K_{\mathrm{I}} f_{ij}^{\mathrm{I}}(\theta) + K_{\mathrm{II}} f_{ij}^{\mathrm{II}}(\theta) + K_{\mathrm{III}} f_{ij}^{\mathrm{III}}(\theta) \right] + (O) \quad \text{for } i,j = x,y,z \quad , \quad (2.1)$$

where K_{I}, K_{II}, and K_{III} are the stress intensity factors. They correspond to the three modes of crack surface displacements discussed in Fig. 2.1. (O) are terms of higher order with respect to the radial coordinate and their influence vanishes as the radial coordinate approaches zero. The stress field close to the crack tip is dominated by the singular term in Eq. (2.1). f_{ij}^{I}, f_{ij}^{II}, and f_{ij}^{III} are functions of the angle θ which, for instance, are derived following the complex stress function approach developed by Westergaard [76].

The displacement field is given by,

$$u_i(r,\theta) = \frac{1}{2G} \sqrt{\frac{r}{2\pi}} \left[K_{\mathrm{I}} g_i^{\mathrm{I}}(\theta) + K_{\mathrm{II}} g_i^{\mathrm{II}}(\theta) + K_{\mathrm{III}} g_i^{\mathrm{III}}(\theta) \right] + (O) \quad \text{for } i = x,y,z \quad , \quad (2.2)$$

where (O) are terms of higher order with respect to the radial coordinate. Their influence vanishes as the radial coordinate approaches zero and the displacement field close to the crack tip is dominated by the square root term in Eq. (2.2). g_i^{I}, g_i^{II}, and g_i^{III} are functions of the angle θ which, for instance, are derived following the Westergaard approach.

Equation (2.1) shows the typical $1/\sqrt{r}$ singularity of the stresses at the crack tip. Equation
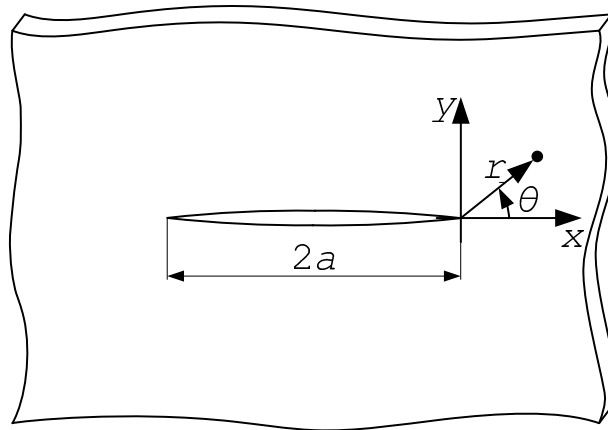
Figure 2.2: Infinite wide body of isotropic material containing a plane crack of total length $2a$.

(2.2) shows that the displacements of the crack surfaces are dominated by a $\sqrt{r}$ term which leads to parabolic crack opening close to the crack tip.

Mode I and Mode II Loading

The stress and displacement fields at the crack tip are now derived for the case of an infinite body loaded at the boundary by uniform normal stresses, σ_{yy}^∞, and uniform shear stresses, $\sigma_{xy}^\infty = \sigma_{yx}^\infty$. Solving the complex stress functions for these boundary conditions yields equations for the stress and displacement fields [24]. The stresses ahead of the crack tip along the x–axis (i.e. $\theta = 0$) are given as,

$$\left\{ \begin{array}{c} \sigma_{yy} \\ \sigma_{xy} \end{array} \right\} = \frac{1}{\sqrt{2\pi r}} \left\{ \begin{array}{c} K_\mathrm{I} \\ K_\mathrm{II} \end{array} \right\} \quad , \tag{2.3}$$

where the stress intensity factors are defined as,

$$\begin{aligned} K_\mathrm{I} &= \sigma_{yy}^\infty \sqrt{\pi a} \quad , \\ K_\mathrm{II} &= \sigma_{xy}^\infty \sqrt{\pi a} \quad . \end{aligned} \tag{2.4}$$

The displacement of the upper crack surface (i.e. $\theta = +\pi$) and the lower crack surface (i.e. $\theta = -\pi$) read,

$$\left\{ \begin{array}{c} u_x \\ u_y \end{array} \right\} = \pm \frac{\kappa + 1}{2G} \sqrt{\frac{r}{2\pi}} \left\{ \begin{array}{c} K_\mathrm{II} \\ K_\mathrm{I} \end{array} \right\} \quad , \tag{2.5}$$

where u_x is the displacement of the crack surface in x–direction, u_y is the displacement in y–direction, and κ is an elastic parameter, which depends on the boundary conditions

applied in z–direction. It is defined as,

$$\begin{aligned} \kappa &= 3 - 4\nu \quad \text{for plane strain} \quad, \\ \kappa &= \frac{3-\nu}{1+\nu} \quad \text{for plane stress} \quad, \end{aligned} \tag{2.6}$$

where ν is the Poisson's ratio.

Mode III Loading

The body shown in Fig. 2.2 is now loaded at the boundary by some uniform shear stresses, $\sigma_{zy}^{\infty} = \sigma_{yz}^{\infty}$. These stresses will lead to displacements u_z perpendicular to the xy–plane while the displacements in x–direction and y–direction will remain zero. The stresses ahead of the crack tip along the x–axis (i.e. $\theta = 0$) read [24],

$$\sigma_{yz} = \frac{1}{\sqrt{2\pi r}} K_{\text{III}} \quad, \tag{2.7}$$

and the mode III stress intensity factor is defined as,

$$K_{\text{III}} = \sigma_{yz}^{\infty} \sqrt{\pi a} \quad. \tag{2.8}$$

The displacements of the upper and the lower crack surface (i.e. $\theta = \pm\pi$) read,

$$u_z = \pm \frac{4K_{\text{III}}}{G} \sqrt{\frac{r}{2\pi}} \quad. \tag{2.9}$$

The above equations describe the stress and displacement fields for a crack in a homogeneous isotropic material. A delamination between plies of the same orientation can be considered as a crack within a homogeneous orthotropic material, where the xz–plane is a plane of material symmetry. The stress and displacement fields for such cracks are derived from the solutions for isotropic materials by multiplying the normal stresses, σ_{yy}, and the displacements in y–direction, u_y, by a factor that is a function of the elastic properties of

the material. The shear stresses, σ_{xy} and σ_{yz}, and the displacements in $x-$ and $z-$direction remain unchanged, see [45] for details.

Critical Stress Intensity Factor

According to Irwin [32] a crack loaded in pure mode I, mode II, or mode III will grow if the stress intensity factor reaches some critical value. Consider for example a crack loaded in pure mode I, it will grow if,

$$K_{\mathrm{I}} \geqslant K_{\mathrm{Ic}} \quad , \tag{2.10}$$

where K_{Ic} is the critical stress intensity factor for pure mode I loading. It can be determined in experimental testing. Equivalent criteria and critical stress intensity factors can be given for pure mode II and pure mode III loading. For the case of mixed mode loading, i.e. loading by some combination of mode I, mode II, and mode III, the crack growth criterion can be written in the general form,

$$f\left(K_{\mathrm{I}}, K_{\mathrm{II}}, K_{\mathrm{III}}, K_{\mathrm{Ic}}, K_{\mathrm{IIc}}, K_{\mathrm{IIIc}}\right) \geqslant 1 \quad . \tag{2.11}$$

In order to take the mode interaction at the crack tip into account various functions, f, have been developed, see e.g. [24].

Next the question in which direction a crack will grow is discussed. In the case of pure mode I loading the plane crack shown in Fig. 2.2 will grow in $x-$direction and will remain planar. In case of a combination of mode I and mode II loading the crack growth direction will deviate from the $x-$direction, i.e. the crack will kink. Kinking of a crack loaded in mode III is rarely treated in the literature and is not considered here. Several criteria have been proposed to predict the angle by which the crack will kink [24]. All such criteria predict that crack kinking is driven by the ratio of mode I to mode II loading. The interfaces between the plies of FRP laminates are typically considered to possess a smaller critical energy release rate than the ply itself as they are not reinforced by any fiber. For unidirectionally

reinforced laminates where the delamination front is orthogonal to the fiber direction the delamination is assumed to grow along the interface and does not kink, irrespective of the fracture mode. The fibers used for reinforcement of the plies would bridge the delamination if it is growing into one of the plies. Different behavior might be obtained in the case of a delamination front that is parallel to the fibers of a unidirectionally reinforced ply. In this case the delamination can grow into the ply without any fiber bridging. Such cases are discussed in Chapter 6.

2.1.2 Energy Release Rate

Griffith [23] was the first who considered the equilibrium of the energy released at crack growth and the energy required to create new crack surface for the prediction of crack propagation. The energy released per unit area if the crack is extended by an area ∂A is called energy release rate and reads,

$$\mathcal{G} = -\frac{\partial \left(\Pi_{\text{int}} + \Pi_{\text{ext}} \right)}{\partial A} \quad , \tag{2.12}$$

where Π_{int} is the elastic potential and Π_{ext} is the potential of external forces. Note that the potential of external forces decreases by the work performed by these forces, i.e. $\partial \Pi_{\text{ext}} = -\partial W_{\text{ext}}$, see [39, 24].

The energy release rate can be computed from the stress intensity factors as shown in the following. Crack growth leads to the formation of new traction free crack surfaces. The energy released during crack growth is equal to the work required to close the crack again, i.e. to bring the relative displacement of the newly formed crack surfaces to zero. Following Irwin's crack closure integral [33], the work required to close the crack can be computed by the stresses ahead of the new crack tip and the relative displacement of the crack surfaces with respect to each other. For planar structures of unit thickness and pure

mode I loading, the work required to close the crack over a length of Δa is given as,

$$
\begin{aligned}
\Delta W &= \frac{1}{2} \int_0^{\Delta a} \sigma_{yy}(x) \left(u_y^+(\Delta a - x) - u_y^-(\Delta a - x) \right) dx \\
&= \frac{\kappa + 1}{4\pi G} \int_0^{\Delta a} \frac{K_{\mathrm{I}}(a)}{\sqrt{x}} K_{\mathrm{I}}(a + \Delta a) \sqrt{\Delta a - x} \, dx \quad .
\end{aligned}
\tag{2.13}
$$

For structures containing a through–the–width crack with straight front the crack area is equal to the crack length, i.e. $\Delta A = \Delta a$, and the energy release rate reads,

$$
\begin{aligned}
\mathcal{G}_{\mathrm{I}} &= \lim_{\Delta a \to 0} \frac{\Delta W}{\Delta a} \\
&= \frac{\kappa + 1}{4\pi G} K_{\mathrm{I}}^2(a) \underbrace{\lim_{\Delta a \to 0} \frac{1}{\Delta a} \int_0^{\Delta a} \sqrt{\frac{\Delta a - x}{x}} dx}_{\frac{\pi}{2}} \quad .
\end{aligned}
\tag{2.14}
$$

Equivalent equations can be derived for pure mode II and pure mode III loading by considering the corresponding shear stresses and displacements. The energy release rates read,

$$
\begin{aligned}
\mathcal{G}_{\mathrm{I}} &= \frac{\kappa + 1}{8G} K_{\mathrm{I}}^2 \quad , \\
\mathcal{G}_{\mathrm{II}} &= \frac{\kappa + 1}{8G} K_{\mathrm{II}}^2 \quad , \\
\mathcal{G}_{\mathrm{III}} &= \frac{1}{2G} K_{\mathrm{III}}^2 \quad .
\end{aligned}
\tag{2.15}
$$

This means that for linear elastic materials the concept of stress intensity factors developed by Irwin and the concept of energy release rates developed by Griffith are equivalent. For the prediction of delamination growth, however, the concept of energy release rates is commonly used since energy release rates can be more easily derived from results of experimental tests [49].

Crack Growth and Crack Growth Stability

According to Griffith a crack will grow if the energy released at crack growth is equal to
or greater than the energy required to create new crack area. For pure mode I loading the
growth condition reads,

$$\mathcal{G}_{\mathrm{I}} \geqslant \mathcal{G}_{\mathrm{Ic}} \quad , \tag{2.16}$$

where $\mathcal{G}_{\mathrm{Ic}}$ is the critical energy release rate for pure mode I loading. Equivalent criteria
and critical energy release rates, $\mathcal{G}_{\mathrm{IIc}}$, and $\mathcal{G}_{\mathrm{IIIc}}$, can be defined for pure mode II and pure
mode III loading, respectively. Some remarks concerning experimental testing of critical
energy release rates of FRP laminates are given at end of this subsection.
For the case of a crack loaded by combination of mode I, mode II, and mode III, the growth
criterion can be written in the general form,

$$g\left(\mathcal{G}_{\mathrm{I}}, \mathcal{G}_{\mathrm{II}}, \mathcal{G}_{\mathrm{III}}, \mathcal{G}_{\mathrm{Ic}}, \mathcal{G}_{\mathrm{IIc}}, \mathcal{G}_{\mathrm{IIIc}}\right) \geqslant 1 \quad . \tag{2.17}$$

In order to take into account the mode interaction at the delamination front, various
functions, g, have been developed, see [35, 73] for an overview. For the materials considered
in the present work a quadratic interaction criterion is suitable and the growth condition
is given as,

$$\left(\frac{\mathcal{G}_{\mathrm{I}}}{\mathcal{G}_{\mathrm{Ic}}}\right)^2 + \left(\frac{\mathcal{G}_{\mathrm{II}}}{\mathcal{G}_{\mathrm{IIc}}}\right)^2 + \left(\frac{\mathcal{G}_{\mathrm{III}}}{\mathcal{G}_{\mathrm{IIIc}}}\right)^2 \geqslant 1 \quad . \tag{2.18}$$

For the definition of equilibrium growth condition and its stability it is favorable to for-
mulate the growth criterion in terms of the total energy release rate,

$$\mathcal{G} = \mathcal{G}_{\mathrm{I}} + \mathcal{G}_{\mathrm{II}} + \mathcal{G}_{\mathrm{III}} \quad . \tag{2.19}$$

Then the growth condition reads,

$$\mathcal{G} \geqslant \mathcal{G}_{\mathrm{c}} \quad , \tag{2.20}$$

where $\mathcal{G}_{\text{c}}$ is the critical energy release rate for the actual loading. It is a function of the critical energy release rates for pure mode I, mode II, and mode III loading as well as the actual mode mix situation. Considering the quadratic interaction criterion, Eq. (2.18), the critical energy release rate is defined by,

$$\left(\frac{\mathcal{G}}{\mathcal{G}_{\text{c}}}\right)^2 = \left(\frac{\mathcal{G}_{\text{I}}}{\mathcal{G}_{\text{Ic}}}\right)^2 + \left(\frac{\mathcal{G}_{\text{II}}}{\mathcal{G}_{\text{IIc}}}\right)^2 + \left(\frac{\mathcal{G}_{\text{III}}}{\mathcal{G}_{\text{IIIc}}}\right)^2 \quad . \tag{2.21}$$

Substituting Eq.(2.12) in Eq. (2.20) yields the growth condition in terms of the potentials,

$$\frac{\partial\left(\Pi_{\text{int}} + \Pi_{\text{ext}}\right)}{\partial a} + \mathcal{G}_{\text{c}} \begin{cases} > 0 & \text{no growth} \\ = 0 & \text{equilibrium growth} \\ < 0 & \text{non–equilibrium growth} \end{cases} \quad . \tag{2.22}$$

Equilibrium growth takes place if all energy released is required to create new delaminated area. If more energy is released during delamination growth than required the structure is not in static equilibrium and non–equilibrium delamination growth, accompanied by dynamic effects, takes place. Such non–equilibrium states are always unstable.

The condition for stability of equilibrium growth (i.e. a small increase in the applied load leads to limited increase of the delaminated area) reads,

$$\frac{\partial^2\left(\Pi_{\text{int}} + \Pi_{\text{ext}}\right)}{\partial a^2} + \frac{\partial\mathcal{G}_{\text{c}}}{\partial a} > 0 \quad . \tag{2.23}$$

Note that if the mode mix changes during delamination growth also the critical energy release rate changes (i.e. $\frac{\partial\mathcal{G}_{\text{c}}}{\partial a} \neq 0$). If the left hand side of Eq. (2.23) is smaller than zero growth is unstable. In case that the left hand side of Eq. (2.23) is zero, derivatives of higher order have to be considered to determine the stability of the equilibrium state [9].

For FRP laminates critical energy release rates can be determined by experimental testing, though this may be quite difficult. Test procedures are evaluated and standardized by

ASTM and other national and international standards organizations [48, 12]. For experimental testing of critical mode I energy release rates the Double Cantilever Beam (DCB) test is widely used for FRP laminates [16]. For experimental determination of critical mode II energy release rates of FRP laminates, End Notched Flexure (ENF) specimens are used. They can be loaded in three or four point bending mode, see [64]. A critical review of the ENF test, including a discussion of the influence of friction effects is given in [47]. There is no accepted test for determining the mode III critical energy release rate. To circumvent this problem it is assumed that the critical energy release rate for mode III and mode II are equal, i.e. $\mathcal{G}_{\mathrm{IIIc}} = \mathcal{G}_{\mathrm{IIc}}$ [49].

It is shown in [5] that for some FRP the critical energy release rate depends on the orientation of the delamination front with respect to the fibers in the plies adjacent to the delamination. In the present work such effects are not taken into account and it is assumed that the critical energy release rates depend neither on the fiber orientation nor on the delamination length.

2.1.3   Bimaterial Problems

Delaminations between plies with different orientations have to be considered as cracks in a bimaterial interface. Such problems are discussed in detail e.g. in [71, 24, 39]. An example of a crack at the interface between two homogeneous, isotropic materials A and B with elastic mechanical properties $E_{\mathrm{A}}, G_{\mathrm{A}}$ and $E_{\mathrm{B}}, G_{\mathrm{B}}$ is shown in Fig. 2.3. The normal and shear stresses ahead of the crack tip along the x–axis (i.e. $\theta = 0$) can be written as [24],

$$\sigma_{yy} + \mathrm{i}\sigma_{xy} = \frac{K}{(2l)^{\mathrm{i}\epsilon}} \frac{r^{\mathrm{i}\epsilon}}{\sqrt{2\pi r}} \quad , \tag{2.24}$$

where $K = K_1 + \mathrm{i}K_2$ is the complex stress intensity factor with the real part K_1 and the complex part K_2. l is a reference length that corresponds to the crack size (e.g. the crack length). In the following half of the total crack length is used as reference length, i.e. $l = a$.

ϵ is the so called bimaterial parameter

$$\epsilon = \frac{1}{2\pi} \ln \frac{G_B \kappa_A + G_A}{G_A \kappa_B + G_B} \quad , \tag{2.25}$$

where κ is computed for material A and material B, respectively, by Eq. (2.6). If the structure is loaded at the boundary by uniform normal stresses, σ_{yy}^{∞}, and uniform shear stresses, $\sigma_{xy}^{\infty} = \sigma_{yx}^{\infty}$ the complex stress intensity factor reads [24]

$$K = (\sigma_{xx}^{\infty} + i\sigma_{xy}^{\infty})\sqrt{\pi a}(1 + 2i\epsilon) \quad . \tag{2.26}$$

Equations (2.24) and (2.26) show that the normal and shear stresses at the interface ahead of the crack tip are inherently related to each other and no separation into mode I and mode II loading is possible. Hence, no loading state exists for which the entire interface is loaded by normal stresses or by shear stresses only. Note that the stress intensity factors K_1 and K_2 do not correspond to the stress intensity factors K_{I} and K_{II} defined for a crack in a homogeneous isotropic material. For cracks in a homogeneous material the bimaterial parameter is zero and Eqs. (2.24) and (2.26) reduce to Eqs. (2.3) and (2.4), respectively.

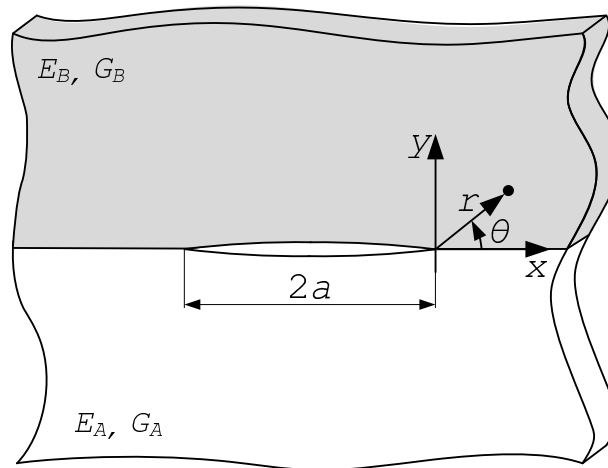The relative opening and sliding displacements of the crack surfaces with respect to each

Figure 2.3: Crack at the interface between two homogeneous, isotropic materials with mechanical properties E_A, G_A and E_B, G_B .

other are given as

$$\left(u_y^+ - u_y^-\right) + \mathrm{i}\left(u_x^+ - u_x^-\right) = \frac{K}{(2a)^{\mathrm{i}\epsilon}}\, r^{\mathrm{i}\epsilon} \sqrt{\frac{r}{2\pi}} \frac{c_\mathrm{A} + c_\mathrm{B}}{2\,(1 + 2\mathrm{i}\epsilon)\cosh \pi\epsilon} \quad , \tag{2.27}$$

where the constants c_A and c_B are defined as,

$$c_j = \frac{1 + \kappa_j}{G_j} \quad \text{for} \;\; j = \mathrm{A}, \mathrm{B} \quad . \tag{2.28}$$

The relative crack opening $\left(u_y^+ - u_y^-\right)$ defined in Eq. (2.27) oscillates as the radial coordinate approaches zero, and crack fronts are predicted to overlap. As this is physically not possible, contact between the crack surfaces takes place. However, linear elastic fracture mechanics is based on the assumption of traction free crack surfaces and can only be used to predict the stress and displacement field outside the region where contact takes place. For practical material combinations and loading by uniform normal and shear stresses, it can be shown that the size of the zone where the oscillatory terms play a role is some orders of magnitude smaller than the crack length [59, 24]. As a consequence the zone where the oscillatory terms play a role is negligibly small.

Loading by some uniform shear stresses, $\sigma_{yz}^\infty = \sigma_{zy}^\infty$ (i.e. mode III loading), leads to the same stress and displacement fields as presented for the crack in an isotropic material [71].

The stress and the displacement fields at the crack tip are defined in a unique manner by a modified stress intensity factor $\widetilde{K} = (K_1 + \mathrm{i}K_2)(2a)^{-\mathrm{i}\epsilon}$. Note that the the modified stress intensity factor depends on the reference length a. Considering the magnitude, $|K|$, and the argument, ψ, of the complex stress intensity factor,

$$|K| = \sqrt{K_1^2 + K_2^2} \quad , \qquad \tan\psi = \frac{K_2}{K_1} \quad , \tag{2.29}$$

the modified stress intensity factor is defined as [24, 39],

$$\widetilde{K} = \frac{|K|e^{\mathrm{i}\psi}}{(2a)^{\mathrm{i}\epsilon}} \quad . \tag{2.30}$$

For the prediction of crack growth, a criterion in the form $\widetilde{K} \geqslant \widetilde{K_c}$ might be formulated. However, the definition of $\widetilde{K_c}$ is difficult. For the case of two different crack lengths (i.e. two different reference lengths a and a^*) the stresses at the interface are equal if,

$$\frac{|K^*| e^{i\psi^*}}{(2a^*)^{i\epsilon}} = \frac{|K| e^{i\psi}}{(2a)^{i\epsilon}} \quad . \tag{2.31}$$

This is equivalent to the requirement that,

$$|K^*| = |K| \quad , \qquad \psi^* = \psi - \epsilon \ln \frac{a}{a^*} \quad . \tag{2.32}$$

Hence, different crack lengths require different values of the argument of the complex stress intensity factors. This makes the transfer from experimentally determined data to structures with different geometry complicated. A pragmatic solution to this problem was proposed by Rice [59]. For most material combinations of practical relevance the bimaterial parameter is very small. Consequently, the zone where the oscillatory terms play a role is small and the stress field is dominated by the singular term only. Using the phase angle that corresponds to a fixed reference length $\hat{l}$ (e.g. the initial crack length, the ply thickness), instead of the phase angle that corresponds to the actual crack length, one can write,

$$K_I + i K_{II} \approx \widetilde{K} 2 \hat{l}^{i\epsilon} \quad . \tag{2.33}$$

This means that the stress state that exists at a distance $\hat{l}$ ahead of the crack tip is used to describe the stress field and the real and the complex parts of the stress intensity factor can be interpreted as the mode I and mode II stress intensity factors of a crack in an isotropic material.

The total energy released at crack growth can be computed by means of the crack closure integral defined in Eq. (2.13) and is given as [24],

$$\mathcal{G} = \frac{(c_A + c_B)(K_1^2 + K_2^2)}{16 \cosh^2(\pi\epsilon)} \quad . \tag{2.34}$$

Due to the oscillatory nature of the stress and displacement fields no crack closure integrals for mode I or mode II exist and the mode I and mode II energy release rates cannot be computed. Hence, conventional linear elastic fracture mechanics does not allow to define a mode I and a mode II energy release rate for bimaterial problems only the total energy release rate can be computed.

A delamination between plies with different fiber orientations can be considered as a crack between two different homogeneous orthotropic materials. The stresses and displacements at the tip of a crack in such an interface can be derived from the results for a crack between two isotropic materials and a bimaterial parameter [45]. The latter is a function of the difference in elastic properties of the materials; the corresponding equations are given in [71, 45]. The results show that the oscillatory nature of the stresses and displacements remains.

2.1.4 Virtual Crack Closure Technique

Within the FEM several methods exist to compute energy release rates. One of the most successfully used is the VCCT, which is briefly reviewed in the following. For a detailed discussion see [35].

If a crack is advanced by a length Δa, the energy released is assumed to be equal to the work required to close the crack over the same distance (Eq.(2.13)). Within the FEM the work to close a crack is computed easily from the relative distance which the nodes need to be moved to close the crack and the corresponding nodal forces, see Fig. 2.4. For planar elements with four nodes and linear shape functions the work required to close the crack over a length of Δa, which is equal to the element length, is computed as,

$$\Delta W = \frac{1}{2}(F_x \Delta u_x + F_y \Delta u_y) \quad , \tag{2.35}$$

where F_x and F_y are the nodal forces computed for the closed crack and Δu_x and Δu_y are the relative nodal displacements computed for the open crack. Hence, two analyses are required, one for a crack length of a and one for a crack length of $a + \Delta a$.

It is assumed now that crack growth is self similar, i.e. the shape of the crack does not change during crack growth (i.e. no crack kinking takes place) and the increment in crack length, Δa, is small compared to the total crack length, a. Consequently, the stress state at the crack tip does not alter significantly during crack growth. For a crack in an isotropic material the stresses in Irwin's crack closure integral, Eq.(2.13), can be substituted by functions of the nodal forces and the relative crack surface displacements can be substituted by functions of the nodal displacements [56]. The equation obtained allows to compute the energy release rate for pure mode I loading. For configurations of unit thickness it is given as,

$$\mathcal{G}_\text{I} \;=\; \lim_{\Delta a \to 0} \frac{1}{2\Delta a} (F_{y,\,j}\,\Delta u_{y,\,i}) \quad . \tag{2.36}$$

$F_{y,\,j}$ is the force at node j in y–direction and $u_{y,\,i}$ is the relative nodal displacement in y–direction between nodes $i\,''$ and $i\,'$, see Fig. 2.5. The limit indicates that the element length at the crack tip needs to be small. For sufficiently small element lengths the limit can be dropped [56]. If, as an approximation, the forces at the crack tip and the displacements behind the crack tip are used, only one analysis is required. Equation (2.36) was proposed
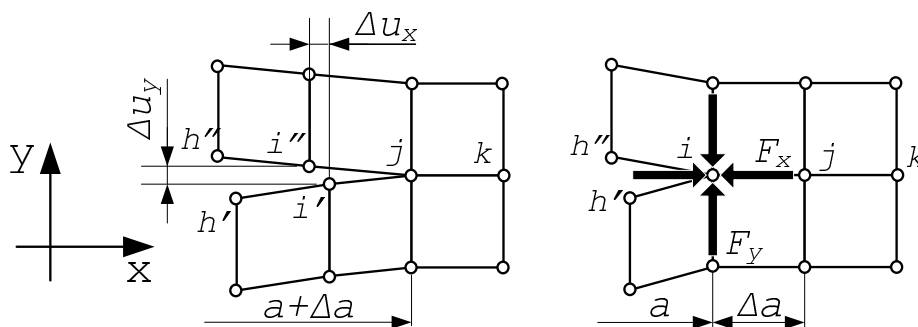

Figure 2.4: Work required to close the crack computed from the nodal forces and nodal displacements.

first in [62] based on some heuristic arguments. Their validity has been proven in [56] and equivalent equations for elements of higher order and quarter point elements have been derived [56]. If the elements ahead and behind the crack tip have different lengths a correction factor is required [35].

Consideration of the nodal forces and relative nodal displacements in x–, y–, and z–directions allows the computation of the energy release rate for mode I, mode II, and mode III,

$$
\begin{aligned}
\mathcal{G}_{\mathrm{I}} &= \frac{1}{2\Delta a}(F_{y,\,j}\Delta u_{y,\,i}) \quad, \\
\mathcal{G}_{\mathrm{II}} &= \frac{1}{2\Delta a}(F_{x,\,j}\Delta u_{x,\,i}) \quad, \\
\mathcal{G}_{\mathrm{III}} &= \frac{1}{2\Delta a}(F_{z,\,j}\Delta u_{z,\,i}) \quad.
\end{aligned}
\tag{2.37}
$$

The z–direction is defined by the local direction of the crack front and the y–direction is defined to be perpendicular to the crack plane, see Fig.2.6.

A mesh that is locally orthogonal to the delamination front is required to allow for a proper definition of the relative displacements of the nodes behind the delamination front in x– and z–directions. Care has to be taken if the delamination front is not smooth. At kinks and corners it is not possible to define the local z–direction in a unique manner. Consequently
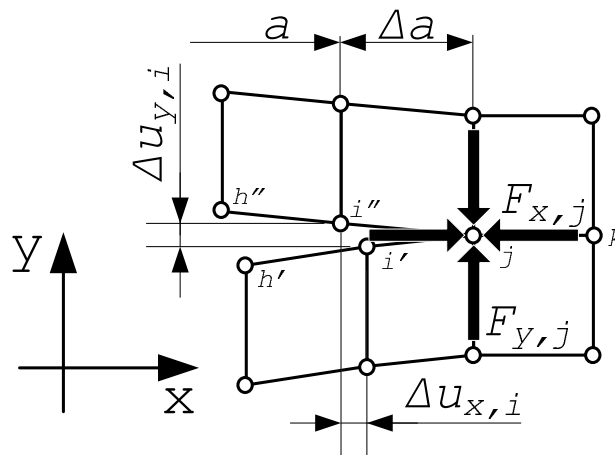

Figure 2.5: Definition of forces and displacements used for computation of energy release rates within the Virtual Crack Closure Technique.

the mode II and mode III energy release rates cannot be defined. A pragmatic solution of this problem is to model such corners as fillets and to use a mesh that is fine enough to allow for a smooth delamination front along the fillet [35].

A delamination located between plies oriented in the same direction can be considered as a crack in a homogeneous orthotropic material (see Section 2.1.1). The energy release rates can be computed by Eq. (2.37). A delamination located between plies with different orientation can be considered as a crack at the interface between two different orthotropic solids. For such bimaterial problems an oscillatory singularity is predicted at the delamination front as discussed in detail in the previous section. Due to the oscillatory field only the total energy release rate is defined and can be computed by means of the VCCT [35]. If one tries to compute mode I and mode II energy release rates by means of the VCCT the computed values start to oscillate if the size of the elements at the crack tip becomes too small (i.e. if the element size becomes smaller than the zone where the oscillatory terms play a role).

Several approaches have been proposed to circumvent this problem. The first one is the introduction of an artificial, thin, homogeneous, and isotropic layer that is assumed to exist between the plies [56]. Consequently, delamination propagation occurs in a homogeneous, isotropic material and the problem of oscillatory singularities does not exist. Another ap-
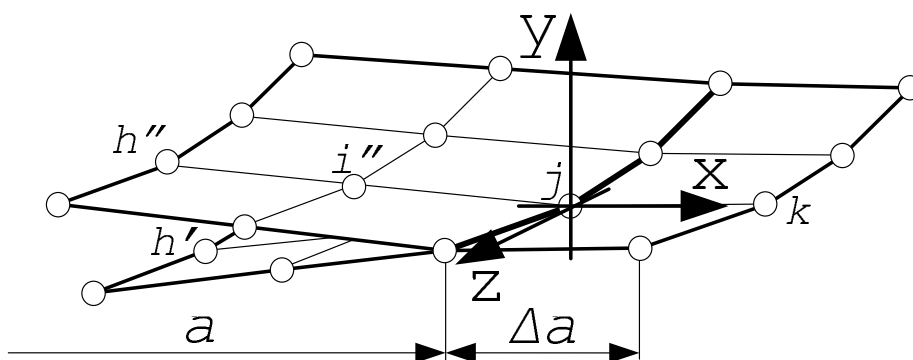

Figure 2.6: Definition of the local orientation of the delamination front used within the Virtual Crack Closure Technique; Nodes and faces defining the crack surfaces and the crack front shown only.

proach is to take into account the contact of the crack surfaces, which is predicted for the region close to the crack tip [29]. Very fine meshes and appropriate contact conditions at the crack surfaces are applied and the predicted stress field does not show any oscillations. Hence, the computed mode I and mode II energy release rates converge to asymptotically constant values as the size of the elements at the crack tip decreases. To summarize, it can be said that assuming a homogeneous layer or taking into account the contact of the crack surfaces allows to compute the mode I and mode II energy release rates for bimaterial problems The results obtained by both approaches are similar [35], but, very fine meshes are required.

A more convenient and numerically more efficient way to compute mode I and mode II energy release rates is the usage of an element size that is small enough to resolve the local deformation at the crack tip but large enough to avoid oscillatory results [70, 56, 31]. A reasonable lower limit for the element size is a length equal to five to ten times the fiber diameter. For smaller elements the assumption of a homogeneous orthotropic material is no longer valid and the local distribution of fibers has to be taken into account. The ply thickness is a reasonable upper limit of the element size in thickness direction. Larger elements would require to represent more than one ply by one element, i.e. to smear the properties of different plies over one element. Numerical studies have shown that the variations in the computed mode I and mode II energy release rate between these upper and lower bounds are typically small and their accuracy proves acceptable for practical application [35]. To minimize innaccuracies the same mesh size should be used for the evaluation of experimental tests and for the prediction of delamination growth in structural problems.

FEM Implementation

A VCCT tool is provided by *ABAQUS*, it is based on the *ABAQUS* contact capability [1]. The tool is capable of computing the mode I, mode II, and mode III energy release rates at nodes at the crack front, of evaluating the energy release rates by means of a growth

criterion, and of propagating the crack if indicated.

The crack path needs to be defined in advance and the regions adjacent to the crack path are meshed separately, so that the elements on both sides of the crack path do not have any nodes in common. In the region of the crack path that is yet uncracked the degrees of freedom of the nodes of the elements adjacent to the crack path are coupled by kinematic conditions. For conventional continuum elements the translational degrees of freedom are coupled. For shell elements the question arises if the translational and the rotational degrees of freedom should be coupled. Numerical investigations showed that coupling only the translational degrees of freedom yields more accurate results [57]. Note, that for the definition of coupling conditions the shell thickness has to be taken into account properly, i.e. the displacements of the faces of the shell elements need to be coupled.

At nodes where the growth criterion is met the delamination propagates. To aid convergence the kinematic coupling conditions are replaced by coupling forces, and the coupling forces are incrementally reduced to zero.

The VCCT tool provided by *ABAQUS* can only be used in combination with linear elements and no correction is applied if the element size ahead and behind the crack tip is different or if the mesh is locally not orthogonal to the delamination front (i.e. if such meshes are used the computed energy release rates are inaccurate).

2.2 Elastic–Plastic Fracture Mechanics

The use of linear elastic fracture mechanics leads to the prediction of infinite stresses at the crack tip. However, most materials of practical relevance yield and a plastic zone is formed at the crack tip. Local yielding at the crack tip was first taken into account by Dugdale [19]. He considered a plastic zone ahead of the crack tip in an elastic, ideally plastic material and assumed that the effective crack is longer than its nominal length. The plastic zone is assumed to be thin compared to its length, hence, the model is also called strip yield model. A similar model has been proposed by Barenblatt [8], who defined the traction

acting on the plastic zone as function of the separation of the crack surfaces. This function
is called traction–separation law or cohesive law. Cohesive laws are frequently used in
the simulation of growth of a crack along a predefined paths in homogeneous materials as
well as in bimaterial problems. Needlemann [46] used cohesive laws to describe the failure
of interfaces. He considered cohesive zone models particularly attractive when interfacial
strengths are relatively low compared to the strength of the adjoining material.

2.2.1 Cohesive Zone Elements

Based on the work of Dugdale and Barenblatt, Cohesive Zone Elements have been devel-
oped within the framework of the FEM [14, 13, 4]. The proposed constitutive equations
for the interface are phenomenological mechanical relations between the tractions at the
interface and the separation of the interface. With increasing interfacial separation the
tractions acting on the interface reach a maximum, decrease, and vanish when complete
decohesion occurs. Commonly used for the simulation of delamination are piecewise linear
traction separation relations as shown in Fig. 2.7. The initial response is defined by the
initial stiffness, E. The onset of damage is defined by a critical interface traction, t_c, or
by a critical separation distance of the interface, δ_c. Further increase of the separation
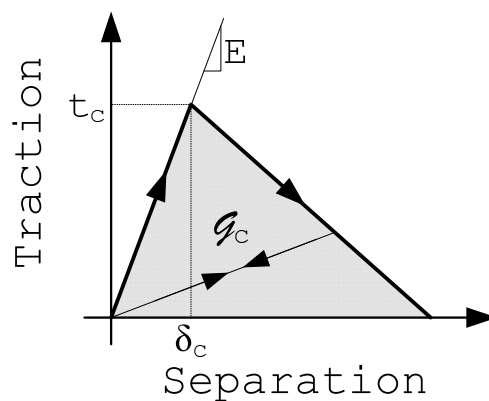

Figure 2.7: Bilinear traction separation law to describe the interface behavior of Cohesive
Zone Elements.

leads to damage evolution, the tractions and the stiffness decrease linearly up to complete separation of the crack surfaces. The energy required to separate the crack surfaces (i.e. the area underneath the traction–separation curve) is equal to the the critical energy release rate, $\mathcal{G}_\mathrm{c}$. Such piecewise linear laws can be defined for mode I, mode II, and mode III loading by considering the normal and shear tractions acting on the interface and the corresponding separations. In order to distinguish the mode II and the mode III shear tractions the local orientation of the delamination front must be known. To simplify this problem the total shear traction is commonly considered instead of the separate mode II and mode III components. Hence, two traction–separation laws are defined, one for the normal traction and one for the shear traction. If the interface is loaded by a combination of normal and shear traction some interaction criteria are required for the prediction of damage onset and damage evolution, see e.g. [14].

For the simulation of crack growth using CZE a mesh is required that is fine enough to adequately represent the process zone. A detailed discussion concerning the mesh size including some guideline for choosing an appropriate one is given in [75]. Small load increments are required to capture damage evolution and the associated stress redistribution adequately. Due to their formulation CZE can be used to simulate the onset of interface damage, i.e. the formation of a first flaw at an interface, as well as crack propagation along a predefined path.

Planar CZE with four nodes and three–dimensional CZE with eight nodes are provided by *ABAQUS*. Both elements use linear shape functions and a finite initial thickness. The initial stiffness of these elements is defined by their thickness and their Young's modulus and shear modulus. For the prediction of the onset and evolution of damage various criteria are available. For the case of mixed mode loading it is assumed that the mode mix does not change in the considered element during damage evolution, i.e. the ratio between the normal and shear separation is assumed to be constant as long as the considered element belongs to the process zone.

Chapter 3

Emergence of Delaminations

The delamination process from the perfect, i.e. flawless structure up to final failure of the structure is considered as a two step process. In the first step an initial delamination emerges at the intact interface and in the second step the delamination grows. Strength criteria can be applied to predict the onset of interface damage, which can be considered as the onset of formation of a delamination, but cannot directly be applied to predict open initial delaminations. LEFM, on the other hand, can be used to predict the propagation of delaminations, provided an initial delamination exists. In the present chapter an approach for the prediction of emergence of delaminations is presented that combines these methods and bridges the gap between them.

The proposed approach allows to predict emergence of delaminations in a numerically efficient and robust manner. Delaminations emerging inside a structure can be handled as well as delaminations emerging from free edges, where stress singularities are present theoretically. A linear FEM analysis of the pristine structure is conducted and regions of overloaded interface regions are predicted with the Puck FPF criterion. Within such regions, delamination initiation is assumed to occur and initial delaminations are introduced. The onset of propagation of these initial delaminations is predicted using the Griffith criterion which is evaluated by means of the VCCT within linear FEM analyses. The smallest

delamination size which fullfills the initiation criterion and the propagation criterion is the *critical initial delamination*. The load at which this delamination emerges is called *delamination load*. These findings allow for a conservative estimate of the load carrying capacity of the structure. In addition, the sensitivity of the load carrying capacity with respect to changes in the interface properties (i.e. strength and critical energy release rate) can be assessed. Once the size of the critical initial delamination and the delamination load are determined, the entire delamination process and the corresponding non–linear structural response can be predicted by a non–linear FEM analysis.

Two examples are investigated in Section 3.3, delamination inside a curved laminate and delamination emerging from a stress singularity at a corner in a Double–Lap–Shear (DLS) test specimen. For verification of the proposed approach CZE are used. All FEM analyses are carried out by means of the FEM program *ABAQUS*.

3.1   Strength/Energy Approach

In the following, an approach is presented which combines a strength criterion that predicts delamination initiation and an energy criterion that predicts the onset of delamination propagation. Here, the Puck FPF criterion and the VCCT are employed for this purpose. However, it should be noted that any strength criterion can be used which is suitable for predicting interface failure. In [72], for example, a quadratic strength criterion is used for the prediction of the failure of the interface between two plies. For predicting delamination propagation any fracture criterion suitable for this purpose can be used.

3.1.1   Puck First Ply Failure Criterion

The Puck FPF criterion is a local failure criterion for triaxial stress states for FRP laminates. In the following a brief description of this criterion is given, for a more detailed

discussion see [54, 52, 63]. A general introduction concerning failure criteria for FRP laminates is given in [66].

The Puck FPF criterion evaluates the stresses at the ply level and is suitable for plies made of unidirectional continuous fiber reinforced polymers. The criterion allows to distinguish between fiber failure and several modes of matrix dominated failure. For the prediction of fiber failure a maximum stress criterion is utilized. For the prediction of matrix dominated failure, Mohr's fracture hypothesis for brittle materials is used which states that fracture occurs in the plane with the lowest resistance against the tractions acting on that plane. Depending on the predicted orientation of the fracture plane, different modes of matrix dominated failure are distinguished. Delamination is considered as that matrix dominated failure mode, for which the fracture plane is oriented parallel to the ply.

The Puck FPF criterion was implemented into $ABAQUS$ as a post processing tool [63, 65]. It evaluates the stresses in each Gauss point of each element and predicts the spatial distribution of the load factor and the corresponding failure mode (i.e. fiber failure, matrix failure, and delamination). The load factor is defined as the scalar value by which the stress tensor needs to be multiplied to reach the failure stress state. Therefore, a load factor being smaller than unity indicates that the failure load has been exceeded. The Puck FPF criterion allows to find out whether or not delamination is the critical failure mode for the considered problem.

3.1.2   Analysis Procedure

In the following the analysis procedure for the prediction of emergence of delaminations is presented. As result of this procedure conservative estimates of the delamination load and the load carrying capacity of the structure is obtained. The procedure is based on the assumption that an initial delamination is formed at the lowest load for which the delamination initiation and the delamination propagation criteria are fullfilled. The critical initial delamination which fullfills both criteria is defined by the intersection of two curves

in a load–delamination size diagram, one curve that defines delamination initiation and one curve that defines delamination propagation. The way these curves are computed is discussed in detail in the following.

A linear FEM analysis of the flaw free structure loaded by a mechanical load is performed and the stresses are evaluated using the Puck FPF criterion. From this analysis the spatial distributions of the load factor and the corresponding failure modes are obtained. The FPF load of the structure is computed by scaling the applied load by the load factor at the location most prone for failure. Note that only these cases are considered here, for which the failure mode at the failure critical location is predicted to be delamination. The applied load is scaled incrementally beyond the FPF load, leading to the prediction of a region where the stresses exceed the strength of the interface. Initial delaminations with the sizes of the overloaded interfacial region are assumed to form there. Considering various load levels above the FPF load allows to derive a relation between the applied load and the size of the initial delamination. The size of the delamination can be defined by its length or by the square root of the delaminated area. This relation is called *delamination initiation curve*; generic examples are shown in Fig. 3.1 (bold solid lines). Of course, the curves show
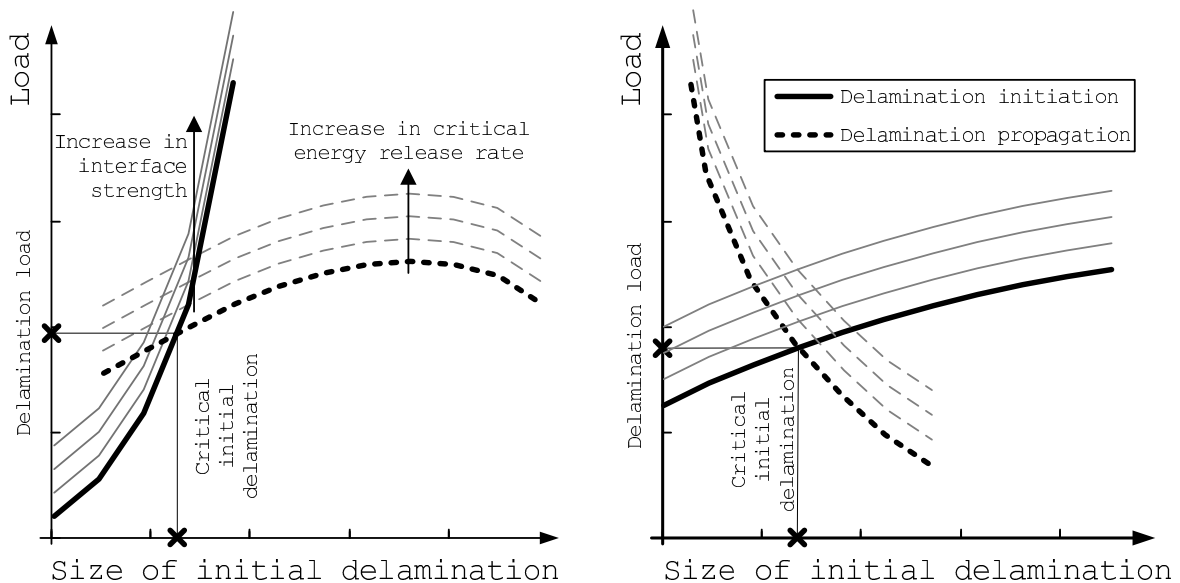

Figure 3.1: Generic examples of delamination initiation curves and delamination propagation curves.

that the higher the load is, the larger is the size of the predicted initial delamination. The entire delamination initiation curve can be derived by scaling the results of one single linear FEM analysis.

Care has to be taken if an overloaded region is predicted at a free edge or a sharp notch. Theoretically, stress singularities are present at such locations and the stresses computed with conventional FEM depend on the mesh size. For the prediction of the overloaded region the FEM mesh size has to be chosen sufficiently fine to ensure that the stresses at the distal edge of the predicted overloaded region are well represented.

To determine which size of initial delamination is critical the VCCT is used. From the results of the delamination initiation a series of initial delaminations of different sizes is selected, introduced into the FEM model, and for each delamination the load required to cause delamination propagation is computed. The relation between the size of the initial delamination and the load required to propagate it is called *delamination propagation curve*, Fig. 3.1 (thick dashed lines). The slope of this curve provides information about the stability of delamination growth. If the slope is positive an increase in the delamination size leads to an increase in the load required to cause delamination propagation, i.e. the load needs to be increased continuously to cause further delamination growth. This growth process is stable and it is entirely controlled by the applied load. If the slope of the delamination propagation curve is negative the growth process is unstable and not controlled by the applied load. The generic delamination propagation curve in Fig. 3.1, (left, dashed line) predicts stable growth for small delaminations and unstable growth for large delaminations. The delamination propagation curve in Fig. 3.1, (right, dashed line) predicts unstable growth for all delamination sizes.

The intersection of the delamination initiation curve and the delamination propagation curve defines the initial delamination size. For this size the load required to fullfill the initiation and the propagation criteria is smallest. Hence, this delamination is called *critical initial delamination*, the load at which such a delamination emerges is called *delamination load.*

The load carrying capacity of the structure is equal to or greater than the delamination

load, depending on the stability of delamination growth. In Fig. 3.1 (left) growth is stable for the predicted delamination load, which means that the load has to be increased in order to cause delamination growth. Thus, the load carrying capacity is higher than the delamination load. In Fig. 3.1, (right) growth is predicted to be unstable. The critical initial delamination will grow without any further load increase as soon as it emerges and the load carrying capacity is equal to the delamination load. As a consequence, a conservative estimate of the load carrying capacity of the structure is obtained from the critical initial delamination (for further discussion see 3.3.1).

The proposed strength/energy approach allows to determine the size and the position of the critical initial delamination as well as load at which delaminations emerge. Based on these results the non–linear structural response caused by the delamination process can predicted in a non–linear analysis. An FEM model with bonded surface conditions at the location of the critical initial delamination is set up and loaded up to the delamination load. Then the critical initial delamination is introduced by removing the bonding conditions, and delamination growth is simulated using the delamination propagation capability of the VCCT–tool provided by *ABAQUS*.

Several assumptions are made to derive the delamination initiation curve from the FEM data which are summarized in the following. First, for the FPF analysis the stresses at the Gauss points of the continuum elements are assessed instead of the stresses at the interface. However, the interface tractions are continuous and the respective stress components at the Gauss points are similar to the stress components at the interface provided that the stress gradients are small. Second, for the prediction of the delamination initiation curve, the load is increased beyond the FPF load without considering non–linear interface behavior. Third, initial delaminations are introduced at locations for which the load factor is predicted to be smaller than one. It is assumed that sufficient energy is available for the formation of these initial delaminations (i.e. no energy criterion is employed to check this assumption).

3.1.3 Sensitivity of the Predictions

The proposed strength/energy approach allows to study the sensitivity of the predicted structural response with respect to a change of the interface properties. This allows to evaluate the effects of uncertainties in interface properties on the predicted results. An increase of the interface strength increases the load required to cause delamination initiation and shifts the delamination initiation curve upwards (Fig. 3.1, thin solid lines). An increase of the critical energy release rate increases the load required to cause delamination propagation and shifts the delamination propagation curve upwards (Fig. 3.1, thin dashed lines). In the generic example shown in Fig. 3.1 (left) an increase in the critical energy release rate affects the delamination load much more than an increase in the interface strength. The load carrying capacity is reached during the delamination growth process and is determined by the critical energy release rate, but not by the interface strength. Only changes of the critical energy release rate affect the load carrying capacity, whereas changes in the interface strength hardly affect the behavior. In the generic example shown in Fig. 3.1 (right) the load carrying capacity is equal to the delamination load and it is a little more sensitive to a change in the interface strength than to a change in the critical energy release rate.

3.2 Comparison to Cohesive Zone Elements

For verification of the proposed strength/energy approach CZE with linear shape functions provided by *ABAQUS* are used. The non–linear constitutive behavior of the CZE is defined by a piecewise linear traction–separation law, see Fig. 2.7. These elements are used within a non–linear FEM analysis for simulation of emergence and growth of delaminations. For the prediction of damage onset in the CZE a quadratic stress criterion is used, see [1]. For the prediction of damage evolution the quadratic energy criterion given by Eq. (2.18) is utilized.

The same material properties used within the proposed strength energy approach are now used to define the non–linear constitutive behavior of the CZE. Hence, the maximum tractions of the CZE are equal to the interface strength (the same strength values are considered in the Puck criterion) and the energy release rate of the CZE is equal to the critical energy release rate of the interface (the same rates are used for prediction of delamination propagation by means of the VCCT).

3.3 Examples

3.3.1 Curved Laminate

The first example considered is an L–shaped structure made from a laminated composite. Details concerning the geometry are shown in Fig. 3.2, all dimensions are given in mm. The laminate consists of 15 plies of a unidirectional carbon fiber reinforced epoxy resin. The plies are oriented in alternating 0° and 90° orientations, where the angle is measured from the xy–plane (Fig. 3.2). The first and the last ply are oriented in 0°–direction. The displacements in x– and y–direction are fixed along the lower leg. The displacements are coupled at the upper end of the left leg of the structure and a load (displacement or force) in x–direction is applied. Material and interface properties are taken from the literature [42], see Table 3.1. The Young's modulus and the normal strength of such unidirectional carbon fiber reinforced epoxy resin can be determined by uniaxial testing of single plies. To determine the shear modulus and the shear strength of such a material laminates with a +45°/-45°layup are tested in a uniaxial manner. Test procedures to determine such properties are evaluated and standardized by ASTM and other national and international standards organizations. An overview about methods to test mechanical properties of FRP is given in [2]. Methods for determining critical energy release rates are briefly discussed in 2.1.2.

The material data is defined with respect to the local material coordinate system (l is the fiber direction, q is the in–plane direction normal to the fibers and n is the out–of–ply direction). R_{ll} is the strength in fiber direction, R_{qq} is the in–plane strength normal to the fiber direction, and R_{lq} is the in–plane shear strength. Strength values for tensile and compressive loading are given. p_{lq} and p_{qn} are parameters required for the definition of the failure surface. Estimates for physically realistic values of these parameters for carbon fiber reinforced epoxy resins are taken from [53]. f_{weak} is called weakening factor for the interface strength and it is defined as the ratio of the normal strength of the interface between the plies and the in–plane normal strength of the plies in direction transverse to the fibers. The weakening factor is used within the Puck criterion to consider the fact that the interface strength might be smaller than strength of the ply in transverse direction. Hence, the weakening factor allows to compute estimates of the interface strength values from given ply strength values, see [52] for details.

The structure has a considerable length in z–direction, so that generalized plane strain
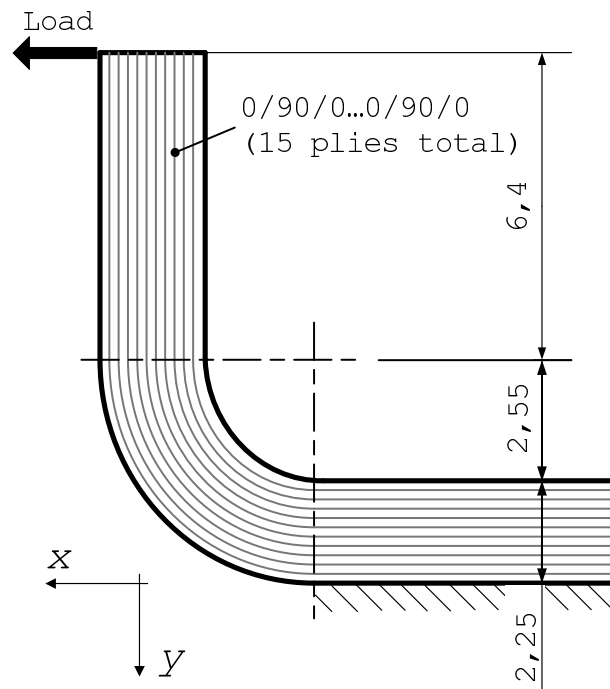

Figure 3.2: Geometry and boundary conditions of the curved, laminated structure.

Table 3.1: Material and interface properties of plies made of a unidirectional carbon fiber reinforced epoxy layer *T300/976*, data taken from [42] (* following Puck's guidelines for carbon fiber materials [53]).

Elastic constants				
E_l	$E_q = E_n$	$G_{lq} = G_{ln}$	$\nu_{lq} = \nu_{ln}$	ν_{qn}
139.3 GPa	9.72 GPa	5.59 GPa	0.29	0.40

Coefficients of thermal expansion	
α_{ll}	$\alpha_{qq} = \alpha_{nn}$
0.41 10^{-6} K^{-1}	36.0 10^{-6} K^{-1}

Strength						
	R_{ll}	R_{qq}	R_{lq}	p_{lq}	p_{qn}	f_{weak}
tension	1517 MPa	45 MPa	107 MPa	0.35 *	0.27 *	0.9 *
compression	1593 MPa	253 MPa	107 MPa	0.3 *	0.27 *	0.9 *

Critical energy release rates	
$\mathcal{G}_{\text{Ic}}$	$\mathcal{G}_{\text{IIc}}$
193 J/m^2	455 J/m^2

conditions are assumed. The structure is modeled using plane strain continuum elements with linear shape functions. Each ply is represented by three elements over the ply thickness and all element aspect ratios are close to unity.

Displacement Controlled Loading

A unit displacement is prescribed and a linear FEM analysis is conducted. The resulting ply stresses are evaluated by means of the Puck criterion. In Fig. 3.3 the predicted spatial distributions of the load factor (left) and the failure mode (right) are shown, indicating

that the critical location is at the interface between ply five and ply six in the curved part
of the laminate. Due to the curvature of the structure high normal stresses in out–of–ply
direction are present in this region. The corresponding failure mode is delamination.

The delamination initiation curve is determined as described in Section 3.1.2. The re-
sult is shown in Fig. 3.4 (top, solid line) in a displacement–delamination length diagram.
The delamination initiation curve shows that for applied displacement loads smaller than
0.31 mm no initial delamination is predicted. Above this load, a small increase in the ap-
plied displacement load leads to a considerable increase in the size of the predicted initial
delamination. The delamination propagation curve is determined as described in Section
3.1.2, the result is shown in Fig. 3.4 (top, dashed line). The curve has a negative slope,
indicating that delamination growth is unstable for all delamination sizes. The intersection
of the delamination initiation and the delamination propagation curve yields the delami-
nation load (0.315 mm) and the size of the critical initial delamination (0.86 mm). Since
delamination growth is predicted to be unstable, the load carrying capacity is equal to the
delamination load.

From the strength/energy approach the size and the location of the critical initial delami-
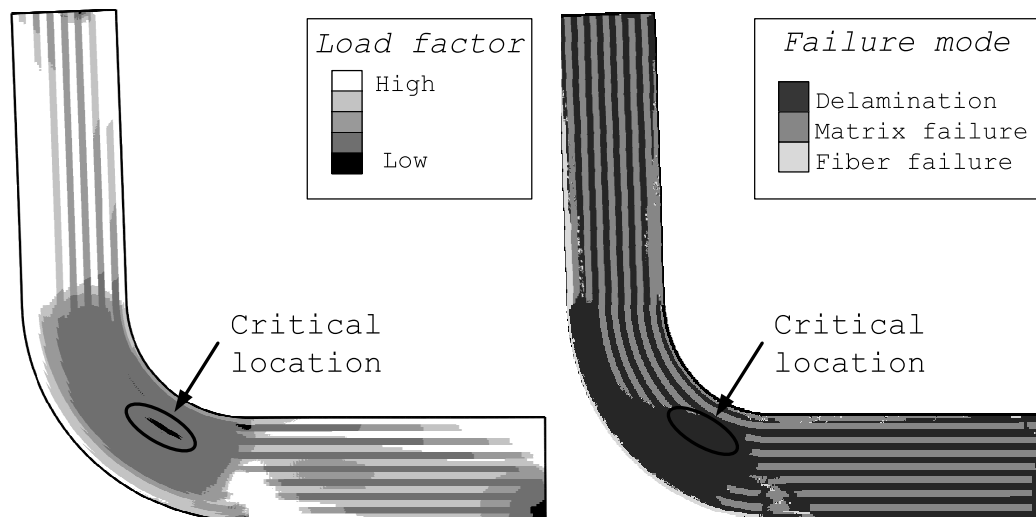

Figure 3.3: Puck FPF predictions of the curved, laminated structure loaded by a unit
displacement; load factor (left), failure mode (right).

nation, as well as the delamination load, are known. Based on these results the non–linear structural response caused by the delamination process is predicted by a non–linear FEM analysis, Fig. 3.4 (bottom, solid line). The perfect structure is loaded and in point 1 the FPF load is reached for the first time in a small region. In point 2, the delamination load predicted above is reached and the critical initial delamination is introduced into the model, while keeping the applied displacement load constant. This leads to a change of the structural stiffness and to a reduction of the reaction force, point 3. Beyond point 3, still
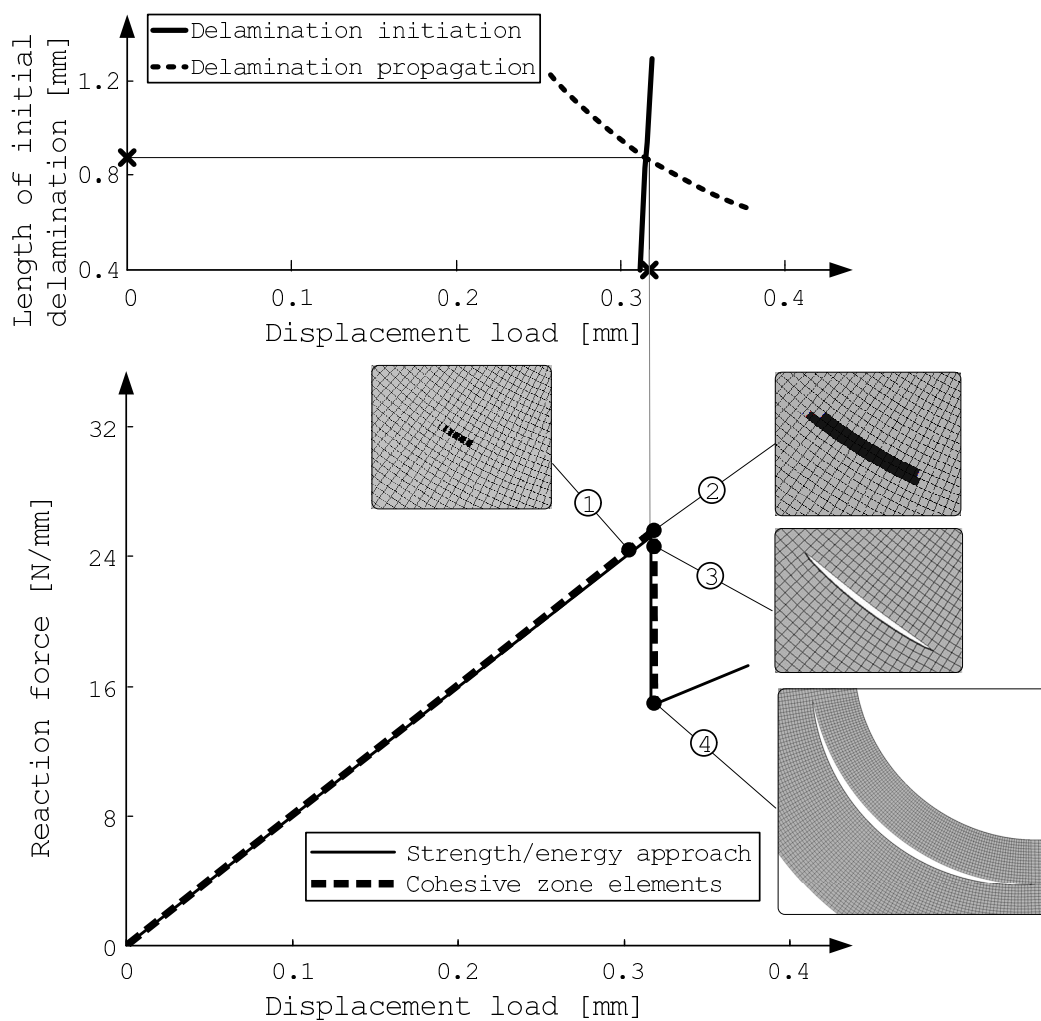

Figure 3.4: Predicted emergence and growth of delaminations in the curved, laminated structure loaded in displacement controlled manner; delamination initiation curve and delamination propagation curve (top), structural responses predicted by the strength/energy approach and by CZE (bottom).

maintaining the same displacement load, unstable delamination growth takes place which leads to a considerable increase in the size of the delamination. In point 4, delamination growth changes from unstable to stable, hence, the prescribed displacement has to be increased to cause further delamination growth. Between points 3 and 4 unstable growth accompanied by dynamic effects takes place. These effects, however, are not considered in the present analysis. Unstable delamination growth is discussed in detail in Chapter 4. Finally, the sensitivity of the predicted delamination load with respect to changes of the interface properties is discussed, following the argumentation presented in Section 3.1.3. An increase of the interface strength shifts the delamination initiation curve in Fig. 3.4 (top) to the right. An increase of the critical energy release rate shifts the delamination propagation curve in the same direction. The slopes of these curves at their intersection show that the predicted delamination load is much more sensitive to a change in the interface strength than to a change in the critical energy release rate.

The assumption that the critical initial delamination provides conservative estimates of the load carrying capacity is discussed in the following for displacement controlled loading conditions. The same non–linear FEM analysis procedure as discussed in Fig. 3.4 is followed for this purpose, but different sizes of initial delaminations are considered now. The non–linear structural response caused by the delamination process is predicted for various sizes of initial delaminations, see Fig. 3.5 (left). Comparison of the results will show that the predicted critical size of the initial delamination leads indeed to conservative estimates of the load carring capacity. The structure is loaded above the FPF load and an overloaded region is predicted by the Puck FPF criterion (dots). An initial delamination is assumed and introduced, while keeping the applied displacement load constant (stars). Growth of the initial delaminations is simulated using the VCCT. For small initial delaminations a load increase is required in order to start delamination growth (diamonds); large initial delaminations grow as soon as they are introduced.

Taking all the predicted responses together, an envelope can be formed. Displacement loads within this envelope do not cause delamination. To emphasize this, two sizes of initial

delaminations, one that is smaller and one that is larger than the critical one are considered in detail, see Fig. 3.5 (left). The small initial delamination is initiated at a load level below the delamination load, but propagation is retarded and only starts at a load level above the delamination load. Thus, the delamination load and the load carrying capacity would be higher than the one predicted for the critical initial delamination. The large initial delamination initiates at a load level above the delamination load and propagates as soon as it is introduced. Again, the delamination load would be higher than the one predicted in the case of the critical initial delamination. Thus, the critical initial delamination provides conservative estimates of the delamination load and the load carrying capacity of the structure.
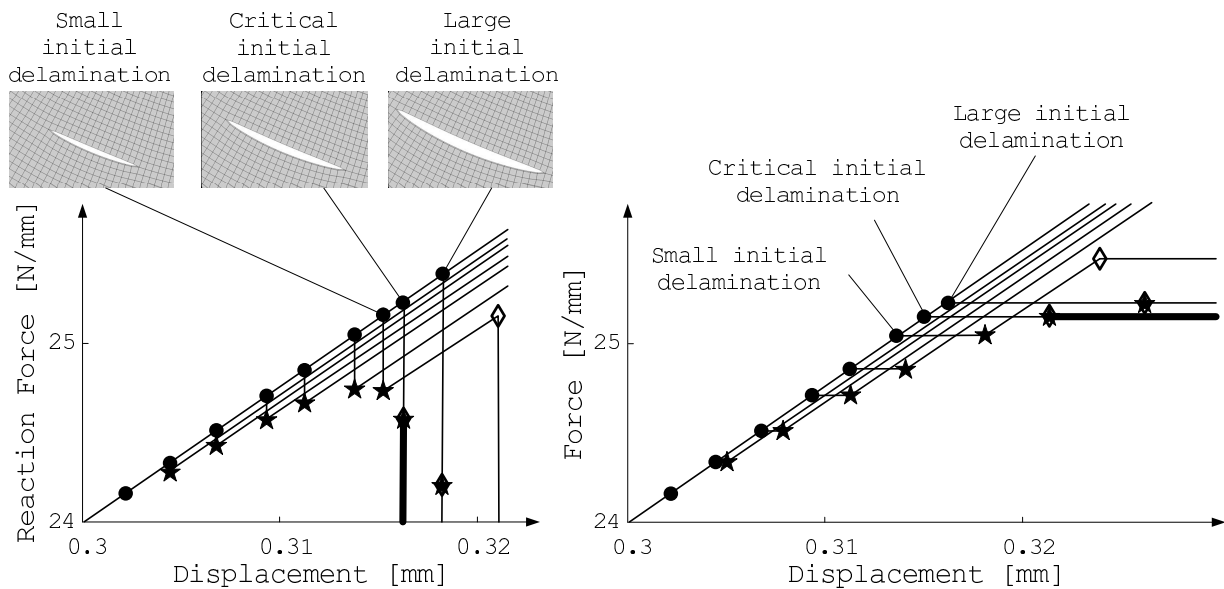

Figure 3.5: Predicted structural response of the curved, laminated structure for several sizes of initial delaminations; the critical initial delamination provides conservative estimates of the load carrying capacity; displacement controlled loading (left), force controlled loading (right).

Verification of the Results

For verification of the structural response predicted by the strength/energy approach, an
alternative modeling technique is employed within the FEM framework. CZE are placed
in each interface of the laminated structure, the non–linear constitutive behavior of these
elements is discussed in Section 3.2. The thickness of the interface elements is $1\,\mu$m, the to-
tal thickness of the structure remains unchanged. The piecewise linear traction–separation
law of the CZE, shown for mode I loading in Fig. 2.7, is described according to the material
data of the UD–layer presented in Table 3.1. The initial Young's modulus of the CZE is
assumed to be equal to the Young's modulus of the UD–layer in out–of–ply direction. Their
shear modulus is equal to the out–of–ply shear modulus G_{qn}. The critical normal interface
tractions of the CZE is equal to the tensile normal strength of the plies in direction normal
to the fibers, R_{qq}, times the weakening factor. The critical shear interface tractions is equal
to the shear strength of the plies, R_{lq}, times the weakening factor, f_{weak}.
A non–linear FEM analysis is conducted and the resulting structural response is shown
in Fig. 3.4 (bottom, dashed line). Comparing the results obtained from the CZE to the
results predicted by the strength/energy approach shows reasonably good agreement con-
cerning the size as well as the location of the initial delamination, the delamination load,
the stability delamination growth process, and the load carrying capacity of the structure.
It is noted that the application of CZE requires a fine spatial discretization at the delam-
ination tip in order to represent the cohesive zone adequately. Furthermore, small load
increments are required to capture the damage process in the CZE. For the present exam-
ple the usage of CZE requires about ten times the computational time compared to the
proposed strength/energy approach.

Force Controlled Loading

Loading of the curved laminate, Fig. 3.2, by a concentrated force is considered in the following. In Fig. 3.6 (left), the delamination initiation and delamination propagation curves are shown for this load case in a force–delamination length diagram. Note that these curves can be obtained from the results for displacement controlled loading by considering the reaction force at the load introduction point in place of the displacement. The slope of the delamination propagation curve shows that growth is unstable for all sizes of delaminations considered. The intersection of the curves defines the length of the critical initial delamination (0.825 mm) and the delamination load (25.1 N/mm) which is equal to the load carrying capacity of the structure. The size of the critical initial delamination is slightly smaller in force controlled loading than in displacement controlled loading. This can be explained by the fact that the structural stiffness decreases with increasing delamination size and thus the delamination propagation curve changes slightly. In Fig. 3.6 (right), the non–linear structural response is shown. Up to the delamination load, the structural re-
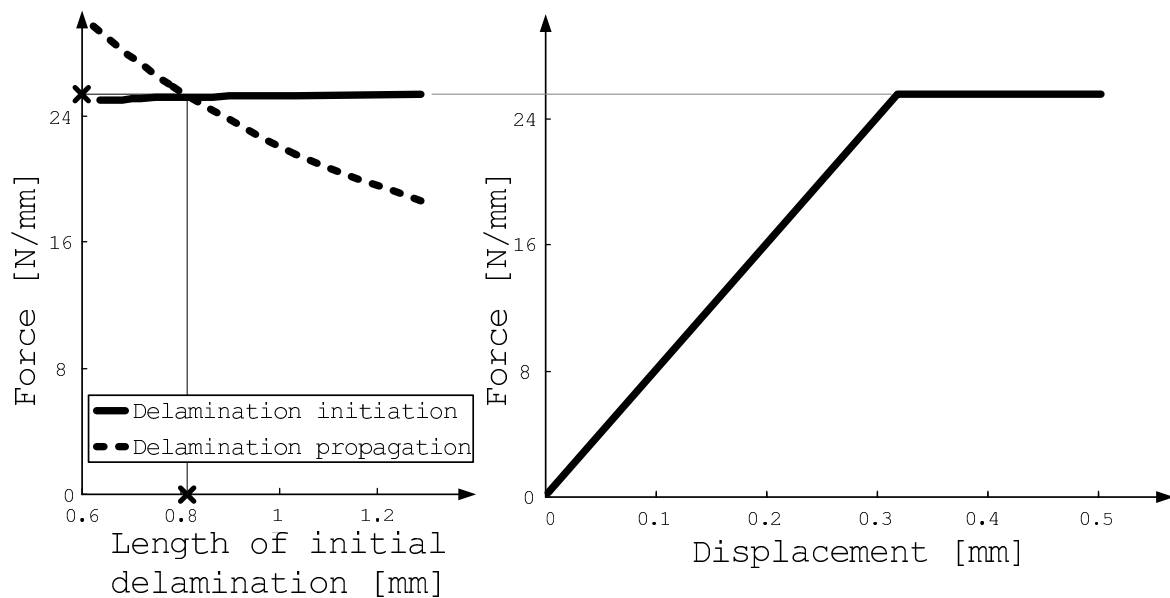

Figure 3.6: Predicted emergence and growth of delaminations in the curved, laminated structure loaded in force controlled manner; delamination initiation curve and delamination propagation curve (left), structural response (right).

sponse is linear. Beyond this load unstable delamination growth takes place.

The fact that the intersection of the delamination initiation and the delamination propagation curve defines a critical initial delamination is cross checked in Fig. 3.5 (right) for force controlled loading. The non–linear structural response is predicted for a set of initial delaminations with different sizes. The responses form an envelope and forces below this envelope do not cause delamination. So the critical initial delamination again provides conservative estimates of the load carrying capacity of the structure.

3.3.2   Double–Lap–Shear Test Specimen

As second example, a Double–Lap–Shear (DLS) test specimen is analyzed. The DLS test was introduced in [20] for the experimental determination of the interlaminar shear strength of laminated composites. A discussion of the DLS test including a comparison of numerical and experimental results is given in [51].

The structure analyzed here is made of 20 plies of a unidirectional carbon fiber reinforced epoxy resin, all plies are oriented in the longitudinal direction of the specimen. Material and interface properties are presented in Table 3.1. Details concerning the geometry of the DLS specimen are shown in Fig. 3.7, the corners of the notch are modeled as perfectly sharp. On the right hand side the displacements in x–direction are coupled and a load in this direction is applied. Due to the symmetry with respect to geometry, loading, and material, only the upper half of the structure is modeled. The structure has a considerable width, so that plane strain conditions are considered. It is modeled using plane strain continuum elements with linear shape functions. Overall, each ply is represented by four elements through the ply thickness, except for the region near the corner of the notch of the specimen where 64 elements per ply thickness are used. All element aspect ratios are close to unity.

Displacement Controlled Loading

A linear FEM analysis of the specimen loaded by a unit displacement load is conducted. Within this analysis the stresses are computed and evaluated by means of the Puck FPF criterion. The sharp corners at the notch lead to the theoretical prediction of stress singularities and it should be noted that the stress fields close to such corners cannot be represented adequately by conventional FEM. However, the results for the elements close to the notch are not relevant in the present approach. The predicted distribution of the load factor and the failure mode are shown in Fig. 3.8 indicating that emergence of delaminations at the corner is the expected failure mode. The delamination initiation curve is shown in Fig. 3.9 (top, solid line). Even for small loads an initial delamination is predicted due to the stress singularity. If the latter were fully resolved the delamination initiation curve would pass through the origin. The delamination propagation curve, Fig. 3.9 (top, dashed line), shows a non–monotonous behavior; growth is stable for small delaminations and unstable for larger ones. This behavior is attributed to the fact that for small initial delaminations the stress field caused by the corner is dominant, whereas for larger initial delaminations the stress field caused by the delamination dominates. The size of the critical initial delamination is $0.3\,\mathrm{mm}$ and the applied displacement load giving rise to delamination is $0.0205\,\mathrm{mm}$. Growth of the critical initial delamination is predicted to be
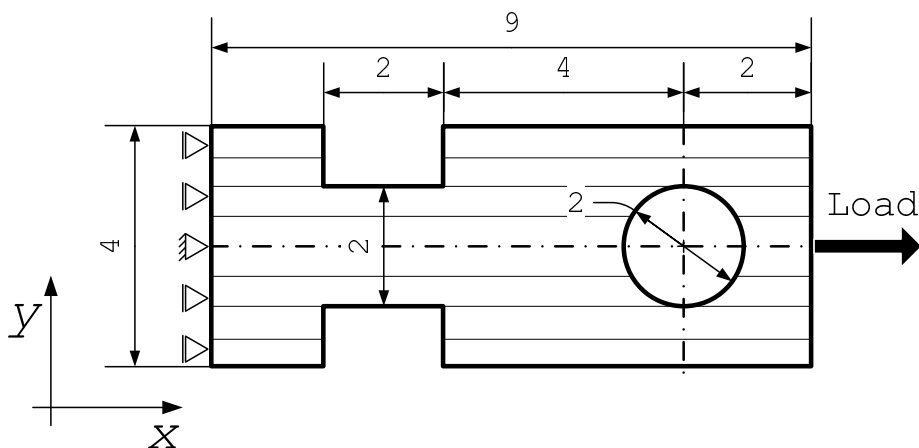

Figure 3.7: Geometry and boundary conditions of a Double–Lap–Shear test specimen.

stable at first and changes to unstable growth when the delamination reaches a length of
0.45 mm. The corresponding displacement load which is equal to the load carrying capac-
ity is 0.021 mm. It should be noted that the difference between the delamination load and
the load carrying capacity is very small and would not be distinguishable in experimental
tests.

The structural response of the DLS test specimen caused by the delamination process is
shown in Fig. 3.9 (bottom). The specimen is loaded in displacement controlled manner and
in point 1 FPF is predicted for the first material point. Due to the stress singularity at
the corner the predicted FPF load is mesh dependent, which is not relevant for the present
approach. In point 2, the delamination load is reached and the critical initial delamination
is introduced into the FEM model. Keeping the prescribed delamination load constant, the
introduction of the initial delamination leads to a decrease of the structural stiffness and
causes a decrease of the reaction force, point 3. At this point, the VCCT tool is activated
and the displacement can be increased further because stable delamination growth takes
place. As the load carrying capacity is reached, point 4, the growth behavior changes to
unstable, and the delamination size increases considerably, point 5. At point 5 final failure
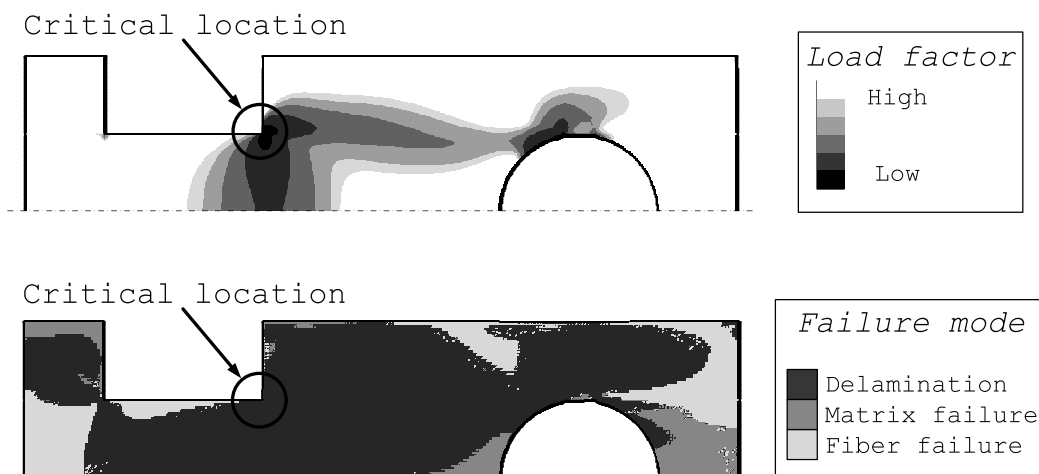takes place and the structure breaks apart.

Figure 3.8: Puck FPF predictions of the DLS test specimen loaded in displacement con-
trolled manner; load factor (top), failure mode (bottom).

An increase in one of the interface properties (i.e. strength or critical energy release rate) shifts the delamination initiation or the delamination propagation curve in Fig. 3.9 (top) to the right. The slopes of these curves at their intersection show that the predicted delamination load is more sensitive to a change in the critical energy release rate than to a change in the interface strength. The load carrying capacity of the structure is reached during delamination growth and depends solely on the critical energy release rate. Although the DLS test was designed to determine the interface strength of laminated composites, the load carrying capacity of the DLS test specimen considered here is mainly determined by the critical energy release rate of the interface.

Force Controlled Loading

In Fig. 3.10 (left), the delamination initiation and the delamination propagation curves for force controlled loading are shown. The size of the critical initial delamination is $0.28\,\mathrm{mm}$ and is smaller than the critical initial delamination in displacement controlled loading. The delamination load is $215\,\mathrm{N/mm}$. Delamination growth is predicted to be unstable for the critical initial delamination Therefore, the load carrying capacity of the structure is equal to the delamination load.

The non–linear structural response of the DLS test specimen for force controlled loading is shown in Fig. 3.10 (right). A linear response is found before the delamination load is reached, then the initial delamination is introduced and unstable growth takes place.

Verification of the Results

For verification of the predictions a non–linear FEM analysis employing CZE is carried out. CZE are placed at interface that starts at the corner. The thickness of the CZE is $1\,\mu\mathrm{m}$, the total thickness of the structure remains unchanged. For definition of the non–linear constitutive behavior of the CZE the material data presented in Table 3.1 is used,

see Section 3.3.1 for details. The result of the analysis show that the mode mix within each CZE changes considerably during damage evolution. However, the CZE available in *ABAQUS* are based on the assumption that the mode mix does not change in the considered element during damage evolution, i.e. the ratio between the normal and shear separation is assumed to be constant as long as the considered element belongs to the process zone (see discussion in Section 2.2.1). As a consequence delamination in the DLS test specimen cannot be simulated satisfactorily with the CZE available in *ABAQUS*.
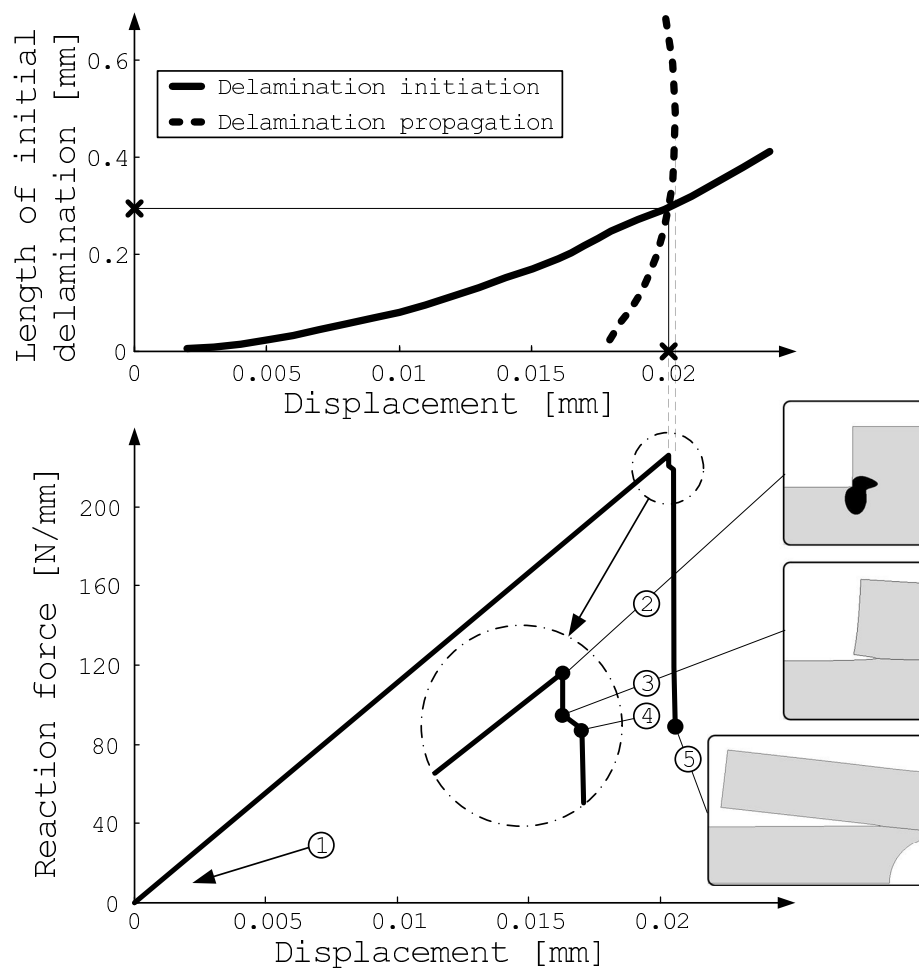

Figure 3.9: Predicted delamination growth in a DLS test specimen loaded in displacement controlled manner; delamination initiation curve and delamination propagation curve (top), structural response (bottom).

3.4   Summary

A strength/energy approach for the prediction of emergence of delaminations in laminated composite components is proposed. The approach can handle delaminations emerging inside a structure as well as delaminations emerging from free edges where stress singularities are present. The Puck FPF criterion is utilized to evaluate delamination initiation and delamination propagation is evaluated using the VCCT. The combination of an initiation criterion and a propagation criterion provides conservative estimates of the size and the location of the critical initial delamination, the delamination load, and the load carrying capacity of the structure. Furthermore, the stability of the growth process and the sensitivity of the load carrying capacity with respect to changes of interface properties can be assessed. Once the critical initial delamination and the delamination load are found with the proposed strength/energy approach the non–linear structural response caused by the delamination process is predicted using non–linear FEM.

Two examples are investigated, emergence of delaminations inside a curved laminate and
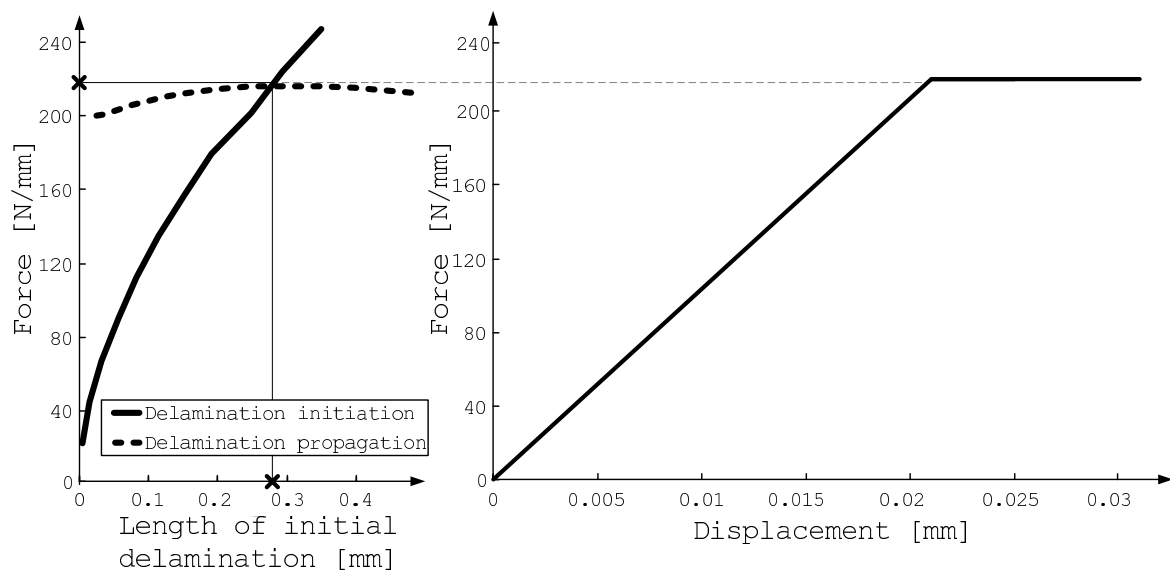
Figure 3.10: Predicted delamination growth in a DLS test specimen loaded in force controlled manner; delamination initiation curve and delamination propagation curve (left), structural response (right).

emergence of delaminations at a sharp corner in a DLS test specimen. For verification of the predicted delamination and the predicted non–linear structural response, CZE are utilized. For the curved laminate it is found that both methods predict the same structural response but the proposed strength/energy approach is numerically much more efficient and robust than the use of CZE. For the DLS test specimen delamination cannot be simulated satisfactorily with the CZE available in *ABAQUS* due to some implementation details.

Chapter 4

Growth of Delaminations with Straight Fronts

Within the framework of FEM several methods for the prediction of delamination growth in FRP laminates have been developed. Frequently used are VCCT and CZE. However, every particular size and position of delaminations of interest have to be investigated separately in a non–linear FEM analysis. This is numerically expensive and only specific information about the particular size and position of the delamination considered in the FEM analysis is obtained. Furthermore, numerical problems arise if unstable delamination growth takes place.

To overcome these shortcomings a computationally efficient semi–analytical approach for the prediction of delamination growth is proposed. It provides a complete picture of a delamination problem in a given structure and offers systematic understanding of the influence of size and position of a delamination on the growth, on the stability of the growth process, and on the structural response. Within the proposed approach the energy release rate is computed from the decrease of the potential energy of a structure effectuated by an increase of the delaminated area. The potential energy is derived from the applied loads

and the structural stiffness. The latter is computed in the present study by means of the FEM but any other suitable numerical method can be used for this purpose. Structures loaded by arbitrary combinations of concentrated or distributed forces, forces of inertia, displacements, temperature, and moisture loads can be handled. Load cases where all loads vary with the same frequency can be treated as well as load cases where some or all load components are constant.

In order to show the application and the capabilities of the proposed approach delamination in a curved laminate and delamination in a T–joint are investigated in detail.

4.1 Semi–Analytical Approach

In the following, a semi–analytical approach for the prediction of delamination growth in structures loaded by quasi–static or cyclic loads is presented. First, equations are derived that allow to compute the energy release rate for general load cases. Second, a Griffith–type growth criterion is employed to predict the load required to cause quasi–static equilibrium delamination growth as well as the stability of the growth process and the structural response. Third, a Paris–type growth law is presented to predict delamination growth in structures loaded by cyclic loads.

4.1.1 Energy Release Rate

The proposed semi–analytical approach can handle arbitrary combinations of mechanical, temperature, and moisture loads. In the following three load cases are discussed in detail, i.e. loading by a homogeneous temperature change and concentrated forces, loading by a homogeneous temperature change and prescribed displacements, as well as loading by a homogeneous temperature change, a concentrated force, and a prescribed displacement.

Loading by Concentrated Forces

In Fig. 4.1 (left) a generic example of a structure loaded by a homogeneous temperature change, two orthogonal, concentrated forces and a moment is shown. The total displacement of the load introduction point is the sum of the elastic displacements, $\mathbf{u}_{\mathrm{el}}$, and thermal displacements, $\mathbf{u}_{\mathrm{th}}$, and reads,

$$
\begin{bmatrix} u_1 \\ u_2 \\ u_3 \end{bmatrix} = \underbrace{\begin{bmatrix} C_{11} & C_{12} & C_{13} \\ C_{12} & C_{22} & C_{23} \\ C_{13} & C_{23} & C_{33} \end{bmatrix} \begin{bmatrix} F_1 \\ F_2 \\ F_3 \end{bmatrix}}_{\mathbf{u}_{\mathrm{el}}} + \underbrace{\begin{bmatrix} \alpha_1 \\ \alpha_2 \\ \alpha_3 \end{bmatrix} \Delta T}_{\mathbf{u}_{\mathrm{th}}} \quad , \tag{4.1}
$$

where $\mathbf{u} = [u_1, \ u_2, \ u_3]^{\mathrm{T}}$ is the displacement vector of the load introduction point. $\mathbf{F} = [F_1, \ F_2, \ F_3]^{\mathrm{T}}$ is the force vector acting at that point and $\mathbf{C}$ is the structural compliance. $\boldsymbol{\alpha} = [\alpha_1, \ \alpha_2, \ \alpha_3]^{\mathrm{T}}$ is the vector of coefficients of thermal deformation of the load introduction point caused by a homogeneous temperature change of $1\,\mathrm{K}$. ΔT is the homogeneous temperature change with respect to the stress free state. The indices 1 and 2 refer to the components of the vectors in 1– and 2– direction, 3 refers to the rotational
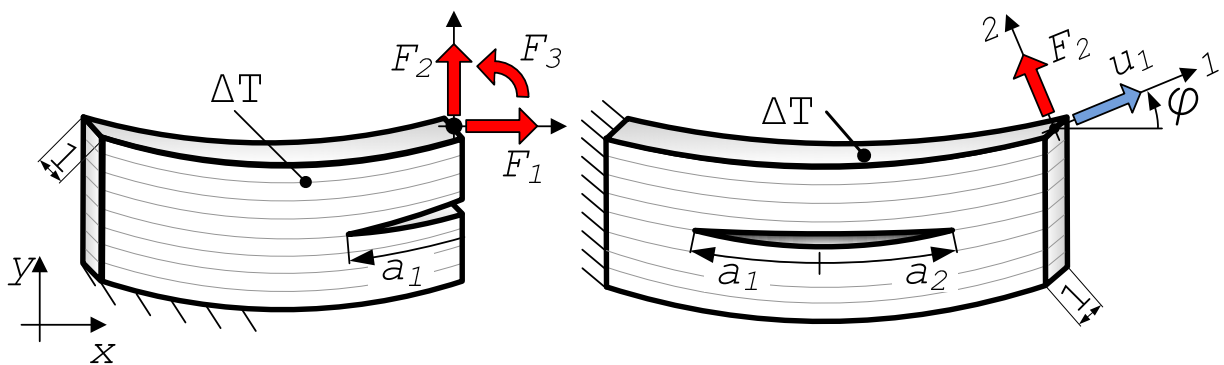

Figure 4.1: Laminated composites with through–the–width delaminations loaded by a homogeneous temperature change, prescribed displacements, and concentrated forces; delaminations described by one (left) or two (right) delamination coordinates; definition of the rotation angle φ (right).

component, respectively.

In the linear elastic range the strain energy of a structure is equal to the work performed by the mechanical loads acting on the structure plus the strain energy caused by a homogeneous temperature change. The latter is caused by stacking together differently oriented plies with orthotropic thermal expansion behavior. In the present load case the work performed by the mechanical loads is equal to one half of the force acting on the load introduction point times the elastic displacement of the load introduction point. The latter is given in Eq.(4.1) and the strain energy reads,

$$\Pi_{\text{int}} = \frac{1}{2} \left(\mathbf{F}^{\text{T}} \, \mathbf{C} \, \mathbf{F} + \gamma \, \Delta T^2 \right) \quad , \tag{4.2}$$

where γ is a measure for the strain energy of the structure caused by a homogeneous temperature change of $1\,\text{K}$ with respect to the stress free state.

For computing energy release rates by means of Eq. (2.12), the change of the potential of external forces caused by an increase of delaminated area is required. The change of the potential of external forces is defined as the negative work performed by the external forces. For the present load case it is computed from the forces applied at the loading point and the change of the total displacement of the loading point and reads,

$$\partial \Pi_{\text{ext}} = -\partial W_{\text{ext}} = - \, \mathbf{F}^{\text{T}} \, \partial \mathbf{u} \quad . \tag{4.3}$$

Integration of Eq. (4.3) for constant forces and consideration of the definition of the total displacement of the loading point given in Eq. (4.1) yields an expression for the potential of external forces,

$$\Pi_{\text{ext}} = -\mathbf{F}^{\text{T}} \left(\mathbf{C} \, \mathbf{F} + \boldsymbol{\alpha} \, \Delta T \right) + c \quad . \tag{4.4}$$

The constant, c, is not defined. However, only the change of the potential of external forces is relevant for computation of energy release rates. By substitution of Eqs. (4.2) and (4.4)

into Eq. (2.12) an expression for the energy release rate is obtained as,

$$\mathcal{G} = \frac{1}{2}\left(\mathbf{F}^{\mathrm{T}}\frac{\partial \mathbf{C}}{\partial A}\mathbf{F}\right) + \mathbf{F}^{\mathrm{T}}\frac{\partial \boldsymbol{\alpha}}{\partial A}\Delta T - \frac{1}{2}\left(\frac{\partial \gamma}{\partial A}\Delta T^2\right) \quad . \tag{4.5}$$

The delaminated area, A, can be described by some delamination front coordinates a_i. For problems with through–the–width delaminations with straight delamination fronts (i.e. problems that can be investigated by two–dimensional FEM models) the delaminated area is entirely described by a limited number of delamination front coordinates. In Fig. 4.1 two generic examples of structures with through–the–width delaminations are shown where one (left) and two (right) delamination coordinates are required to describe the delamination entirely. In structures with constant width the increase in delaminated area can be expressed by the increase in the delamination coordinates. In the present study structures of unit width are considered and the energy released is computed at each delamination front as,

$$\mathcal{G}_i = \frac{1}{2}\left(\mathbf{F}^{\mathrm{T}}\frac{\partial \mathbf{C}}{\partial a_i}\mathbf{F}\right) + \mathbf{F}^{\mathrm{T}}\frac{\partial \boldsymbol{\alpha}}{\partial a_i}\Delta T - \frac{1}{2}\left(\frac{\partial \gamma}{\partial a_i}\Delta T^2\right) \quad . \tag{4.6}$$

The proposed semi–analytical approach can be used for three–dimensional problems with curved delamination fronts, but some approximations concerning the shape of the delamination are required, to limit the number of delamination coordinates. Note that no information about the local distribution of the energy release rate along the delamination front is obtained in such cases.

The above equations are based on the assumption that the compliance is load independent. In the case of closed delaminations this assumption is violated as friction may occur and contact states may change. However, many delamination problems of practical relevance have open delaminations and can be treated with the proposed semi–analytical approach.

Loading by Prescribed Displacements

In a structure loaded by a homogeneous temperature change and a total prescribed displacement the reaction force at the load introduction point is computed from the structural stiffness and the elastic displacement of the load introduction point. The latter is computed by means of the first term of Eq. (4.1) and the reaction force reads,

$$\mathbf{F} = \mathbf{K}\left(\mathbf{u} - \boldsymbol{\alpha}\,\Delta T\right) \quad, \tag{4.7}$$

where the structural stiffness is defined as, $\mathbf{K} = \mathbf{C}^{-1}$. The strain energy of the structure is computed from the reaction force at the load introduction point, the elastic displacement of the load introduction point, and the strain energy caused by a homogeneous temperature change and reads,

$$\Pi_{\text{int}} = \frac{1}{2}\left(\mathbf{F}^{\text{T}}\mathbf{u}_{\text{el}} + \gamma\,\Delta T^2\right) \quad. \tag{4.8}$$

Substitution of Eq. (4.7) in Eq. (4.8) yields an expression for the strain energy,

$$\Pi_{\text{int}} = \frac{1}{2}\left(\mathbf{u}^{\text{T}}\,\mathbf{K}\,\mathbf{u} + \boldsymbol{\alpha}^{\text{T}}\,\mathbf{K}\,\boldsymbol{\alpha}\,\Delta T^2 - 2\mathbf{u}^{\text{T}}\,\mathbf{K}\,\boldsymbol{\alpha}\,\Delta T + \gamma\,\Delta T^2\right) \quad. \tag{4.9}$$

The potential of external forces is zero in case of displacement controlled loading [21]. By substitution of Eq. (4.9) in Eq. (2.12) an equation for the computation of the energy released at delamination growth along delamination coordinate a_i is obtained,

$$\mathcal{G}_i = -\frac{1}{2}\left(\left(\mathbf{u} - \boldsymbol{\alpha}\Delta T\right)^{\text{T}}\left(\frac{\partial \mathbf{K}}{\partial a_i}\left(\mathbf{u} - \boldsymbol{\alpha}\Delta T\right) - 2\mathbf{K}\frac{\partial \boldsymbol{\alpha}}{\partial a_i}\Delta T\right) + \frac{\partial \gamma}{\partial a_i}\Delta T^2\right) \quad. \tag{4.10}$$

Loading by Forces and Displacements

If the structure is loaded by concentrated forces as well as prescribed displacements some modifications of the above equations are required. This will be shown for an example with a homogeneous temperature change, a prescribed displacement in 1–direction, a force in

2–direction, and a zero moment in 3–direction, see Fig. 4.1 (right). The strain energy of the structure is computed from the forces acting on the load introduction point, the elastic displacement of the load introduction point, and the strain energy caused by a temperature change and reads,

$$\Pi_{\text{int}} = \frac{1}{2}\left(u_{\text{el},1}\,F_1 + u_{\text{el},2}\,F_2 + \gamma\Delta T^2\right) \quad . \tag{4.11}$$

The force in 1–direction and the elastic displacement in 2–direction are derived in Eq.(4.1) as function of u_1 and F_2 and the strain energy is computed as,

$$\Pi_{\text{int}} = \frac{1}{2}\left\{(u_1 - \alpha_1\,\Delta T)\frac{u_1 - C_{12}\,F_2 - \alpha_1\,\Delta T}{C_{11}} + \right.$$
$$\left. + \left(\frac{C_{12}\,u_1 - C_{12}^2\,F_2}{C_{11}} + C_{22}\,F_2\right)F_2 + \gamma\,\Delta T^2\right\} \quad . \tag{4.12}$$

For the present load case only the force in 2–direction contributes to the potential of external forces and the work performed by this force during delamination growth is given as,

$$\partial\Pi_{\text{ext}} = -\,F_2\,\partial u_2 \quad . \tag{4.13}$$

The total displacement of the load introduction point in 2–direction is computed by means of Eq. (4.1) and the potential of external forces reads,

$$\Pi_{\text{ext}} = -F_2\left(\frac{C_{12}\,u_1 - C_{12}^2\,F_2 - C_{12}\,\alpha_1\,\Delta T}{C_{11}} + C_{22}\,F_2 + \alpha_2\,\Delta T\right) \quad . \tag{4.14}$$

The potential energy of the structure is computed by summation of Eqs.(4.12) and (4.14). To simplify notation this sum is written as,

$$\Pi_{\text{int}} + \Pi_{\text{ext}} = \frac{1}{2}\mathbf{P}^{\text{T}}\mathbf{C}_{\text{gen}}\mathbf{P} \quad , \tag{4.15}$$

where $\mathbf{P} = [u_1,\ F_2,\ \Delta T]^{\mathrm{T}}$ is a generalized load vector and $\mathbf{C}_{\mathrm{gen}}$ is a generalized compliance, defined for the present load case as,

$$\mathbf{C}_{\mathrm{gen}} = \begin{bmatrix} \frac{1}{C_{11}} & -\frac{C_{12}}{C_{11}} & -\frac{\alpha_1}{C_{11}} \\[2ex] -\frac{C_{12}}{C_{11}} & \frac{C_{12}^2}{C_{11}} - C_{22} & \frac{3\,C_{12}\,\alpha_1}{2\,C_{11}} - \alpha_2 \\[2ex] -\frac{\alpha_1}{C_{11}} & \frac{3\,C_{12}\,\alpha_1}{2\,C_{11}} - \alpha_2 & \frac{\alpha_1^2}{C_{11}} + \gamma \end{bmatrix} \quad . \tag{4.16}$$

Finally, the energy released at delamination growth along delamination coordinate a_i is computed as,

$$\mathcal{G}_i = -\frac{1}{2}\mathbf{P}^{\mathrm{T}}\,\frac{\partial \mathbf{C}_{\mathrm{gen}}}{\partial a_i}\,\mathbf{P} \quad . \tag{4.17}$$

Equivalent equations can be derived for all admissible combinations of displacements, forces, and temperature loads.

Loading in Arbitrary Directions

Equation (4.17) allows to compute energy release rates for structures loaded by vertical and horizontal forces and displacements as shown in Fig. 4.1 (left). In order to handle arbitrary loading directions an appropriate rotation transformation, $\mathbf{T}$, is introduced. The angle, φ, by which the local *12* load coordinate system is rotated with respect to the global *xy* coordinate system is defined in Fig. 4.1 (right). The displacement vector, the force vector, the vector of coefficients of thermal deformation, and the compliance written in terms of the rotated coordinate system read

$$\tilde{\mathbf{u}} = \mathbf{T}\mathbf{u} \quad \tilde{\mathbf{F}} = \mathbf{T}\mathbf{F} \quad \tilde{\boldsymbol{\alpha}} = \mathbf{T}\boldsymbol{\alpha} \quad \tilde{\mathbf{C}} = \mathbf{T}\mathbf{C}\mathbf{T}^{-1} \quad . \tag{4.18}$$

Substitution of $\boldsymbol{\alpha}$ by $\tilde{\boldsymbol{\alpha}}$ and $\boldsymbol{C}$ by $\tilde{\boldsymbol{C}}$ in Eq. (4.16) yields an expression for the computation of the generalized compliance, $\tilde{\boldsymbol{C}}_{\mathrm{gen}}$, in terms of the rotated coordinate system. The generalized load vector in the rotated coordinate system reads $\tilde{\mathbf{P}} = [\tilde{u}_1,\ \tilde{F}_2,\ \Delta T]^{\mathrm{T}}$ and the

energy release rate at each delamination front can be computed by means of Eq. (4.17).

Mode Mix

From Eq. (4.17) the total energy release rates at each delamination front is computed. For conventional fiber reinforced polymers, however, the critical energy release rate depends on the actual mode mix and, thus, for planar problems the individual mode I and mode II energy release rates, $\mathcal{G}_\mathrm{I}$ and $\mathcal{G}_\mathrm{II}$, respectively, are relevant. Therefore, a mode mix variable is introduced, which allows to split the total energy release rate at each delamination front into its mode I and mode II contributions as,

$$
\begin{aligned}
\mathcal{G}_{\mathrm{I},\,i} &= (1 - m_i)\ \mathcal{G}_i \quad , \\
\mathcal{G}_{\mathrm{II},\,i} &= m_i\, \mathcal{G}_i \quad .
\end{aligned}
\tag{4.19}
$$

The mode mix, m_i, depends on the geometry considered and is a quadratic function with respect to the applied load. Previous analyses [79] have shown that for conventional fiber reinforced polymers the temperature load hardly affects the mode mix. Hence, the influence of the temperature load is not considered here and the mode mix can be computed at each delamination front as,

$$
m_i = \frac{\mathbf{F}^\mathrm{T}\, \mathbf{M}_i\, \mathbf{F}}{\mathcal{G}_i} \quad ,
\tag{4.20}
$$

where $\mathbf{M}_i$ is named mode contribution. It is a symmetric matrix and its evaluation is discussed in the next section. In case of displacement controlled loading or combinations of force and displacement loads, the force acting at the load introduction point has to be computed by means of Eq. (4.1) before Eq. (4.20) can be applied. An equivalent formulation for the mode mix together with a verification is given in [37].

Numerical Evaluation

So far, equations for the computation of energy release rates and their mode I and mode II contributions have been presented. In order to perform these computations the compliance, the coefficients of thermal deformation, the strain energy caused by a homogeneous temperature change, and the mode contribution at each delamination front need to be defined as functions of the delamination coordinates. In general cases analytical solutions for these functions cannot be given, so that a numerical procedure is required. In the present study the FEM package *ABAQUS* is employed for this purpose.

The space of delamination coordinates is discretized in a way that allows to describe all sizes and positions of delaminations of interest. An FEM model parameterized in the delamination coordinates is set up and a set of linearly independent load cases with temperature changes, ΔT, and concentrated forces, $\mathbf{F}$, is defined. For each delamination (i.e. for each combination of delamination coordinates) an FEM model is generated and the total displacement, $\mathbf{u}$, of the load introduction point and the strain energy, Π_{int}, are computed for all load cases within a linear analysis. From the results the stiffness, $\mathbf{C}$, and the coefficients of thermal deformation, $\boldsymbol{\alpha}$, are evaluated by means of Eq. (4.1), the strain energy caused by a temperature change, γ, is evaluated by means of Eq. (4.2). For the computation of the mode contributions, $\mathbf{M}_i$, the VCCT is utilized. The total energy release rate, its mode II component, and the mode mix are computed for each delamination front for a set of load cases and the mode contribution is derived according to Eq. (4.20).

An alternative way for the computation of the mode contributions, which does not require a special tool, is mode–wise delamination closing. Kinematic coupling conditions are defined for the translational degrees of freedom at the nodes behind the delamination tip, which allow to constrain the relative displacements between them. The strain energy of the structure is computed for four different sets of coupling conditions, shown in Fig. 4.2, and

the mode mix can be computed in an approximative manner as,

$$m_i = \frac{1}{2} \frac{(\Pi_{\mathrm{II}} - \Pi_{\mathrm{open}}) + (\Pi_{\mathrm{closed}} - \Pi_{\mathrm{I}})}{\Pi_{\mathrm{closed}} - \Pi_{\mathrm{open}}} \quad , \tag{4.21}$$

where Π_{open} is the strain energy of the structure for an open delamination front where no coupling conditions are applied. Π_{I} and Π_{II} are the strain energies obtained if the relative mode I or mode II displacements between the nodes behind the delamination tip are constrained, respectively. Π_{closed} is the strain energy obtained if both displacements are constrained. Constraining of the relative mode I displacements causes also a change of the relative mode II displacements and vice versa. Hence, mode wise delamination closing allows only to compute the mode mix in an approximative manner.

This procedure is utilized at each delamination front to compute the mode mix for several linearly independent load cases. From the results the mode contributions, $\mathbf{M}_i$, are computed by means of Eq. (4.20).

The generation of the FEM models, the FEM analyses, and the computation of the compliance, the coefficient of thermal deformation, the strain caused by the temperature load, as well as the mode contributions as functions of the delamination coordinates are conducted within a fully automated procedure. The results of the procedure allow for a pointwise de-
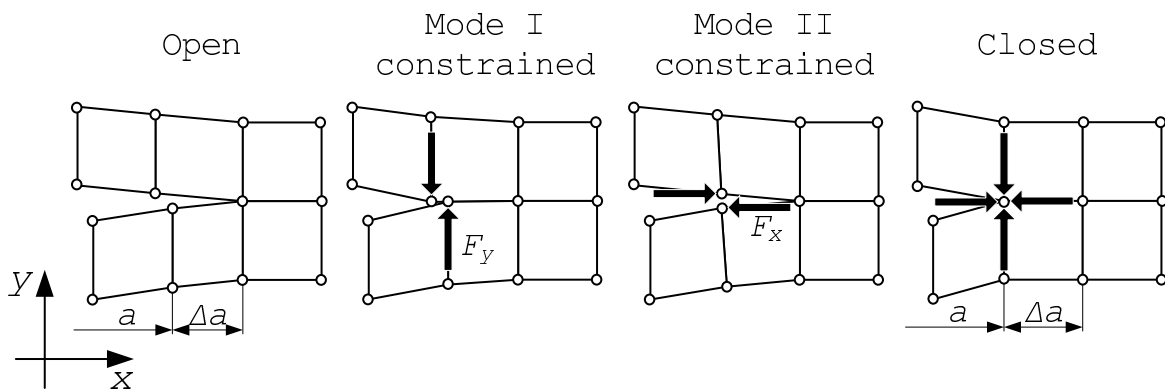

Figure 4.2: Mode–wise delamination closing for computation of the actual mode mix.

scription of the functions. Therefore, the difference quotients are computed instead of the derivatives (i.e. $\frac{\partial \mathbf{C}}{\partial a_i} \Rightarrow \frac{\Delta \mathbf{C}}{\Delta a_i}$). Due to this approximation incremental delamination growth is treated, the size of the increment is equal to the incrementation in the delamination coordinates a_i chosen for discretization of the parameter space.

The compliance is a monotonic and continuous function with respect to the delamination coordinates. Their discretization has to be chosen sufficiently fine to allow for a proper approximation of the compliance as well as its first and second derivatives. Visual inspection of the functions' graphs shows whether or not the approximation is satisfactory in the entire range of delamination coordinates. If not, a finer discretization has to be used at positions where the approximation is not sufficient.

The functions derived allow for computation of energy release rates only for discrete values of the delamination coordinates. For intermediate delamination coordinates the energy release rates are approximated by interpolation. This way energy release rates for delaminations described by any coordinate can be computed.

All the data generated by the automated procedure is stored in a database. Hence, energy release rates can be computed immediately by postprocessing of existing data for all delaminations in the considered space of delamination coordinates for all load cases discussed.

4.1.2 Quasi–Static Loading

According to Griffith a crack will grow if the energy released at delamination growth is equal to or greater than the energy required to create new delaminated area, called critical energy release rate. Using a quadratic criterion, Eq. (2.21), and the mode mix variable defined for planar problems in Eq. (4.19), the critical energy release rate, $\mathcal{G}_{\text{c},\, i}$, at delamination front a_i reads,

$$\left(\frac{1}{\mathcal{G}_{\text{c},\, i}}\right)^2 = \left(\frac{1 - m_i}{\mathcal{G}_{\text{Ic}}}\right)^2 + \left(\frac{m_i}{\mathcal{G}_{\text{IIc}}}\right)^2 \quad . \tag{4.22}$$

Equations for the prediction of equilibrium delamination growth and the growth stability for each delamination front are obtained by substituting of a by a_i and $\mathcal{G}_c$ by $\mathcal{G}_{c,\,i}$ in Eqs. (2.22) and (2.23). Note that Eq. (2.23) is valid only if equilibrium growth at a single delamination front takes place. The stability condition, for the case that the equilibrium growth condition, Eq. (2.22), is fullfilled for more than one delamination front, is discussed in [9]. These stability conditions can be summarized by the intuitive result that equilibrium delamination growth is stable if an increase in the applied load is required to increase the size of the delamination.

For structures loaded by concentrated forces, the force, $\mathbf{F}_{\mathrm{eq},\,i}$, required to cause equilibrium growth along delamination front a_i is derived by substitution of Eq. (4.6) into Eq. (2.22) and reads,

$$-\frac{1}{2}\left(\mathbf{F}_{\mathrm{eq},\,i}\right)^{\mathrm{T}}\frac{\partial \mathbf{C}}{\partial a_i}\,\mathbf{F}_{\mathrm{eq},\,i}-\left(\mathbf{F}_{\mathrm{eq},\,i}\right)^{\mathrm{T}}\frac{\partial \boldsymbol{\alpha}}{\partial a_i}\Delta T+\frac{1}{2}\frac{\partial \gamma}{\partial a_i}\Delta T^2+\mathcal{G}_{\mathrm{c},\,i}=0 \quad . \tag{4.23}$$

For loading by prescribed displacements, the displacement, $\mathbf{u}_{\mathrm{eq},\,i}$, required to cause equilibrium growth along delamination front a_i is derived by substitution of Eq. (4.10) into Eq. (2.22) and reads,

$$\frac{1}{2}\left((\mathbf{u}_{\mathrm{eq},\,i}-\boldsymbol{\alpha}\Delta T)^{\mathrm{T}}\left(\frac{\partial \mathbf{K}}{\partial a_i}(\mathbf{u}_{\mathrm{eq},\,i}-\boldsymbol{\alpha}\Delta T)-2\mathbf{K}\frac{\partial \boldsymbol{\alpha}}{\partial a_i}\Delta T\right)\right)+\frac{1}{2}\left(\frac{\partial \gamma}{\partial a_i}\Delta T^2\right)+\mathcal{G}_{\mathrm{c},\,i}=0 \quad . \tag{4.24}$$

For structures loaded by a combination of a displacement and a force, the generalized equilibrium load, $\mathbf{P}_{\mathrm{eq},\,i}$, is derived for each delamination front from Eqs. (4.17) and (2.22) as,

$$-\frac{1}{2}\left(\mathbf{P}_{\mathrm{eq},\,i}\right)^{\mathrm{T}}\frac{\partial\,\mathbf{C}^{\mathrm{gen}}}{\partial a_i}\,\mathbf{P}_{\mathrm{eq},\,i}+\mathcal{G}_{\mathrm{c},\,i}=0 \quad . \tag{4.25}$$

Delaminations will grow first at the highest loaded delamination front, leading to a change of the corresponding delamination coordinate. For the grown delamination, again, the load required to propagate it by one increment and the change in the corresponding delamination coordinates is predicted. Repeating these considerations allows a pointwise description of

the delamination growth process and the corresponding structural response.

4.1.3 Cyclic Loading

For the prediction of incremental delamination growth caused by cyclic loads Paris–type growth laws have been proposed [25, 61, 15]. Incremental delamination growth, Δa_{cyc}, is determined by the maximum and minimum energy release rate that occurs during each load cycle. In the follwing the growth law developed in [15] is considered where the growth per load cycle is defined as,

$$
\begin{aligned}
\Delta a_{\text{cyc}} &= g_{\text{I}} \, \frac{E_{\text{q}} \, \mathcal{G}_{\text{Ic}}}{R_{qq}^2} A_{\text{I}}^{g_{\text{I}}} A_{\text{II}}^{g_{\text{II}}} \left[U \left(\frac{\mathcal{G}_{\text{I, max}}}{\mathcal{G}_{\text{Ic}}} + \frac{\mathcal{G}_{\text{II, max}}}{\mathcal{G}_{\text{IIc}}} \right) \right]^{b_{\text{I}} \, g_{\text{I}} + b_{\text{II}} \, g_{\text{II}}} + \\
&\quad + g_{\text{II}} \, \frac{E_{\text{q}} \, \mathcal{G}_{\text{IIc}}}{R_{lq}^2} A_{\text{I}}^{g_{\text{I}}} A_{\text{II}}^{g_{\text{II}}} \left[U \left(\frac{\mathcal{G}_{\text{I, max}}}{\mathcal{G}_{\text{Ic}}} + \frac{\mathcal{G}_{\text{II, max}}}{\mathcal{G}_{\text{IIc}}} \right) \right]^{b_{\text{I}} \, g_{\text{I}} + b_{\text{II}} \, g_{\text{II}}} , \\
g_j &= \frac{\frac{\mathcal{G}_{j, \text{max}}}{\mathcal{G}_{j, \text{c}}}}{\frac{\mathcal{G}_{\text{I, max}}}{\mathcal{G}_{\text{Ic}}} + \frac{\mathcal{G}_{\text{II, max}}}{\mathcal{G}_{\text{IIc}}}} \quad \text{for} \quad j = \text{I}, \text{II} .
\end{aligned}
\tag{4.26}
$$

Here, E_{q} is the Young's modulus of the ply in transverse direction, R_{qq} is the ply transverse tensile strength, R_{lq} is the in–plane shear strength, $\mathcal{G}_{\text{min}}, \mathcal{G}_{\text{max}}$ are the minimum and maximum energy release rates, and $\mathcal{G}_{\text{I, min}}, \mathcal{G}_{\text{I, max}}, \mathcal{G}_{\text{II, min}}, \mathcal{G}_{\text{II, max}}$ are their mode I and mode II contributions. U is a function of $\frac{\mathcal{G}_{\text{min}}}{\mathcal{G}_{\text{max}}}$, $\frac{\mathcal{G}_{\text{I, max}}}{\mathcal{G}_{\text{Ic}}}$, and $\frac{\mathcal{G}_{\text{II, max}}}{\mathcal{G}_{\text{IIc}}}$ the form of which depends on whether or not there is shear reversal at the delamination front during each load cycle. In the absence of shear reversal one set of shear cracks is formed ahead of the delamination tip and all cracks are aligned in the same direction. For this case U is defined as,

$$
U = \left(1 - \frac{\mathcal{G}_{\text{min}}}{\mathcal{G}_{\text{max}}} \right) \left[1 + \frac{\mathcal{G}_{\text{min}}}{\mathcal{G}_{\text{max}}} \left(1 - \left(\frac{\mathcal{G}_{\text{I, max}}}{\mathcal{G}_{\text{Ic}}} + \frac{\mathcal{G}_{\text{II, max}}}{\mathcal{G}_{\text{IIc}}} \right) \right) \right]^{u_{\text{I}} \, g_{\text{I}} + u_{\text{II}} \, g_{\text{II}}} .
\tag{4.27}
$$

If there is shear reversal, i.e. the mode II shear stresses ahead the of the delamination tip change their sign during the load cycle, two sets of shear cracks with perpendicular

directions are formed ahead of the crack tip and U reads,

$$U = \frac{\mathcal{G}_{\min}}{\mathcal{G}_{\max}} + \left(\frac{\mathcal{G}_{\text{I, max}}}{\mathcal{G}_{\text{Ic}}} + \frac{\mathcal{G}_{\text{II, max}}}{\mathcal{G}_{\text{IIc}}} \right) \left(1 - \frac{\mathcal{G}_{\min}}{\mathcal{G}_{\max}} \right)^{g_{\text{II}}} \quad . \tag{4.28}$$

The parameters A_{I}, A_{II}, b_{I}, b_{II}, u_{I}, and u_{II} depend on the actual material and have to be determined by cyclic testing (for details see [15]).

Load cases where all loads vary with the same frequency can be treated as well as load cases where some load components are constant. In the case that all load components have the same phasing the minimum and the maximum mode I and mode II energy release rates at each delamination front are directly computed by Eqs.(4.17) and (4.19) from the minimum and the maximum loads that occur during one load cycle. In case that the load components have different phasing some additional procedure is required to find the minimum and the maximum energy release rate during each load cycle. Such cases are not considered here.

The computed maximum and minimum energy release rates serve as input for Eqs. (4.26) - (4.28) and incremental growth, $\Delta a_{\text{cyc}, i}$, at each delamination front is obtained. For the delamination increased in size, again the maximum and the minimum energy release rate are computed. Repeating these considerations allows for a cycle by cycle analysis of the growth process.

In problems with very high numbers of load cycles, however, a cycle by cycle analysis might be computationally very expensive. In such problems a cycle jump strategy can be used. The incremental growth $\Delta a_{\text{cyc}, i}$ is computed for a block of load cycles in an approximate manner by linear scaling of the incremental growth predicted for one load cycle. This way a "block by block" analysis can be performed.

Table 4.1: Material parameters for cyclic delamination growth in a transversely isotropic carbon/epoxy UD–layer, T300/976, data taken from [15].

A_I	A_II	b_I	b_II	u_I	u_II
0.16	0.13	18.0	5.3	-2.0	4.0

4.2 Examples

Two structures, a curved laminate and a T–joint, made of plies of a unidirectional carbon fiber reinforced epoxy resin are analyzed. The elastic properties of the material and the critical energy release rates are taken from [42] and are summarized in Table 3.1, material data concerning cyclic delamination growth is taken from [15] and summarized in Table 4.1. The geometry, the boundary conditions, and the layup of the curved laminate is shown in Figs. 4.3. The orientation of the plies is defined with respect to the xy–plane. Both structures analyzed are assumed to have a considerable width in z–direction and free edge effects are not considered, so that generalized plane strain conditions are utilized. Loading by homogeneous temperature changes superimposed with prescribed displacements and concentrated forces is analyzed. The local load coordinates system (*12*–system) is rotated with respect to the global coordinate system (xy–system) by the angle φ. For each structure an FEM model parameterized in a_i is set up using generalized plane strain elements with linear shape functions and full integration.

4.2.1 Curved Laminate

For the curved laminate growth of delaminations located at the interface between plies five and six, counting from the inside to the outside of the structure, is analyzed. The delamination has two delamination fronts. Accordingly, it can grow in two directions independently and is entirely described by two delamination coordinates, a_1, a_2, see Fig. 4.3. The coordinates are chosen in a way which allows to describe all delaminations of interest

with two positive values. Note that a decrease in a_1 or a_2 is equal to an increase of the delaminated area (i.e. $\frac{\partial A}{\partial a_1} < 0$), hence, ∂a_i has to be replaced by $-\partial a_1$ or $-\partial a_2$ in all equations in Section 4.1.

For the FEM computations each ply is represented by three elements over the ply thickness and all element aspect ratios are close to unity. Sixty discrete values of each delamination coordinate in the range of $1.0\,\mathrm{mm}$ to $9.0\,\mathrm{mm}$ are chosen and all admissible combinations are analyzed within a fully automated procedure. Admissible are all combinations of delamination coordinates for which the sum of the coordinates (i.e. $a_1 + a_2$) is smaller than the total length of the considered interface. In total 1900 delamination configurations are analyzed. The length of the delaminations described by the selected delamination coordinates varies between $0.15\,\mathrm{mm}$ and $10.2\,\mathrm{mm}$. The results allow for a pointwise description of the stiffness, the coefficient of thermal deformation, the strain energy caused by a temperature change, and the mode contributions as functions of the delamination coordinates.
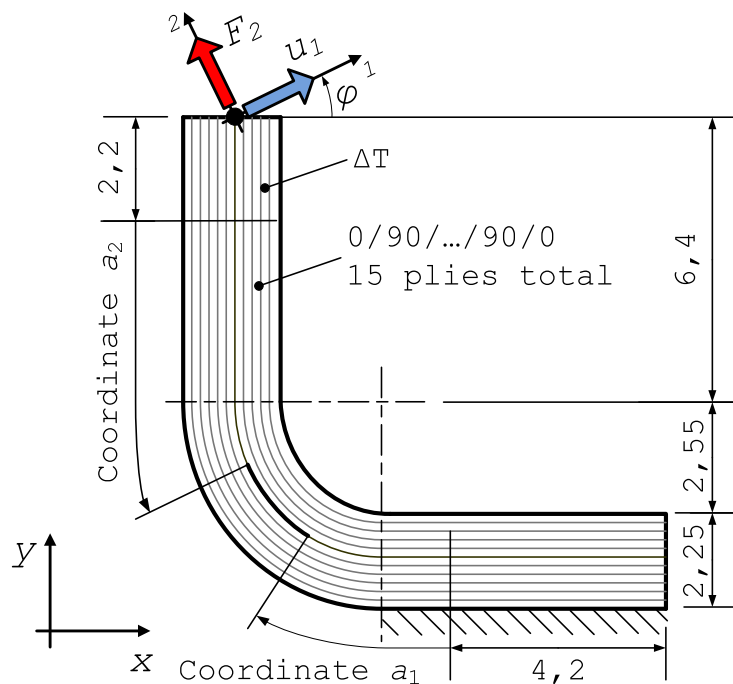

Figure 4.3: Curved laminate with through–the–width delamination between ply five and ply six; definition of the delamination coordinates, a_1 and a_2, as well as the applied load.

Quasi–Static Loading

Equilibrium delamination growth can now be predicted for any load case by postprocessing the data generated in the automated FEM procedure. First, equilibrium growth and its stability are computed for all delaminations in the considered range of coordinates. Second, the structural response is shown for selected delaminations.

In the following two load cases are investigated which allow for comparison of the growth process and its stability under force and displacement controlled loading. At the load introduction point a force or a displacement with variable magnitude by constant direction $\varphi = 206°$ is prescribed, in the orthogonal direction a zero force load is defined. These loads are superimposed by a constant homogeneous temperature change of $\Delta T = $ -75 K. For the displacement load case the generalized load vector defined in Eq. (4.15) reads $\mathbf{P} = [u_1, \ 0, \ -75\,\mathrm{K}]^{\mathrm{T}}$. The force load case reads $\Delta T = $ -75 K, $\mathbf{F} = [F_1, \ 0, \ 0]^{\mathrm{T}}$.

The magnitude of the displacement and the magnitude of the force required to cause equilibrium growth are computed for all delaminations in the considered range of coordinates by applying Eqs. (4.23) and Eq. (4.25). Stability of the equilibrium states is derived according to Eq. (2.23). The results are presented in Fig. 4.4 (left) in terms of the delamination coordinates. Note that delaminations of the same length but different position lie on straight lines with a slope of minus one. All coordinate combinations in the white region describe delaminations which will grow in a stable manner in force and displacement controlled loading. Delaminations described by coordinates in the light gray region will grow stably in the displacement load case, but unstably in the force load case. The dark gray region finally contains all coordinates that describe delaminations which will grow in an unstable manner in both load cases (force and displacement controlled). These findings show that growth stability depends on the loading conditions as well as on the delamination size and its position.

In Fig. 4.4 (left) three starting delaminations are selected, one from each of the three stability regions. For these starting delaminations progressive equilibrium growth is predicted

for both load cases and, of course, the results are identical. The black dots in Fig. 4.4 (left) show the growth process in terms of the change in the delamination coordinates. Delamination (A) grows first in direction a_2, then in direction a_1, and finally in both directions. Delamination (B) and (C) grow first in direction a_1 and direction a_2, respectively, and then in both directions. The figure shows that all three starting delaminations converge to the same final delamination.

In Fig. 4.4 (right) the structural response is plotted in terms of the force in 1–direction, F_1, and the displacement of the load introduction point in 1–direction, u_1. Note that the curves do not start at the origin due to the constant temperature load applied. For the small starting delamination (A) the predicted structural response is linear until the growth load is reached (0.44 mm or 31.9 N), followed by unstable equilibrium delamination growth. The equilibrium load decreases as the delamination size increases, leading to a pronounced snap–back behavior of the structure. As soon as a certain delamination size is
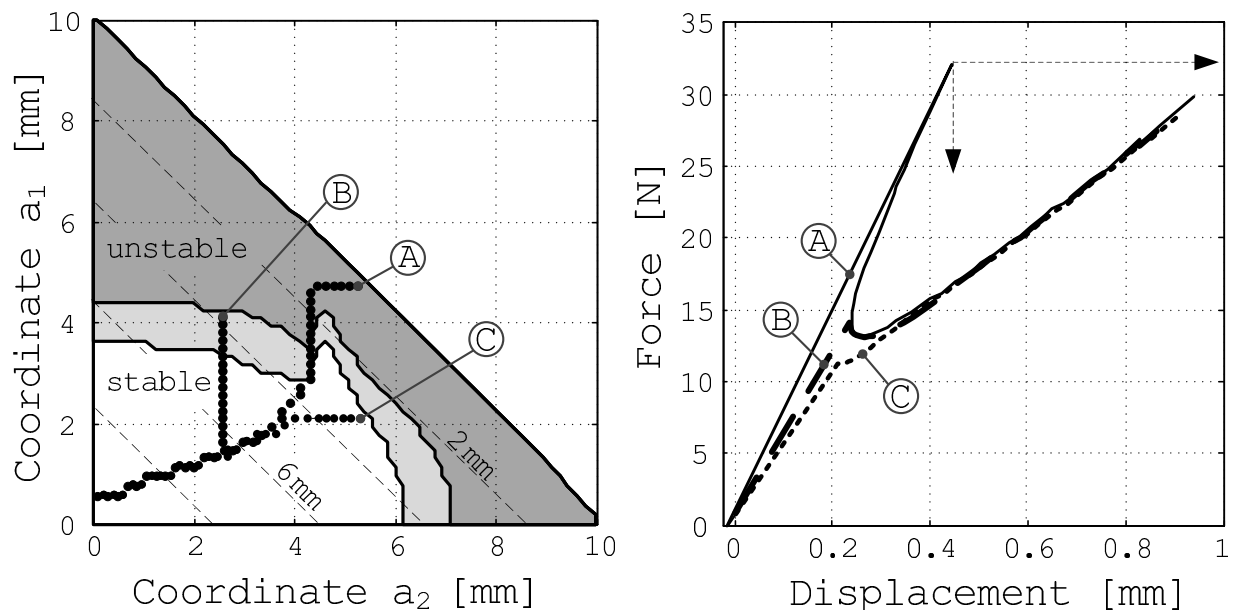

Figure 4.4: Predictions for the curved laminate loaded by a constant homogeneous temperature change superimposed by a quasi–static force or displacement load; stability of the growth process expressed in terms of the delamination coordinates (left); structural response for three selected delaminations (right).

reached growth becomes stable and a load increase is required to propagate the delamination further. Note that such force–displacement curves can only be realized theoretically, in structural experiments unstable delamination growth, including dynamic effects, would take place, as indicated by the dashed lines for monotonously increasing displacement and force loads. For delamination (B) the predicted structural response shows that growth is stable under displacement controlled loading but would be unstable under force controlled loading. These findings correspond to the predicted stability shown in Fig. 4.4. For the third starting delamination (C) delamination growth is predicted to start at a load of about 0.2 mm or 11.3 N and growth is stable for force and displacement controlled loading.

Next, the most detrimental position of a delamination of some given size but undetermined location is analyzed. The most detrimental position is the one for which the load required to propagate the delamination is smallest. The force and the displacement load cases discussed above are considered. The equilibrium growth loads for all delamination configurations are computed and for each delamination size the minimum load is taken. The results are shown in Fig. 4.5 in terms of the delamination size and the minimum force and the minimum displacement required to propagate the delamination. The difference among these curves is caused by the fact that the compliance of the structure depends on the size and the position of the delamination. For small delaminations the results show that the smaller the delamination is the higher is the load required to propagate it. This trend is reversed for large delaminations. Here the load required to propagate the delamination increases with increasing delamination size. These finding coincides with the predicted snap–back behavior, Fig. 4.4 (right), where for small delaminations the equilibrium growth load decreases whereas for large delaminations the growth load increases for increasing delamination size.

As an example a delamination of length 2.0 mm is selected and the load required to propagate it, if it lies in its most detrimental position, is predicted to be 0.215 mm or 14.2 N, respectively. These findings allow a fast and easy interpretation of the results of non–destructive testing procedures. Assuming that a delamination smaller than the resolution

of the inspection method exists somewhere in the interface, the minimum load carrying capacity of the structure can be assessed directly from Fig. 4.5.

Cyclic Loading

In the following incremental delamination growth in the curved structure caused by a cyclic load is analyzed. The applied load is similar to the force load case discussed before. Now the magnitude of the force is cycled between $F_1 = 1\,\text{N}$ and $F_1 = 8\,\text{N}$, its direction ($\varphi = 206°$) and the temperature change ($\Delta T = -75\text{K}$) are kept as before. As example a starting delamination with a length of $3\,\text{mm}$ ($a_1 = 3.1\,\text{mm}$, $a_2 = 3.3\,\text{mm}$) is considered and incremental delamination growth is predicted by postprocessing of the data generated within the fully automated FEM procedure.

The results, Fig. 4.6, show that at about 5000 load cycles considerable growth in direction a_1 starts. At about 10^7 load cycles also some growth in direction a_2 can be observed. Note that this example was chosen to show the capabilities of the semi–analytical approach, the
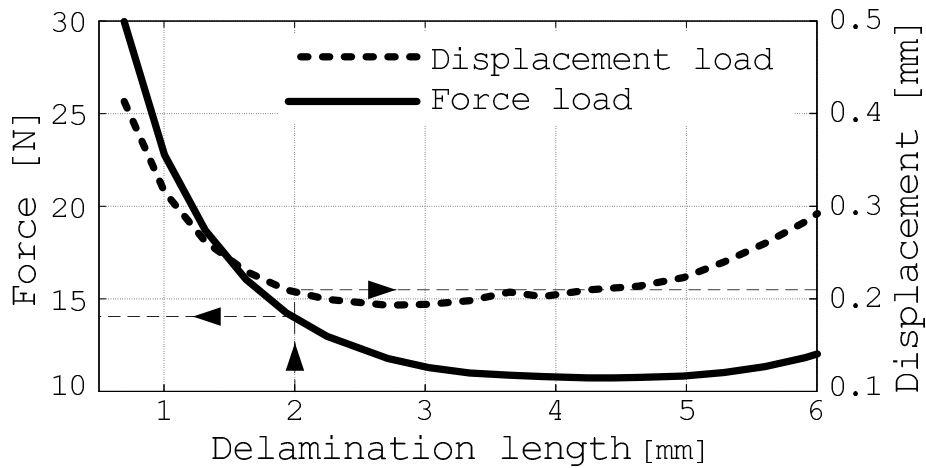

Figure 4.5: Predictions for the curved laminate loaded by a constant homogeneous temperature change superimposed by a quasi–static force or displacement load; minimum force and displacement load required to propagate delaminations of certain size at their most detrimental position.

material data was not verified for such high numbers of load cycles.

Finally, the most detrimental position of delaminations under cyclic loading is analyzed. The most detrimental position of a delamination of some given size is the one for which the predicted final delamination size is largest. The cyclic load discussed before is applied. For all delamination configurations incremental growth is predicted and the final delamination lengths are computed for various numbers of load cycles. From the results the maximum final length is selected for each initial delamination size.

In Fig. 4.7 the results are shown in terms of the initial delamination length and the final delamination length for different numbers of load cycles. The shape of the predicted curves is due to the fact that delaminations in the curvature of the structure grow fast and delaminations in the straight parts of the structure grow slow. The results show that for about 100 load cycles hardly any growth takes place, the final delamination length is almost identical to the size of the starting delamination. For 10^4 load cycles considerable
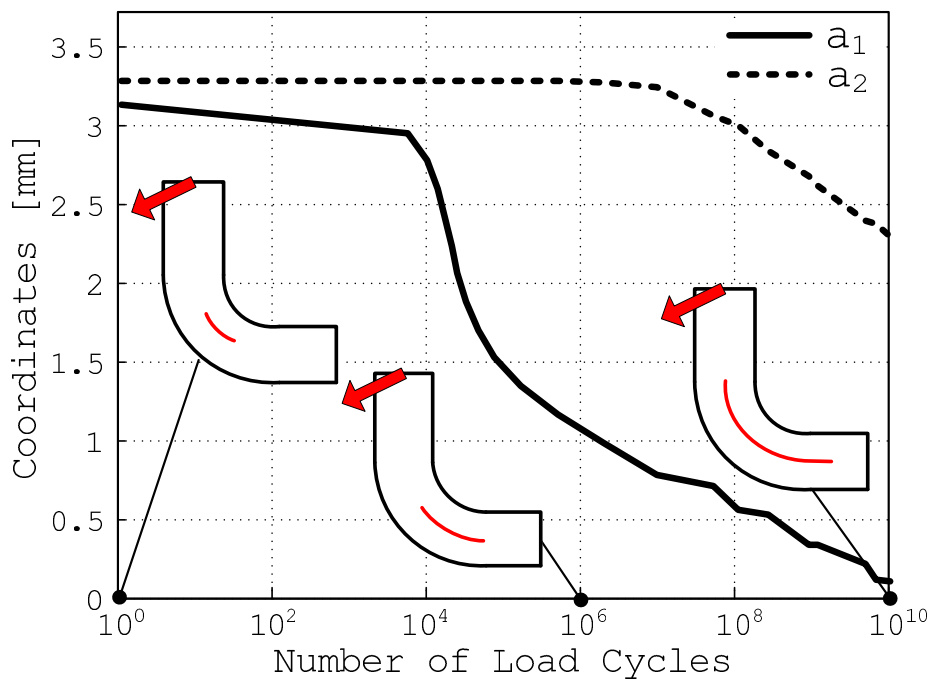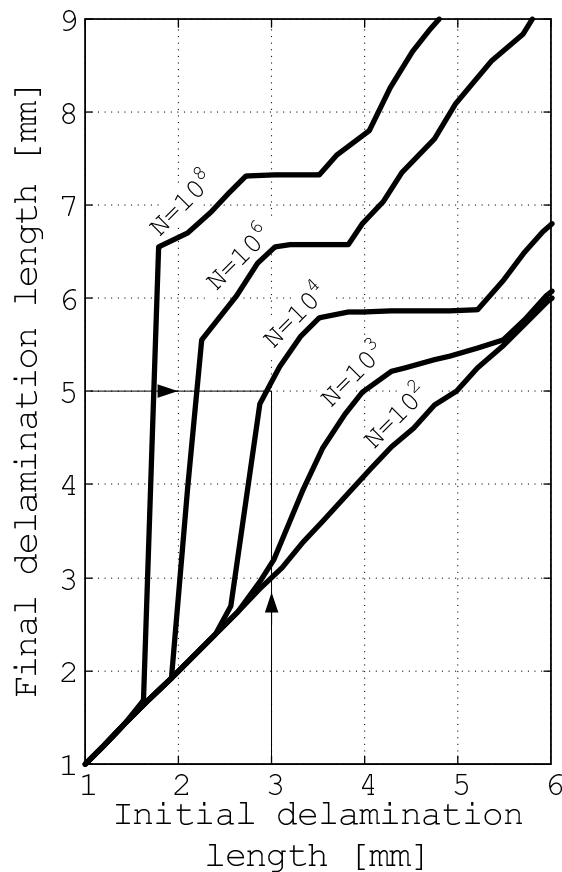

Figure 4.6: Predicted incremental delamination growth for the curved laminate loaded by a constant homogeneous temperature change superimposed by a cyclic force.

growth is observed for delaminations larger than 2.5 mm.

These findings allow now to predict the maximum allowable number of load cycles. As an example it is assumed that the inspection method applied can detect delaminations larger than 3 mm (i.e. initial delaminations of 3 mm might exist anywhere in the interface) and that the maximum allowable delamination length is 5 mm. Figure 4.7 shows that the maximum allowable size is reached after about 10^4 load cycles, hence, at least all 10^4 load cycles an inspection is required. This way the selection of inspection intervals can be assisted.

Figure 4.7: Predictions for the curved laminate loaded by a constant homogeneous temperature change superimposed by a cyclic force; maximum final delamination length for delaminations of certain size at their most detrimental position after N load cycles.

4.2.2   T–Joint

Delaminations emerging from the cavity in the center of the T–joint (Fig. 4.8), which is not filled with resin are analyzed. The T–joint is composed of two flanges and a flat plate. The delaminations can grow independently in three directions, so that three delamination coordinates a_1, a_2, and a_3 are required to describe the delamination. An FEM model of the T–joint is set up where each ply is represented by two elements over the ply thickness and all element aspect ratios are close to unity. For each delamination coordinate, a_1 and a_2, 19 discrete values in the range of 0.0 mm to 9.0 mm and 17 discrete values of the delamination coordinate a_3 in the range of 0.0 mm to 8.5 mm are chosen, i.e. in total 6137 delamination
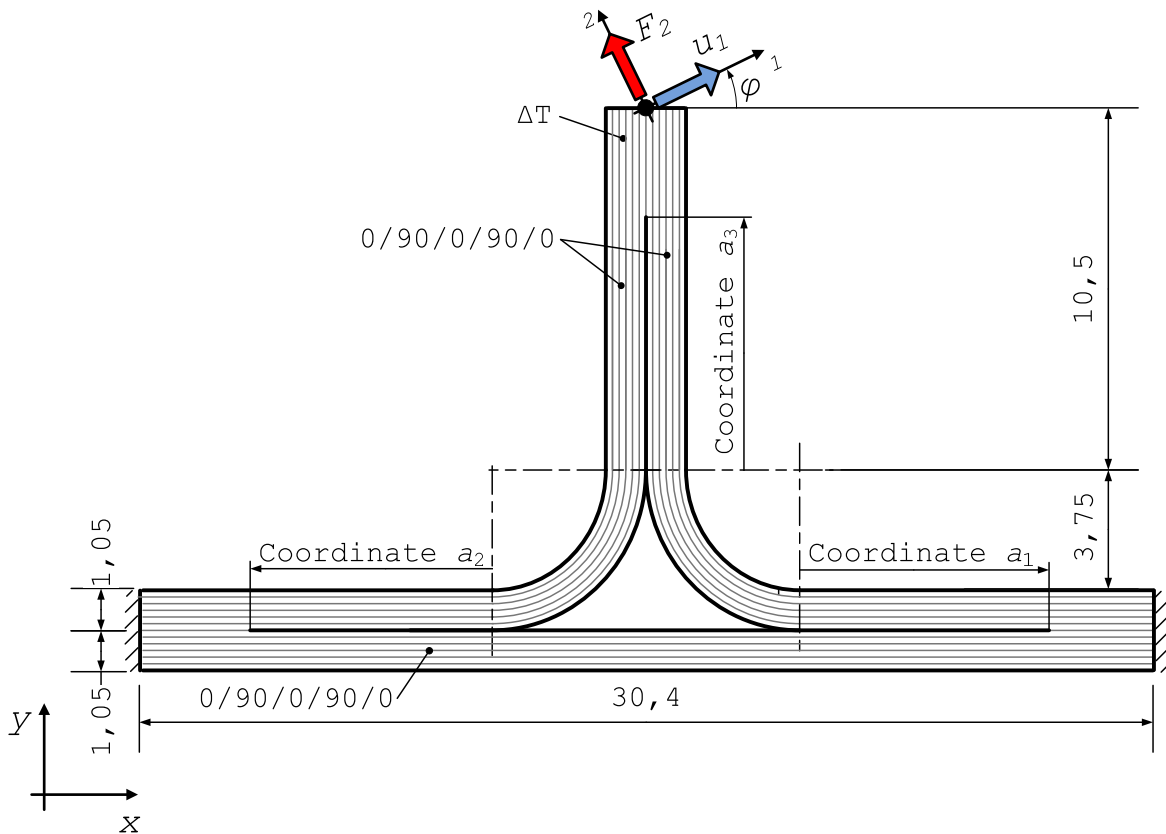

Figure 4.8: T–joint with through–the–width delamination; definition of the delamination coordinates, a_1, a_2, and a_3 and the applied load.

configurations are analyzed.

Quasi–Static Loading

Two quasi–static load cases are selected which allow for a comparison of the stability of the growth process under force and displacement controlled loading. Loading in vertical direction by a prescribed displacement, u_2, and loading in vertical direction by a concentrated force, F_2, is analyzed. The load coordinate system is oriented in direction of the global coordinate system ($\varphi = 0°$). Both loads are superimposed by a homogeneous temperature change $\Delta T = -75\,\mathrm{K}$.

For each delamination the load required to cause equilibrium delamination growth and its stability are computed for both load cases. The predicted stability of the growth process is shown in Fig. 4.9. The considered load cases are symmetric with respect to the yz–plane,
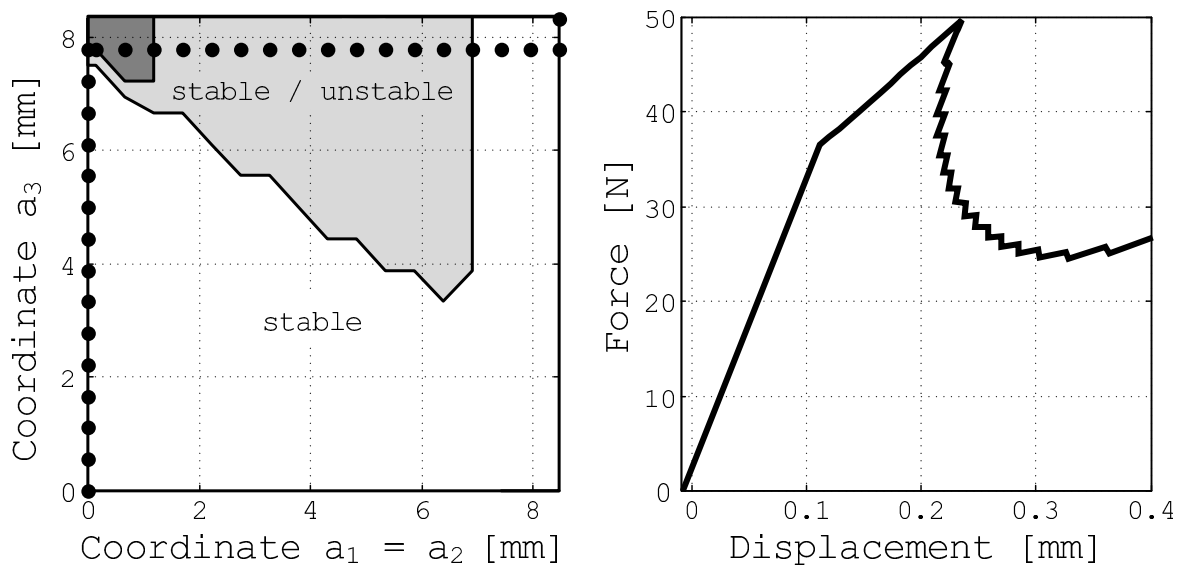

Figure 4.9: Predictions for the T–joint loaded by a constant homogeneous temperature change superimposed by a quasi–static force or displacement load; stability of the growth process expressed in terms of the delamination coordinates (left); structural response (right).

hence the results are symmetric, i.e. $a_1 = a_2$, and the stability of the growth process is plotted in terms of two coordinates, a_1 and a_3. Delamination described by coordinates in the dark–gray region will grow in an unstable way under force and displacement controlled loading, delaminations described by coordinates in the light–gray region will grow in an unstable way under force controlled loading but stably under displacement controlled loading. All delaminations described by coordinates combinations in the white region will grow in a stable manner irrespective of the load type (force or displacement).

The cavity in the center of the T–joint is selected as starting delamination and equilibrium growth is predicted for force and displacement controlled loading and, of course, the results are identical. The growth process in terms of the change in the delamination coordinates is plotted as a dotted line in Fig. 4.9 (left). It shows that the delamination will grow first in direction a_3, followed by simultaneous growth along a_1 and a_2. The structural response caused by equilibrium growth is shown in Fig. 4.9 (right). The structural response is linear until the delamination growth load is reached ($u_1 = 0.11\,\mathrm{mm}$ or $F_2 = 37.5\,\mathrm{N}$), followed by stable growth where the applied load has to be increased in order to propagate the delamination. At a load level of about $0.23\,\mathrm{mm}$ or $49.7\,\mathrm{N}$ unstable growth in direction a_1 and a_2 starts, which again changes to stable growth as soon as a certain delamination size is reached.

Cyclic Loading

Finally the T–joint is loaded by a cyclic load and incremental growth of the delamination emerging from the cavity is analyzed. The load coordinate system is rotated by an angle $\varphi = 80°$ and a displacement in 1–direction and a zero force in 2–direction are applied. The prescribed displacement is cycled between $0.05\,\mathrm{mm}$ and $0.13\,\mathrm{mm}$. This load is superimposed by a constant and homogeneous temperature change of $\Delta T = -75\,\mathrm{K}$.

Incremental delamination growth is predicted and the result, Fig. 4.10, shows that the growth rate is different at each delamination front and considerably changes as the delam-

ination advances. Due to the fact that the considered cyclic load is not symmetric the growth rate is higher in direction a_2 than a_1.

4.3 Summary

A computationally efficient semi–analytical approach for prediction of delamination growth in laminated composites loaded by combinations of displacements, forces, temperature loads, and moisture loads is proposed. Load cases where all loads vary with the same frequency can be treated as well as cases where some loads are constant. Based on the principles of linear elastic fracture mechanics analytical equations for the computation of the energy released at delamination growth and its mode I and mode II components are derived. The coefficients of these equations are determined within a numerical procedure,
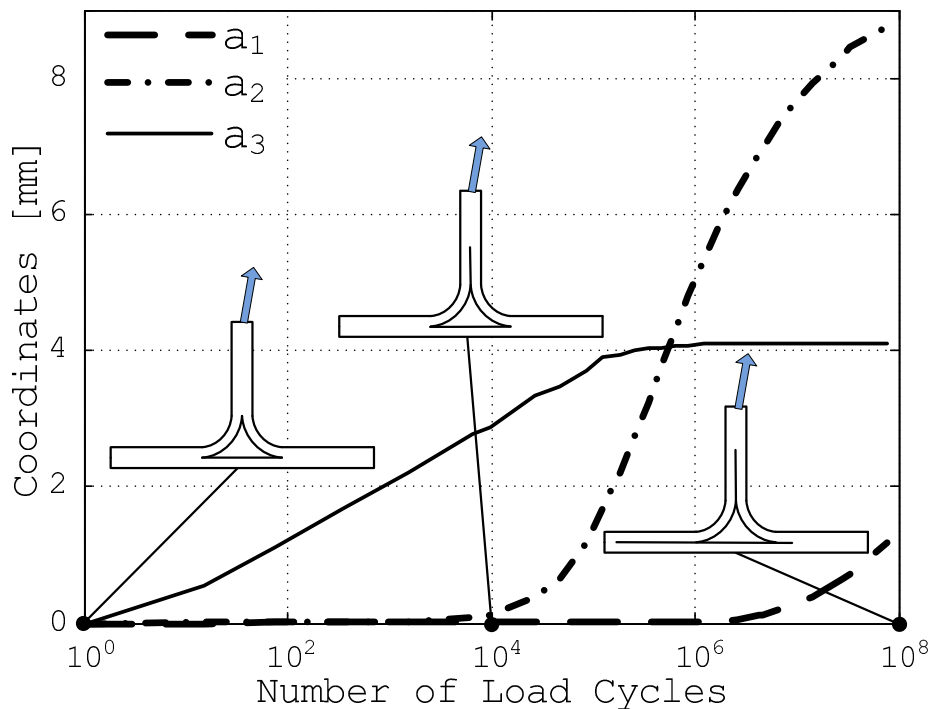

Figure 4.10: Predicted incremental delamination growth for the T–joint loaded by a constant homogeneous temperature change superimposed by a cyclic displacement load.

in the thesis the FEM is used for this purpose. The equations derived are combined with the Griffith criterion to handle quasi–static loads and equilibrium delamination growth, the stability of the growth process, and the non–linear structural response caused by progressive delamination growth are predicted. For the analysis of structures loaded by cyclic loads or by combinations of cyclic and constant loads a Paris–type growth law is employed and incremental delamination growth is predicted. Furthermore, the most detrimental position of a delamination of given size but unknown location is determined. This permits for fast interpretation of results from non–destructive testing.

The proposed approach offers a complete picture of delamination problems, and provides a systematic and general understanding of the influence of size and position of a delamination on the load carring capacity, the stability of the growth process, the structural response, as well as on the cyclic growth rate.

In order to show the application and the capability of the proposed approach, delamination growth in an L–shaped laminate and in a T–joint is analyzed in detail. The results show that for both structures the stability of the growth process depends on the delamination size and that in case of quasi–static loading a pronounced structural snap back behavior is found.

Chapter 5

Growth of Delaminations with Curved Fronts

In the previous chapter, a semi–analytical approach for the prediction of growth of through–the–width delaminations with straight delamination fronts was presented. Growth of such through–the–with delaminations can be predicted by means of two–dimensional models using plane strain or plane stress assumption. Hence, the delamination front reduces to a point and questions concerning the shape of the delamination front do not arise. In the following, growth of delaminations with curved fronts is studied. The investigation of such problems, generally, requires three–dimensional models.

Within the FEM the VCCT can be used to compute energy release rates along curved delamination fronts. For this purpose meshes that allow for a smooth approximation of the delamination front are desired. Furthermore, the mesh needs to be locally orthogonal to the delamination front and the size of the elements ahead and behind the front should be approximately the same. However, the VCCT is not well suited for the simulation of consecutive growth of such delaminations. Following the principles of the VCCT a delamination will grow by an increment equal to the element length at nodes where the growth

criterion is met. As the growth condition is, typically, not fullfilled along the entire delamination front a front with kinks is obtained and growth is no longer self similar. At such kinks the energy release cannot be computed properly by means of the VCCT since the local orientation of the delamination front is not defined there. For a detailed discussion of the limitations of the VCCT see Chapter 2 and [35, 39].

To overcome this problem, moving mesh techniques have been proposed [60, 85, 86]. The growth criterion is evaluated by means of the VCCT and all nodes at the delamination front for which the growth criterion is satisfied are moved by a certain distance in direction of the bonded region. The new nodal coordinates are used to create a new, orthogonal mesh with a smooth delamination front and the analysis is repeated. These moving mesh techniques are numerically expensive, as the distance the delamination front advances needs to be small compared to the total delamination size. Furthermore, the achievement of convergence is tricky if unstable delamination growth takes place.

An alternative way for the simulation of consecutive delamination growth within the FEM is the usage of CZE. These elements can handle curved delamination fronts. Their use, however, is numerically expensive, as very fine meshes and small load increments are required to adequately represent the fracture process zone and the damage evolution within each element (see Chapter 2).

In the following a numerically efficient approach, employing the FEM and the VCCT, for the prediction of consecutive growth of delaminations with curved fronts is presented. Possible shapes of the delamination front are predefined and a delamination growth criterion for the entire delamination front is formulated. The proposed method ensures smooth delamination fronts during the entire growth process.

5.1   Total Delamination Front Criterion

According to Griffith a delamination will grow if the energy released is equal to or greater than the energy required to create new delaminated area, see Eq.(2.20). In FEM analyses employing the conventional VCCT this criterion is evaluated at each node along the delamination front and at nodes where it is satisfied growth is predicted to occur. In the proposed method growth along the entire front is considered instead of predicting growth at individual points. Possible shapes of the new, advanced delamination front are chosen to be continuous, smooth, and geometrically compatible with respect to the current delamination front. Details concerning the way the shapes are selected including a quality check are discussed in the next sections.

In Fig. 5.1 (left) a generic example of a current delamination front with three geometrically compatible, advanced delamination fronts is shown. The delamination will grow from its current front to any of the advanced fronts, if

$$\lambda^2 \frac{\sum_{i=1}^{N} \mathcal{G}_i A_i}{\sum_{i=1}^{N} \mathcal{G}_{c,\,i}\, A_i} = 1 \quad , \tag{5.1}$$
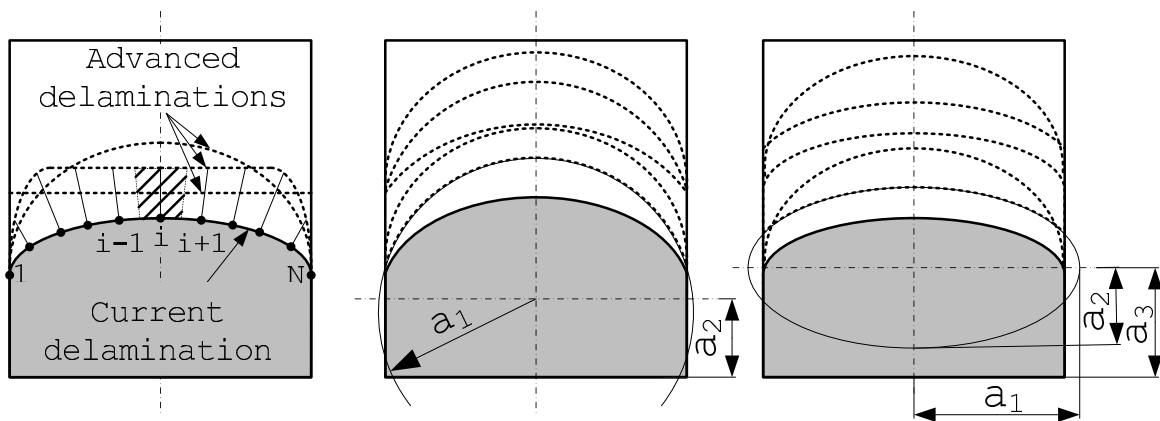

Figure 5.1: Advanced delamination fronts geometrically compatible with the current delamination front; area associated to node i for delamination progress (left); delamination shapes described by two (center) and three (right) delamination coordinates.

where $\mathcal{G}_i$ is the energy release rate at node i. It is computed together with the mode I, mode II, and mode III components for all nodes along the delamination front by means of the VCCT within a linear FEM analysis for a prescribed loading scenario. N is the total number of nodes along the delamination front. A_i is the area associated to each node for delamination progress, which is defined by the current and the advanced delamination front, see Fig. 5.1 for an example. Note that A_i depends on the shape of the advanced delamination front. λ is the load factor by which the magnitude of the prescribed loading scenario has to be increased to propagate the delamination from the current delamination front to the advanced front. The load factor is computed for each advanced delamination front individually. Due to the fact that the energy release rate is a quadratic function of the applied load the square of the load factor is used in Eq. (5.1). $\mathcal{G}_{c,\,i}$ is the critical energy release rate at node i, which depends on the critical energy release rate for pure mode I, mode II, and mode III loading as well as on the actual mode mix. Here a quadratic criterion is used to take the mode interaction into account and the critical energy release rate at node i is defined following Eq. (2.21).

The proposed approach is based on the assumption that the structural compliance is independent of the load. Hence, the energy release rate is a quadratic function of the applied load. In the case of closed delaminations this assumption is violated as friction may occur and contact states may change. However, many delamination problems of practical relevance have open delaminations and can be treated with the proposed total delamination front criterion.

5.1.1 Numerical Evaluation

For simulation of consecutive delamination growth it is assumed that the shape of the delamination front is described by a number of delamination coordinates a_i. In Fig. 5.1 two generic examples are shown; circular delamination fronts (middle) described by two delamination coordinates (the radius, a_1, and the center of the circle, a_2) and elliptical

delamination fronts (right) described by three delamination coordinates (the major axis, a_1, minor axis, a_2, and the center of the ellipse, a_3). Advanced delamination fronts are obtained by proper variation of the delamination coordinates. Note that the delamination size can never decrease. As a consequence all points of the advanced delamination front needs to be at or ahead of the position of the current delamination front. All advanced delamination fronts that fullfill this requirement are geometrically compatible with respect to the current one.

For the prediction of consecutive delamination growth a suitable number of delamination front coordinates has to be chosen to describe the shape of the delamination front. Discrecte values of these delamination coordinates are then selected in a range that allows to describe all delaminations of interest. All combinations of these coordinates describe possible shapes of the delamination front. Consecutive growth is now predicted by selecting one shape after the other out of all predefined shapes.

For the computation of the energy release rate an FEM model parametrized in the delamination coordinates is set up using the FEM package *ABAQUS*. Discrete values of the delamination coordinates are chosen, and for each feasible combination of delamination coordinates an FEM model is generated. The meshes of these models allow for a smooth approximation of the delamination front and are locally orthogonal to the delamination front. The structural stiffness and the energy release rates as well as its mode I, mode II, and mode III components at all nodes along the delamination front are computed for all shapes within a series of linear analyses. The generation of the FEM models and all computations are done within a fully automated procedure and the results are stored in a database. Hence, all delamination fronts described by the choosen delamination coordinates are analyzed and consecutive delamination growth is predicted by postprocessing of existing data, using the data processing capability of *MATLAB*.

For a given current delamination Eq. (5.1) is applied for all geometrically compatible advanced delamination fronts analyzed. From the results the advanced front for which the load factor is smallest is chosen as the new delamination front. The force and the displacement required to propagate the delamination are computed from the load applied in the

prescribed loading scenario, the load factor, and the structural stiffness. Repeating these computations allows to predict incremental delamination growth and the corresponding structural response. The size of the incrementation in delamination size is set by the incrementation chosen for discretization of the delamination coordinates.

5.1.2 Quality Check of the Delamination Front

The proposed approach allows to predict consecutive delamination growth for a prescribed loading scenario by selecting delamination fronts out of a set of predefined ones. Hence, the shape of the delamination front is not a result. However, by considering various shapes one which is well suited for describing the delamination front can be found, as shown in the following.

In Eq. (5.1) only the global energy balance at delamination growth is considered. Locally the energy release rate may be greater or smaller than the critical energy release rate. However, the ratio between energy release rate and critical energy release rate at each node, called *energy ratio* in the following, provides information whether or not the assumed shape allows for a satisfying approximation of the delamination front. First, the energy ratios are normalized by their mean value and plotted along the delamination front for visual inspection. In sections where the normalized energy ratio is greater than unity, delamination growth is underpredicted. In sections where the normalized energy ratio is smaller than unity, delamination growth is overpredicted. A proper description of the shape of the delamination front is found if the normalized energy ratios are equal to unity, or close to unity, along the entire delamination front.

Second, the standard deviation of the normalized energy ratios,

$$s = \frac{N}{\sum_{i=1}^{N} \frac{\mathcal{G}_i}{\mathcal{G}_{c,\,i}}} \sqrt{\frac{1}{N} \sum_{i=1}^{N} \left(\frac{\mathcal{G}_i}{\mathcal{G}_{c,\,i}} - 1 \right)^2} \quad , \qquad (5.2)$$

is defined and used to compare individual shapes of the delamination front. The smaller the standard deviation is the better is the description of the shape of the delaminated front. A proper description of the delamination front is found if the standard deviation is close to zero.

5.2 Examples

Consecutive delamination growth is analyzed in a laminated plate and in a curved laminate, both made of plies of a carbon fiber reinforced epoxy resin. Material data and interface properties are taken from [15, 42] and are summarized in Table 3.1. For the considered material no reliable experimental data for the critical energy release rate for mode III is available. Hence, it is assumed that the critical energy release rate for mode III and mode II are equal (i.e. $\mathcal{G}_{\mathrm{IIIc}} = \mathcal{G}_{\mathrm{IIc}}$).

5.2.1 Laminated Plate

Details concerning geometry and loading of the laminated plate are shown in Fig. 5.2. A $[+45°_{10}/ - 45°_{10}]$ layup is considered, the ply thickness is $0.1\,\mathrm{mm}$ and the orientation of the plies is measured with respect to the x–direction. The structure contains a circular delamination at the midplane of the laminate with a radius of $20\,\mathrm{mm}$ centered at one corner of the plate. The upper sublaminate is loaded at this corner by a prescribed displacement in z–direction, the lower sublaminate is fixed in z–direction at this corner. Appropriate boundary conditions are applied to prohibit rigid body motions but without applying constraints otherwise.

For the FEM computation each sublaminate is modeled using four–noded Krichhoff shell elements with full integration, the element length is about $1\,\mathrm{mm}$. In the region which is not yet delaminated the translational degrees of freedom between the nodes of the two

sublaminates are coupled. Kinematic coupling conditions are applied which enforce the translational displacements of the corresponding surfaces of the sublaminates in the yet not delaminated area to be equal. The rotational degrees of freedom are not coupled as discussed in Chapter 2. Note that such models do not allow to analyze free edge effects.

Shape of the Delamination Front

Various functions for the shape of the delamination front are considered and compared to find out which one is best suited to describing the advanced delamination fronts.

The structure and the considered loading scenario considered (Fig. 5.2) are symmetric with respect to the $+45°$ line. Thus, all advanced delaminations have to be symmetric and only symmetric shapes need to be considered. Four shapes are selected for investigation, see Fig. 5.3, i.e. a straight line, a quarter circle centered at the corner of the plate, and a offset
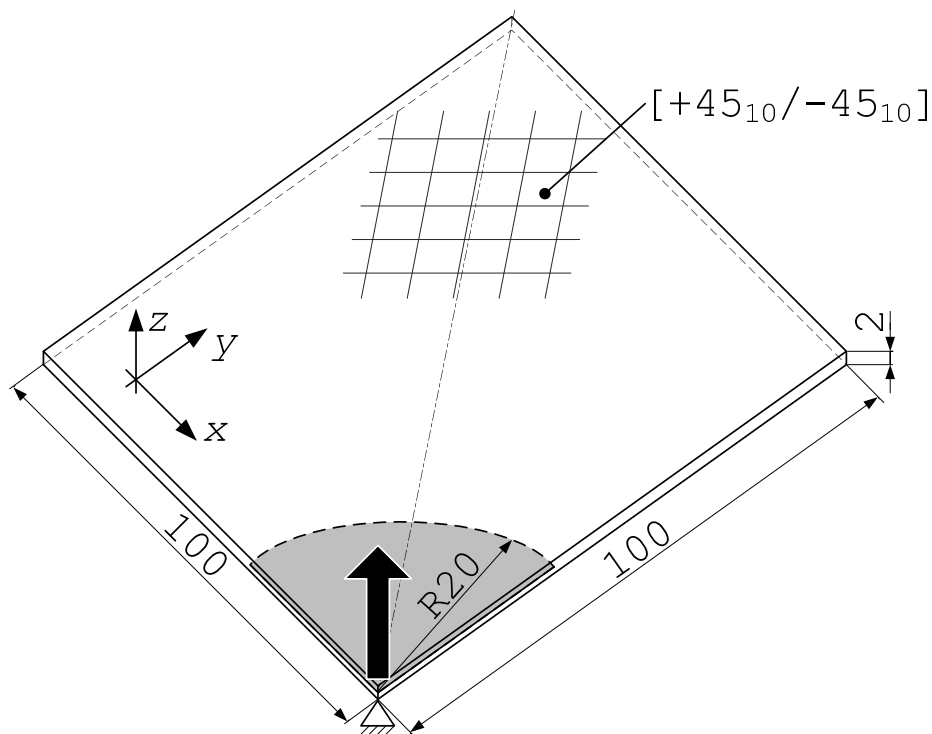

Figure 5.2: Delamination in a laminated plate; definition of geometry, layup, and loading.

circle as well as an ellipse centered somewhere on the symmetry line. The first two shapes are entirely described by one delamination coordinate, the offset circle is described by two delamination coordinates, and for description of the ellipse three delamination coordinates are required.

All four shapes are assumed to pass through the same point at the symmetry line (black star in Fig. 5.3). For the shapes described by one parameter (i.e. the quarter circle and the straight line) the delamination is already entirely defined by this point. For each shape an FEM model with a mesh locally orthogonal to the delamination front is set up and the energy ratios are computed for all nodes along the delamination front within a linear analysis.

For the shapes described by more than one parameter (i.e. the offset circle and the ellipse)
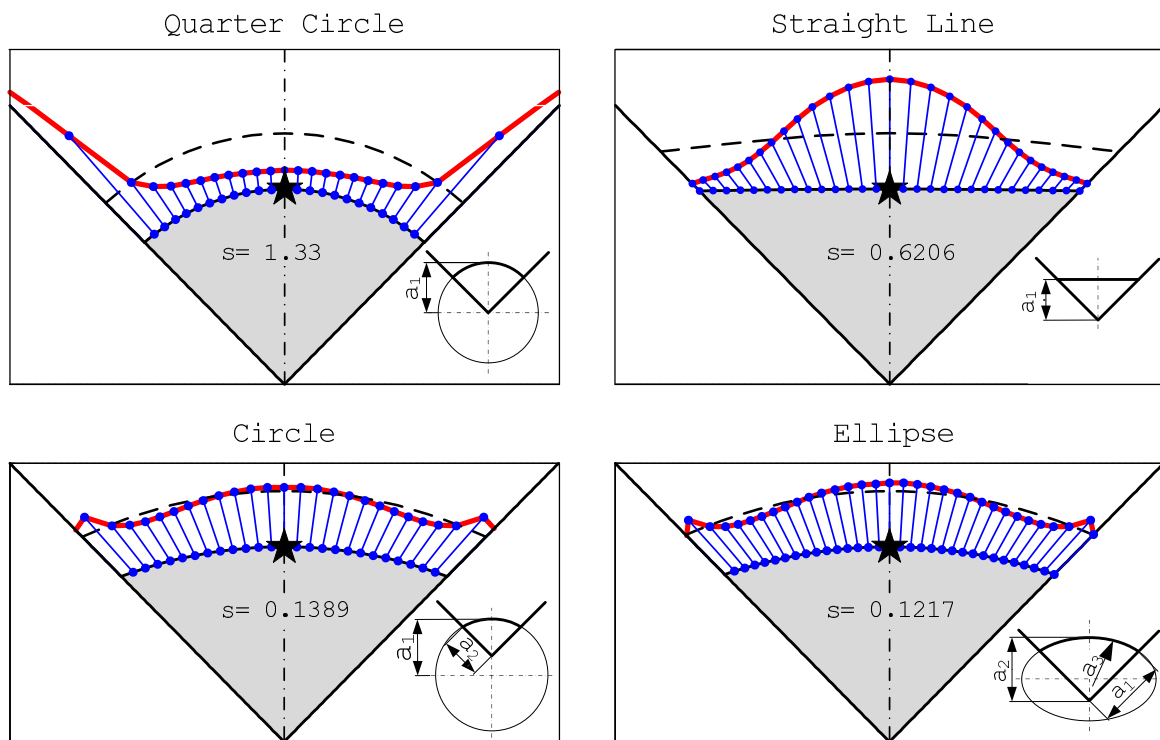

Figure 5.3: Delaminations in the laminated plate loaded by a vertical displacement load; definition of the delamination coordinates; predicted normalized energy ratios and their standard deviations.

discrete values of the delamination coordinates are selected. All combinations of these coordinates which describe shapes that pass through the specified point are investigated. From the results the ones with the smallest standard deviation of the normalized energy ratios are selected.

In Fig. 5.3 the normalized energy ratios are plotted for all nodes along the delamination front for each of the four shapes. For comparison a ratio of unity is plotted as dashed line. It should be noted that the energy ratios computed at the nodes at the free edges might be questionable, e.g. due to free edge effects. For the quarter circle (left, top) the results show that the normalized energy ratio is greater than unity at sections close to the free edges and smaller than unity at sections in the middle of the plate. Based on this graph one could guess that a less curved shape might allow for a better description of the delamination front. For the straight line (right, top) the results show the opposite tendencies, the normalized energy ratio is higher than unity in sections close to the middle and smaller than unity in sections close to the free edge. Hence, one could guess that a shape between a straight line and a quarter circle might be a good description of the delamination front. For the offset circle (left, bottom) as well as for the ellipse (right, bottom) the normalized energy ratios are close to unity along the entire delamination front. Hence, the offset circle and the ellipse allow for a proper description of the shape of the delamination front in the given configuration.

Comparison of the standard deviation of the normalized energy ratios for all four shapes shows that the more delamination coordinates (i.e. more free variables) are used the better is the description of the shape of the delamination front. However, the numerical effort for evaluating all feasible combinations of delamination coordinates increases enormously if the number of delamination coordinates is increased. In Fig. 5.4 the four shapes discussed are plotted. A comparison between the offset circle and the ellipse shows only marginal improvement of the standard deviation of the normalized energy ratios. Therefore, circular delamination fronts described by two delamination coordinates are considered in the following for the analysis of consecutive delamination growth. Note that the shape best suited for describing the delamination front may change during delamination growth.

Consecutive Delamination Growth

Consecutive growth of the circular starting delamination with a radius of 20 mm centered at the corner as shown in Fig. 5.2 is now predicted. Based on the results derived in the previous section it is assumed that during the entire growth process the shape of the delamination is described by a circle centered somewhere on the symmetry line. For numerical evaluation 50 discrete values of delamination coordinate a_1 (Fig. 5.3 left bottom) in the range between 20 mm and 126 mm and 80 discrete values of delamination coordinate a_2 in the range between 20 mm and 178 mm are selected. All combinations of these coordinates which allow to describe a circle centered at the symmetry line are analyzed in an automated procedure. Note that the selected delamination coordinates describe shapes of the delamination front with positive and negative curvature.

Consecutive growth is now predicted by postprocessing of the data generated. In Fig. 5.5 the starting delamination (dark gray region), some intermediate delaminations (dashed lines), and the final delamination (gray region) are shown together with the standard deviation of the normalized energy ratios computed for each delamination front. Comparison of the shapes of the delamination fronts shows that their curvature is negative in the beginning but changes to positive values as the delamination advances. The standard deviations of the normalized energy release rates are small for all delaminations predicted. Hence, it
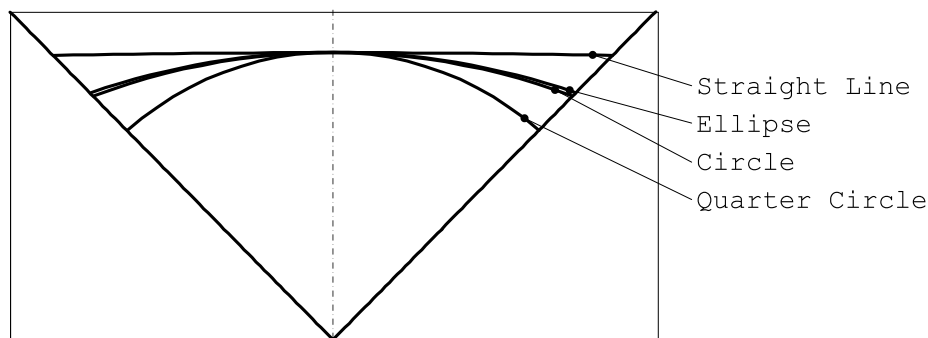

Figure 5.4: Comparison of the delamination shapes used to describe the delamination front in the laminated plate.

can be concluded that the delamination is properly described by the chosen delamination shape (i.e. the offset circle). The variation in the standard deviation might be caused by the incrementation chosen to discretize the delamination coordinates. Concerning the fracture mode the analysis shows that at sections close to the symmetry line growth is mode I dominated, while at sections close to the free edge growth is dominated by mode II and mode III loading.

The predicted structural response is shown in Fig. 5.6 in terms of the prescribed displacement and the reaction force at the loading point. The initial response is linear elastic and at a load of about 4.8 mm or 42 N delamination growth starts. Further increase of the prescribed displacement leads to stable delamination growth up to the point where the delamination front connects the lateral corners of the plate. Somewhat beyond this point delamination growth becomes unstable and the prescribed displacement required to cause
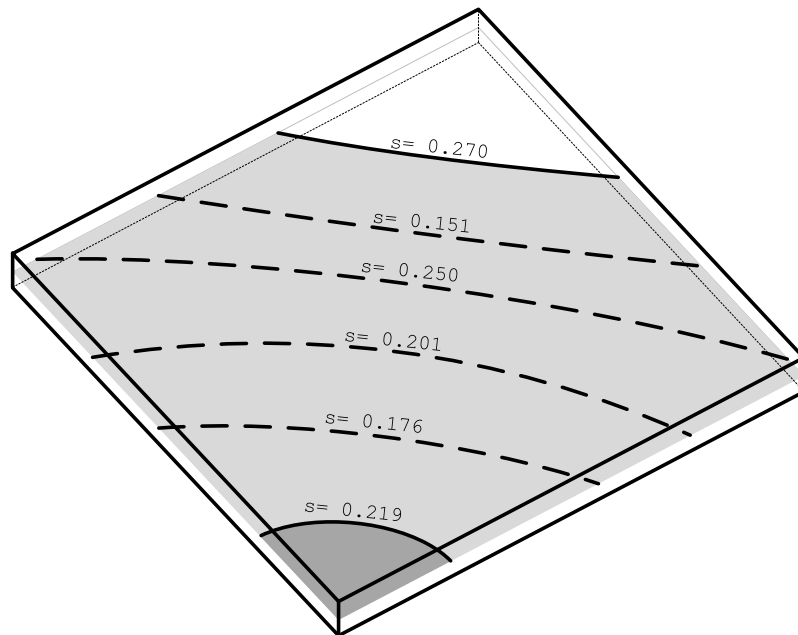

Figure 5.5: Predicted consecutive delamination growth in the laminated plate subject to a vertical displacement load; starting delamination (dark gray region), intermediate delamination fronts (dashed lines), final delamination (gray region); Standard deviation of the normalized energy release rates, s, is given for each front.

equilibrium delamination growth decreases as the size of the delamination increases. As soon as a certain delamination size is reached growth becomes stable again for displacement controlled loading. At the final point of the force–displacement curve only a small not yet delaminated area remains and the analysis is stopped.

Comparison to other approaches

In the following consecutive growth of the circular starting delamination (Fig. 5.2) is predicted using the semi–analytical approach discussed in Chapter 4, an FEM model employing standard VCCT, and an FEM model employing CZE. The results are compared to the predictions obtained by the proposed total delamination front criterion.
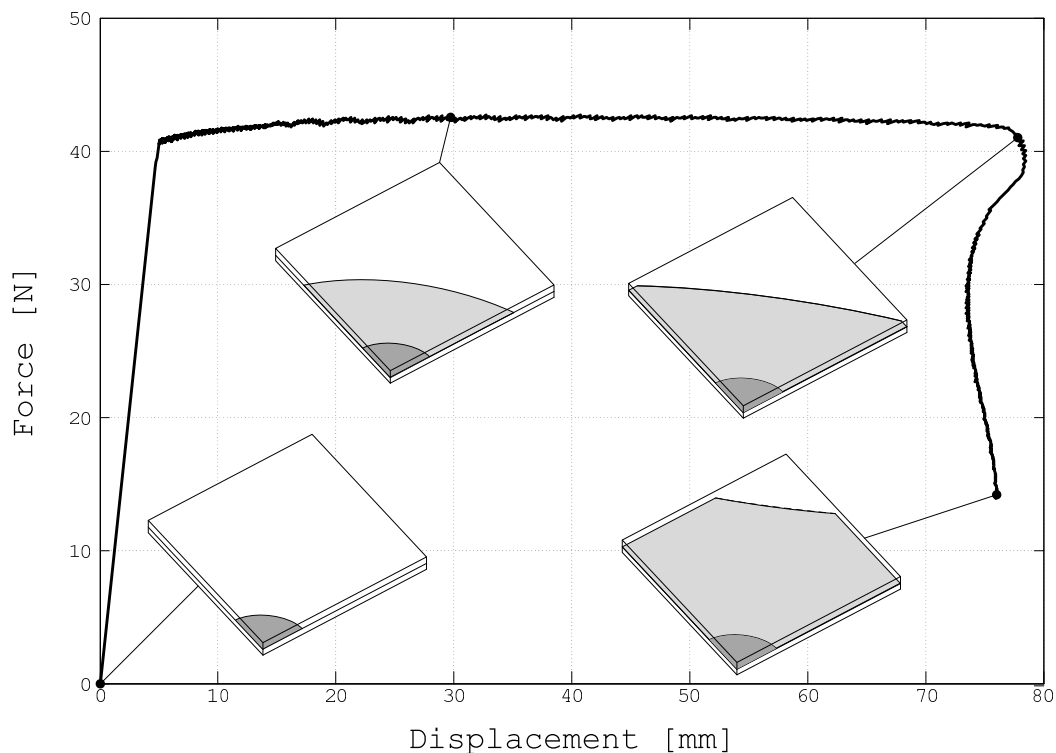

Figure 5.6: Predicted structural response of the plate subject to a vertical displacement load.

Semi–Analytical Approach The semi–analytical approach presented in the Chapter 4 can be used to predict the total energy released for delaminations with curved fronts with some restrictions, i.e. no information about the local distribution of the energy release rates, the mode mix, and the quality of the predefined shapes of the delamination front is obtained. Nevertheless, the semi–analytical approach is used in the following for prediction of consecutive growth of delamination with curved fronts to gain some understanding of the advantages and disadvantages of the proposed methods.

As the mode mix cannot be determined for the current problem with the semi–analytical approach some assumptions need to be made. At first, it is assumed that delamination growth under pure mode I conditions takes place along the entire delamination front. Hence, for the considered material the critical energy release rate takes its smallest possible value and the predicted delamination growth loads are conservative estimates of the load carrying capacity of the plate. Alternatively, it is assumed that the delamination grows in pure mode II conditions, so that the critical energy release rate takes its greatest possible value and an upper estimate of the load carring capacity is obtained.

The compliance for the prescribed loading scenario and its derivatives are directly derived as functions of the delamination coordinates from the numerical data computed for the total delamination front criterion. The load factors required to cause delamination propagation with respect to delamination coordinates a_1 and a_2, respectively, are computed by means of Eq. (4.10). Starting from the circular starting delamination incremental delamination growth is predicted. For the pure mode I assumption the predicted delamination growth load is smaller than the one predicted by the total delamination front criterion, for the pure mode II assumption the growth load is greater than the one predicted by the total delamination front criterion, see Fig. 5.8. This results are in good agreement with the fact that in the analysis employing the total delamination front criterion the fracture mode mix is shown to be in average right in between mode I and mode II.

Virtual Crack Closure Technique The delamination propagation capability of the VCCT–tool provided by *ABAQUS* is used to simulate consecutive delamination growth. As discussed in the introduction some of the principles of the VCCT formulation are violated if consecutive growth of delaminations with curved fronts is simulated. Accordingly the results are questionable and need to be interpreted with care.

A similar FEM model as disscuced before is used, now a simple tiling mesh with an element length of 1 mm is employed. The bonded nodes are chosen in a way that a zig–zag approximation of the smooth starting delamination front is obtained, shown in Fig. 5.7 (left). Hence, the approximation of the delamination front is not smooth and the mesh is not orthogonal to the delamination front. Consecutive delamination growth is simulated within a non–linear FEM analysis and the predicted structural response is shown in Fig. 5.8 in terms of the displacement of the loading point and the reaction force at the loading point. Comparison with the proposed total delamination front criterion shows that a smaller delamination growth load is predicted. This is caused by the zig–zag approximation of the smooth delamination front. For nodes that lie behind the smooth front a much greater energy release rate is computed than for the nodes that lie ahead of this front. Hence,
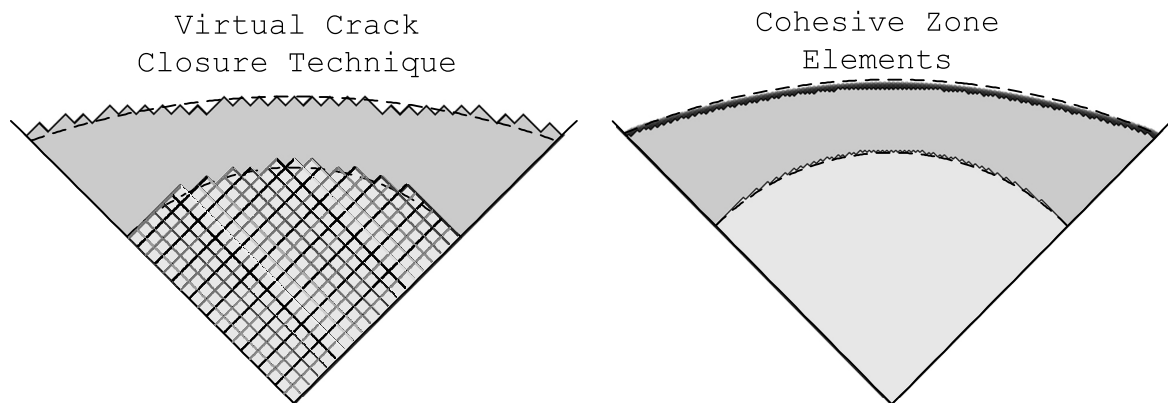

Figure 5.7: Zig–zag approximation of the delamination front for the laminated plate; starting delaminations (light gray region) and some advanced delaminations (dark gray region) predicted by Virtual Crack Closure Technique (left) or cohesive zone elements (right) used; shapes predicted by the proposed total delamination front criterion (dashed line).

delamination growth is always predicted to take place at the nodes behind the smooth front and the growth load predicted is smaller than the growth load predicted with a mesh that allows for a smooth representation of the delamination front.

In Fig. 5.7 (left) intermediate delamination fronts predicted by standard VCCT (dark gray region) and by the proposed approach (dashed line) are shown together with the circular starting delamination. Comparison shows that almost the same intermediate shape of the delamination front is predicted.

Cohesive Zone Elements An alternative approach for the prediction of consecutive delamination growth within the FEM is the usage of CZE. An FEM model similar to the one
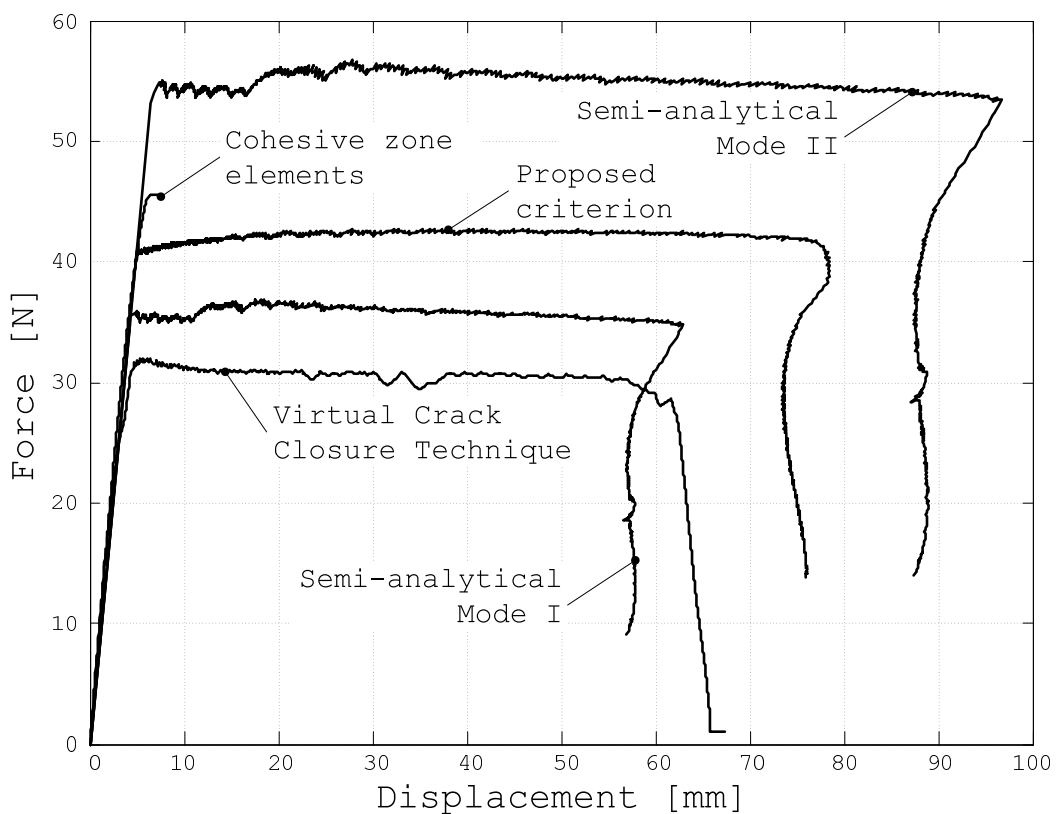

Figure 5.8: Predicted structural response of the plate subject to a vertical displacement load; various methods applied.

used for the proposed total delamination front criterion is employed. As discussed in [75] a fine mesh is required that represents the damage zone adequately. Here an element length of 0.25 mm is used. To keep the numerical effort for the FEM analysis within reasonable limits the plate is loaded only up to a total displacement of 8 mm. Hence, the delamination will propagate by some 10 mm and it is sufficient to study a plate with a reduced size of 40 mm times 40 mm. In the bonded region CZE with a thickness of 0.02 mm are defined to connect the sublaminates and, again, the circular starting delamination is represented in an approximative manner by a zig–zag line, see Fig. 5.7 (right). The stiffness of the CZE as well as the damage onset and the damage evolution law are defined as discussed in Section 3.

Delamination growth is simulated within a non–linear FEM analysis and the corresponding structural response is shown in Fig. 5.8. The predictions show that delamination growth starts at about 45 N. Investigating the damage evolution in selected elements in detail shows that the mode mix in the CZE changes during damage evolution from mode II dominated to mode I dominated. However, the CZE available in *ABAQUS* do not take such changes into account and hence the total energy required to separate the sublaminates is not computed correctly. This might be the reason why the delamination growth load predicted by the model employing CZE is higher than the load computed with the proposed approach.

Comparison of predicted shapes of some intermediate delamination front in Fig. 5.7 (right) shows that the shape predicted by the proposed approach (dashed line) is slightly more curved than the shape predicted by the model employing CZE (dark gray region).

5.2.2   Curved Laminate

Growth of a delamination in a curved laminate is investigated by employing the proposed total delamination front criterion. Details concerning geometry, loading, and layup of the laminate are shown in Fig. 5.9. The orientation of the plies is given with respect to the xy–

plane. A delamination in the midplane of the layup is considered, i.e. the delamination is located between two 0° plies and the laminate is split into two sublaminates with a thickness of 1.05 mm each. The structure is loaded on both legs with a prescribed displacement of 1 mm in positive and negative x–direction, respectively. Hexahedral continuum elements with linear shape functions and full integration are used. Each ply is represented by two elements over the ply thickness and all element aspect ratios are close to unity. The
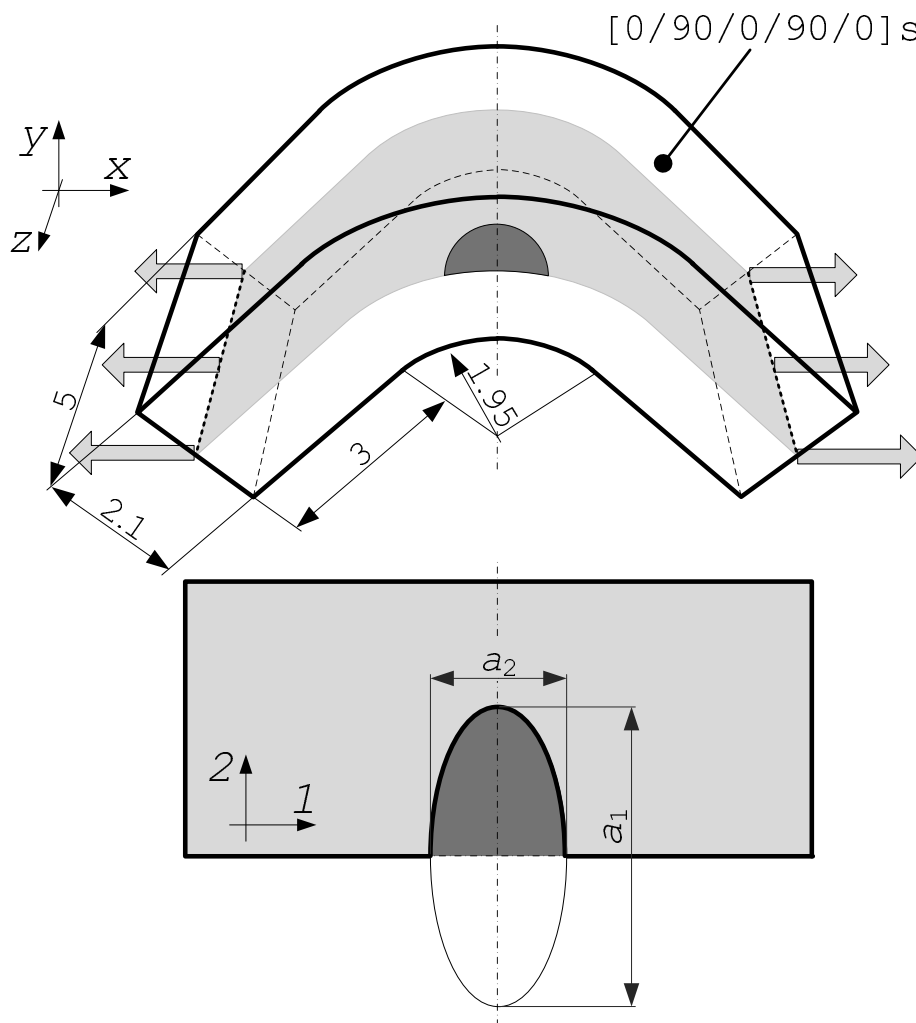

Figure 5.9: Delamination in a curved laminate; definition of geometry, layup, and loading (top); elliptical shape of the delamination front plotted with respect to the unfolded reference plane (bottom).

geometry, the layup, and the loading are symmetric with respect to the yz–plane, thus, only one half of the structure has to be modeled.

To simplify the definition of the shape of the delamination front and the presentation of the results the unfolded symmetry plane is used as reference plane, see Fig. 5.9 (bottom). Within this reference plane the shape of the delamination front is assumed to be described by an ellipse centered at the edge. Hence, two delamination coordinates are required to describe the delamination. In the following the magnitude of the major axis, a_1, and the minor axis, a_2, are used for this purpose.

Consecutive Delamination Growth

An FEM model parametrized in the delamination coordinates is set up and 29 discrete values of delamination coordinate a_1 in the range between 1 mm and 200 mm and 10 discrete values of delamination coordinate a_2 in the range between 1 mm and 9 mm are chosen. For each combination of delamination coordinates an FEM model, with a mesh locally orthogonal to the delamination front, is generated and the structural compliance as well as the energy release rates at each node along the delamination front are computed within a series of linear analyses.

A circular starting delamination with a diameter of 1 mm is considered and consecutive delamination growth is predicted. In Fig. 5.10 the starting delamination (dark gray region), some intermediate delamination fronts (dashed lines), and the final delamination (gray region) are shown for the curved laminate (top) and for the unfolded reference plane (bottom). For reasons of clarity only a limited number of intermediate delamination fronts is shown in the curved laminate. The results show that the delamination first grows in a_1 and a_2 direction and a through–the–width delamination is formed. Further growth is taking place mainly in a_2 direction and the delamination fronts straightens out. The prediction is stopped as the delamination coordinate a_2 reaches a value of 9 mm. Consideration of greater values of the coordinate would result in delaminations that interact with the applied

boundary conditions. The corresponding structural response is shown together with some intermediate delaminations in Fig. 5.11. The predicted response is linear up to the point where the delamination growth load is reached (5.8 mm or 495 N), followed by unstable equilibrium growth. The delamination load decreases as the delamination size increases, leading to a pronounced snap–back behavior of the structure. As soon as a through–the–width delamination is formed growth becomes stable and a load increase is required to propagate the delamination. Concerning the critical energy release rate, the results show that in the beginning growth is mode I dominated but as soon as a through–the–width
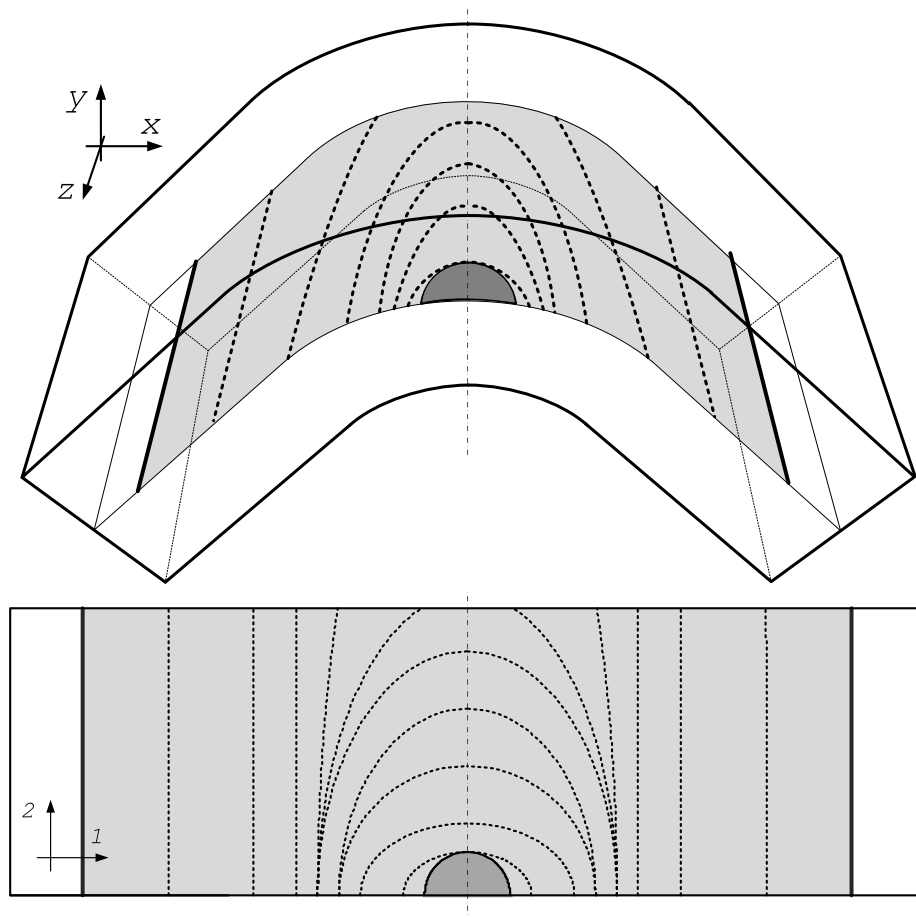

Figure 5.10: Predicted consecutive delamination growth for the curved laminate subject to a horizontal displacement load; starting delamination (dark gray region), intermediate delamination fronts (dashed lines), final delamination (gray region).

delamination is formed growth is mode II dominated.

Quality Check of the Delamination Front

The next question to be answered is whether or not an ellipse centered at the free edge allows for a proper description of the shape of the delamination fronts. In Fig. 5.12 the normalized energy ratios are plotted along the delamination front for selected delaminations. For comparison a ratio of unity is plotted as dashed line. Visual inspection of the results for the circular starting delamination, Fig. 5.12 (top, left), shows that the normalized energy ratio is close to unity along the entire front. The standard deviation of the normalized energy ratio is small (s= 0.036). In Fig. 5.12 (top, right) the delamination front is shown
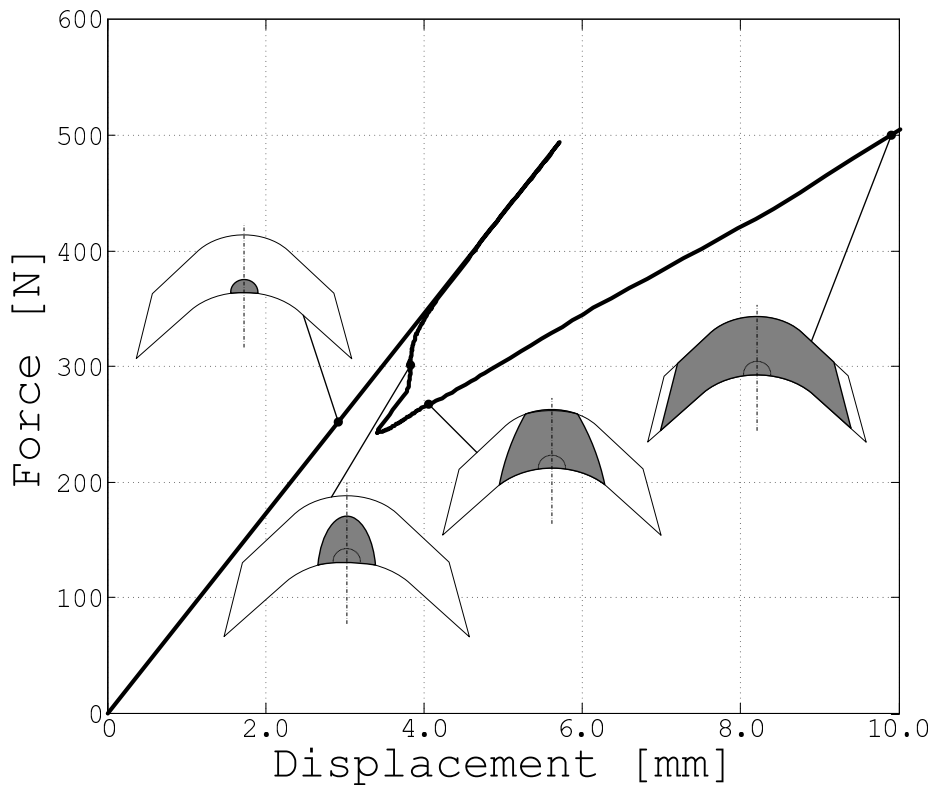

Figure 5.11: Predicted structural response for the curved laminate subject to a horizontal displacement load.

for a state just before a through–the–width delamination is formed. Here the normalized energy ratio is greater than unity at sections where the delamination meets the free edge and smaller than unity at the top. However, the standard deviation of the normalized energy ratios is quite small (s=0.106). The distribution of the normalized energy ratios suggests that the description of the shape improves, if the center of the ellipse is moved in negative 2–direction. Similar results are found for the through–the–width delamination, as shown in Fig. 5.12 (bottom, left). The results for a delamination front close to the final delamination (Fig. 5.12, bottom, right) show that the normalized energy ratio is close to unity along the entire front. To summarize these findings, it can be said that an ellipse centered at the edge allows for a proper definition of the shape of the delamination front during the entire growth process for the geometry studied in this section.
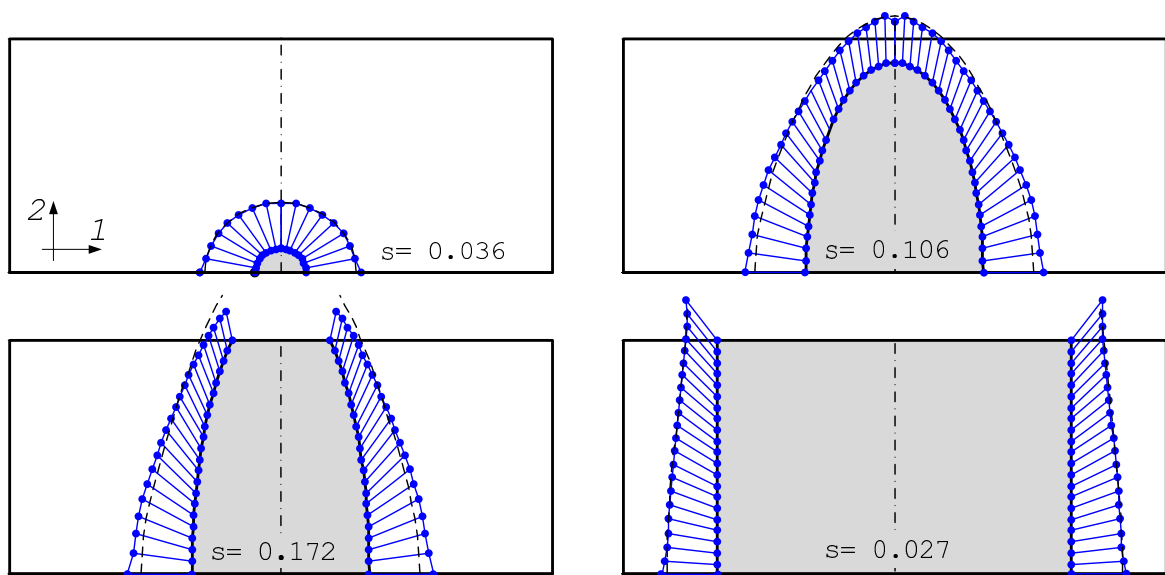

Figure 5.12: Predicted consecutive delamination growth in the curved laminate subject to a horizontal displacement load; normalized energy ratios and their standard deviations for selected delamination fronts.

5.3 Summary

A total delamination front criterion for the prediction of consecutive growth of delaminations with curved fronts is proposed. Growth along the entire delamination front is assumed to take place if the total energy released is equal to the total energy required to create new delaminated area. Possible shapes of the advanced delamination fronts are predefined and are prescribed by a number of delamination coordinates. They are assumed to be continuous, smooth, and geometrically compatible with respect to the current delamination. For computation of the growth load all shapes are analyzed within a fully automated procedure employing the FEM. From all geometrically compatible shapes the one for which the growth load is smallest is selected and incremental delamination growth and the corresponding structural response are predicted. A "quality check" is developed to assess whether or not an assumed shape of the delamination front is a good approximation. This check allows to compare individual shapes and to improve them systematically. The proposed total delamination front criterion allows to handle stable and unstable equilibrium growth in a numerically efficient manner and provides systematic and general understanding of delamination problems.

Delamination growth in a laminated plate and in a curved laminate are analyzed successfully. The delamination in the plate grows stably in the first part and in an unstable way in the second part of the loading scenario. Comparison to results obtained by other methods shows that the proposed approach is more accurate and computationally more efficient. The results show that for the prediction of the delamination growth load it is essential to take the fracture mode mix into account. For the curved laminate structural snap–back behavior is found.

Chapter 6

Computational and Experimental Investigation

Emergence and growth of delaminations in an L–shaped FRP laminate loaded by quasi–static loads is predicted computationally. The predictions are compared to results of experimental tests performed at the *Polymer Competence Center Leoben GmbH* (*PCCL*, Austria). The specimens used for testing were produced by *FACC AG* (Ried, Austria). To avoid the problem of interacting failure modes during experimental testing a specific test setup is proposed that enforces load states for which delamination is the dominant failure mechanism. First, emergence of delaminations in flawless specimens is predicted and tested experimentally. Second, test specimens with initial delaminations of defined size and location are considered and delamination growth and its stability are investigated.

For the prediction of emergence of delaminations the strength/energy approach presented in Chapter 3 is employed. Delamination growth is predicted using the semi–analytical approach presented in Chapter 4.

Table 6.1: Material and interface data of plies made of *Cycom*® *977–2–35%–12KHTA–134–300*; data provided by *FACC AG* (* Estimates following similar materials; ** following Puck's guidelines for carbon fiber materials [53]).

Elastic constants				
E_l	$E_q = E_n$	$G_{lq} = G_{ln}$	$\nu_{lq} = \nu_{ln}$	ν_{qn}
133 GPa	9 GPa	4.4 GPa	0.35*	0.2857*

Strength						
	R_{ll}	R_{qq}	R_{lq}	p_{lq}	p_{qn}	f_{weak}
tension	2104 MPa	82 MPa	103 MPa	0.35**	0.27**	0.86
compression	1407 MPa	249 MPa	103 MPa	0.3**	0.27**	0.86

Critical energy release rates	
$\mathcal{G}_{\text{Ic}}$	$\mathcal{G}_{\text{IIc}}$
133.1 J/m²	458.8 J/m²

6.1 Test and Specimen Design

Delamination in an L–shaped structure build up by plies made of *Cycom*® *977–2–35%–12KHTA–134–300*, which is a unidirectional carbon fiber reinforced epoxy resin with a resin volume content of 35% and a weigth of $134\frac{\text{g}}{\text{m}^2}$, is investigated. The thickness of the plies is 0.125 mm. Their mechanical properties are provided by *FACC AG* and are given in Table 6.1. For definition of the material parameters see Section 3.3.

The test specimens are produced by *FACC AG*. For the production an available hard tool is used, so that the outer radius and the length of the legs of the specimen are fixed. Only 0° and 90° plies are used and the prediction of emergence of delaminations is simplified by grouping together a number of plies with the same orientation. These groups of plies can be assumed to act like a single ply, so that the number of interfaces where delamination might occur is reduced. Various layups, i.e. ply numbers and ply orientations,

are analyzed using the proposed strength/energy approach. Based on the results obtained, a symmetric $[0_3/90_3/0_3/90_3/0_3]_s$ layup with a total thickness of 3.75 mm is selected for the test specimens, i.e. three plies of the same orientation are grouped together and in total 30 plies are used. For this layup delamination is the predicted dominant failure mode and no matrix or fiber failure is expected to occur. The dimensions of the proposed test specimen and the loading device are shown in Fig. 6.1. The ply orientations are measured with respect to the xy–plane. Similar test specimens were investigated in [43, 34] and are used in a standard ASTM procedure [7] for determining the interlaminar out–of–plane strength of plies of FRP.

For the production of the specimens a steel tool is used on the outside and a soft tool (vaccum bag) is used on the inside of the specimens. The prepregs are placed between
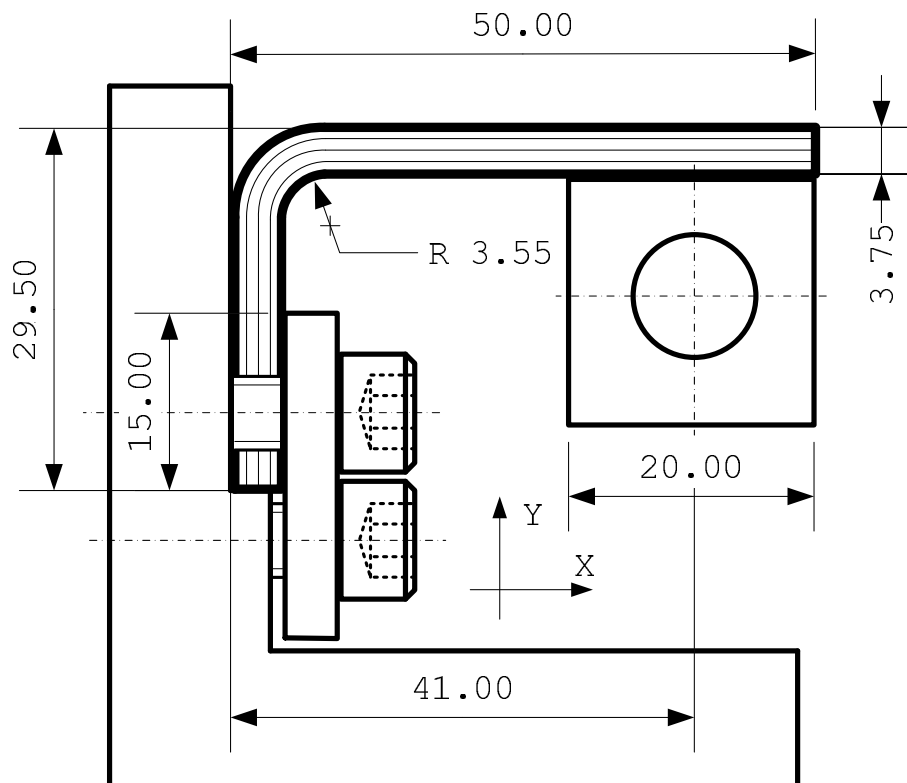

Figure 6.1: Test design of the L–shaped curved laminate with a $[0_3/90_3/0_3/90_3/0_3]_s$ layup; clamped in a loading device and a loading block glued on (dimensions in mm).

these tools and are cured in an autoclave process. This way an L-shaped structure is created which is some 300 mm long. This structure is then cut into ten test specimens with a width of 30 mm each. In Fig. 6.1 the specimen is shown together with the proposed loading device. The specimen is clamped in the loading device at the vertical leg; on the horizontal leg a steel loading block is glued to the specimen and a displacement load in vertical direction is applied. For the specimens with initial delaminations a through–the–width non–adhesive Teflon strip is placed between plies nine and ten. The size and the position of the strip are selected based on the results predicted by the semi–analytical approach, see Section 6.4.1.

Some problems occurred during the production of the test specimens; the soft tool on the inside could not hold the prepregs in place, so that the laminate shows a crimped surface and its thickness is not constant. Varying fiber volume fractions and material properties cannot be excluded. Nevertheless, it is not expected that the qualitative structural behavior is affected.

6.2 Experimental Procedure

The production of the loading device and all experimental tests are done at the *Polymer Competence Center Leoben GmbH* (*PCCL*, Austria). The experimental test setup is shown in Fig. 6.2. The loading device with the specimen (see Fig. 6.2 (left)) is introduced into the wedge–screw grips of a Zwick Z250 universal tensile–compression testing machine (*Zwick GmbH & Co. KG*, Ulm, Germany) and the machine force and displacement are measured. All tests were performed at a cross-head speed of 2 mm/min in a laboratory environment of 23°C and 50% relative humidity. In addition, to determine the local strain distribution, optical full-field strain measurements are performed using the 3D image correlation photogrammetry system *ARAMIS* (*GOM*, Braunschweig, Germany), see Fig. 6.2 (right). For this purpose a stochastic dot pattern is applied on the surface of all specimens by using an

aerosol spray. Prior to testing the system was calibrated with special calibration plates to correct distortions of the lenses and to calibrate the position of the camera.

6.3   Crack Kinking

The semi–analytical approach proposed is based on the assumption that the delamination grows along the interface between two plies. This is true for delaminations between two $0°$ plies where the delamination front is normal to the fiber orientation. In this case the fibers would bridge the delamination if it grew into one of the plies. In the case of delaminations between $0°$ and $90°$ plies, where the delamination front is oriented parallel to the fibers of the $90°$ ply, the delamination can grow into the $90°$ ply without any fiber bridging. The question whether such delaminations grow along the interface or grow into the $90°$ ply is discussed in the following.

For the prediction of kinking of a crack in an isotropic material various criteria have been developed, see e.g. [24]. For mixed mode cracks where the mode I loading is dominant
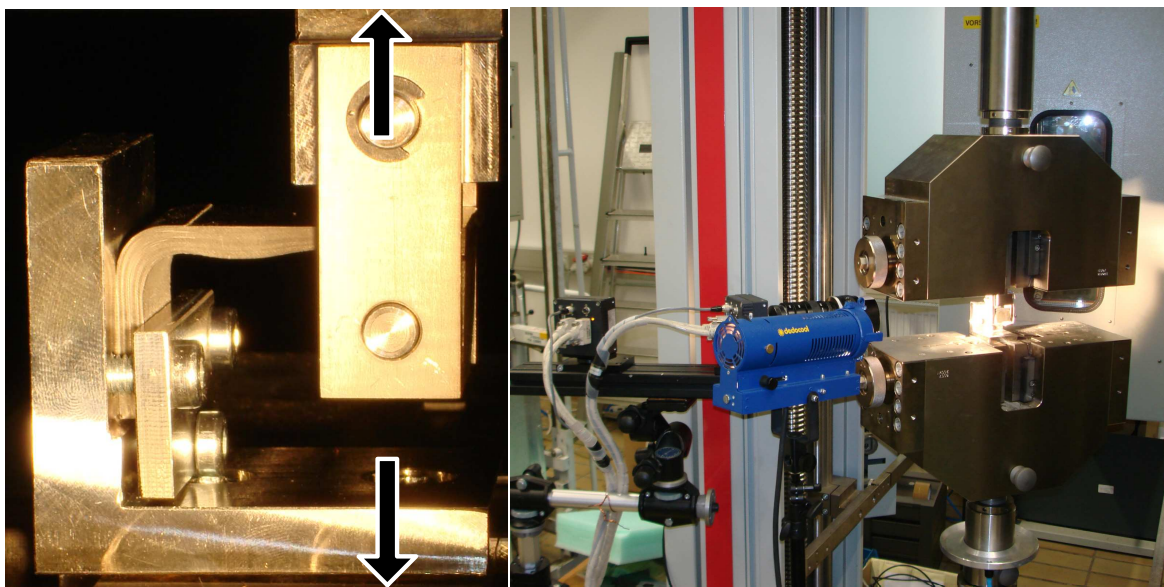

Figure 6.2: Test specimen and loading device (left); experimental test set up (right).

all these criteria lead to the prediction that the crack will kink by an angle φ which is proportional to the negative ratio of the mode II stress intensity factor and the mode I stress intensity factor. For a definition of the kink angle φ see Fig. 6.3. The mode I stress intensity factor is always positive, so the sign of the kinking angle is solely determined by the sign of the mode II stress intensity factor. The latter is proportional to the shear stresses ahead of the crack tip along the $\varphi = 0$ line, so that the sign of the kinking angle is determined by the sign of the shear stresses ahead of the crack tip. If the shear stresses are positive the crack will kink with a negative angle, if the stresses are negative the crack will kink with a positive angle.

The preceding considerations are valid for cracks in an isotropic material with constant fracture toughness and cannot be directly applied to an interface crack. However, an approximative prediction of the kinking tendency of interface cracks can be done following [24]. It is assumed that the interface and the ply have the same fracture toughness and that the delamination has already grown a bit into the 90° ply, see Fig. 6.3. The tip of the delamination front can now be considered to be located within a homogeneous material and the kinking criteria for homogeneous materials can be applied. If the kinking angle is predicted to be negative the delamination will grow towards the 90°/0° interface. As it will not grow into the 0° ply it will grow along the interface. If the kinking angle is predicted to be positive the delamination will grow into the 90° ply and maybe reach its opposite
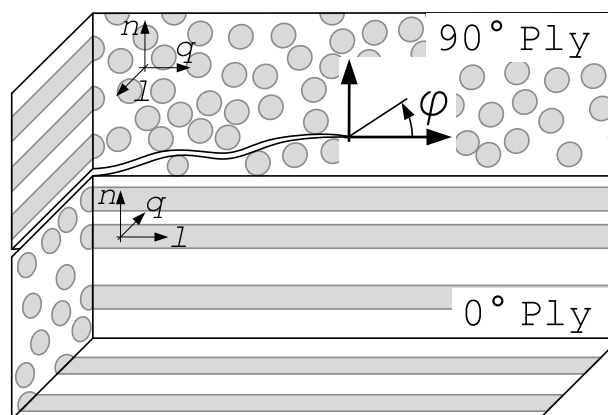

Figure 6.3: Prediction of the direction of crack growth; definition of the kinking angle φ.

interface.

It should be noted that the proposed procedure allows only for a rough estimate of the direction in which a delamination tends to kink. For a more detailed analysis of delamination kinking failure mechanisms on the length scale of the fiber diameter need to be considered and the local distribution of the fibers has to be taken into account.

6.4 Results

6.4.1 Computational Predictions

Free edge effects are not expected to influence the overall structural response. Thus, a two–dimensional generalized plane strain FEM model of the test specimen is set up. Each ply is represented by three linear elements over the ply thickness and all element aspect ratios are close to unity. Previous analyses [81] of similar curved laminates have shown that residual stresses from the curing process hardly affect the delamination process. Such stresses are, therefore, not considered here. The loading and the boundary conditions are shown in Fig. 6.4. At the clamped part of the vertical leg the displacements in horizontal and vertical directions are fixed. In the region to which the loading block is glued a rigid coupling with the loading point is defined. The part of the steel loading device that is in contact with the specimen is also modeled and frictionless contact is modeled.

Emergence of Delaminations

Emergence of delaminations is predicted using the strength–energy approach discussed in detail in Chapter 3. A displacement of 2.4 mm in vertical direction is applied and a geometrically non–linear FEM analysis is conducted. Concerning the contact between the test specimen and the steel loading device the results show that the contact zone is very

small and hardly changes during loading. In all further FEM analyses the displacement in x–direction in the contact zone is, therefore, fixed and contact between the specimen and the loading device is approximated this way.

The stresses computed within the FEM analysis are evaluated with the Puck FPF criterion. The predicted load factor and failure mode are presented in Fig. 6.4, showing a critically loaded region at the interface between plies nine and ten, counting from the inner to the outer radius ($[0_3/90_3/0_3/||/90_3/0_6/90_3/0_3/90_3/0_3]$ where $||$ indicates the overloaded interface). The expected failure mode is delamination, so that in the pristine structure an initial delamination is assumed to form there.

By increasing the applied displacement beyond the FPF load the size of the assumed initial delamination is increased as shown in Fig. 6.5 (top, delamination initiation curve). Onset of growth of initial delaminations of various sizes is analyzed using the VCCT, yielding the delamination propagation curve Fig. 6.5 (top). The intersection of these curves defines
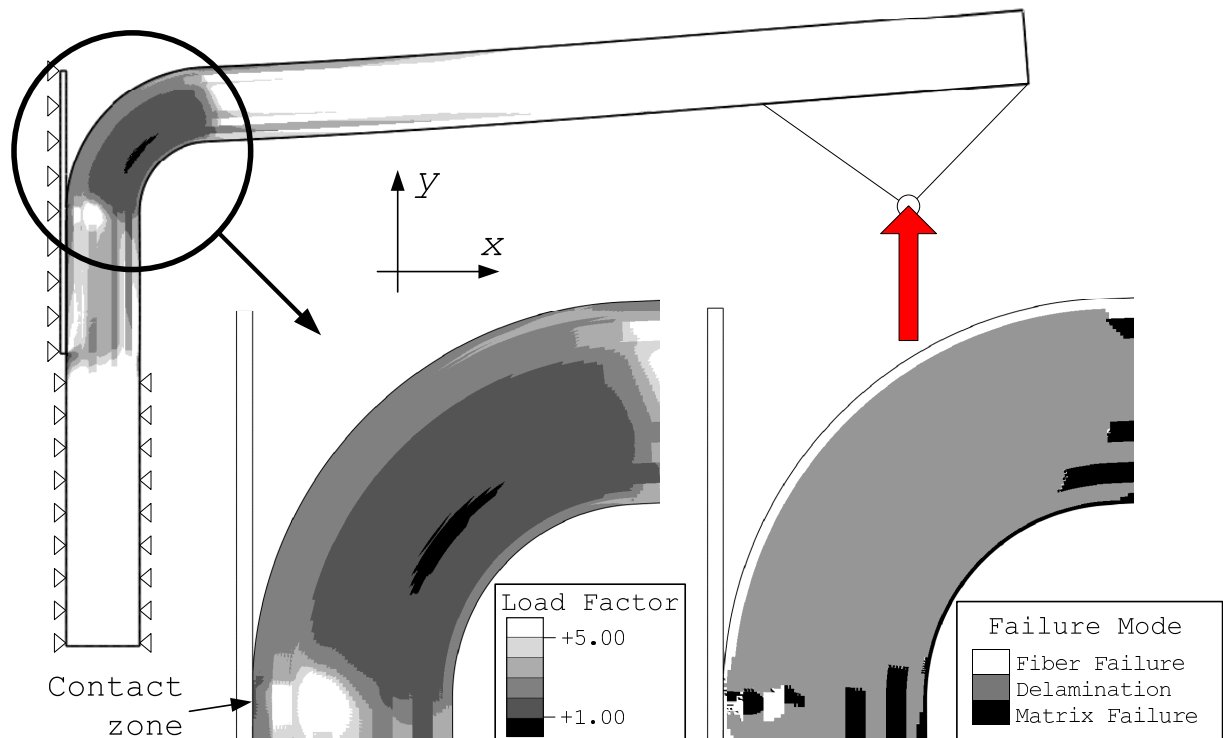

Figure 6.4: Predicted load factor and failure mode in the L–shaped laminate.

the critical initial delamination (0.6 mm) and the load at which this delamination emerges (u= 2.36 mm).

Knowing the size and the location of the critical initial delamination as well as the delamination load the non–linear structural response caused by the delamination process can be predicted within a non–linear FEM analysis, Fig. 6.5 (bottom). The pristine structure is loaded and in point 1 the predicted delamination load is reached. The critical initial delamination is introduced, while keeping the applied displacement constant. This leads to a change of the structural stiffness and to a reduction of the reaction force, point 2. Beyond point 2, still maintaining the same displacement load, unstable delamination growth takes place which leads to a considerable increase of the delaminated area. In point 3
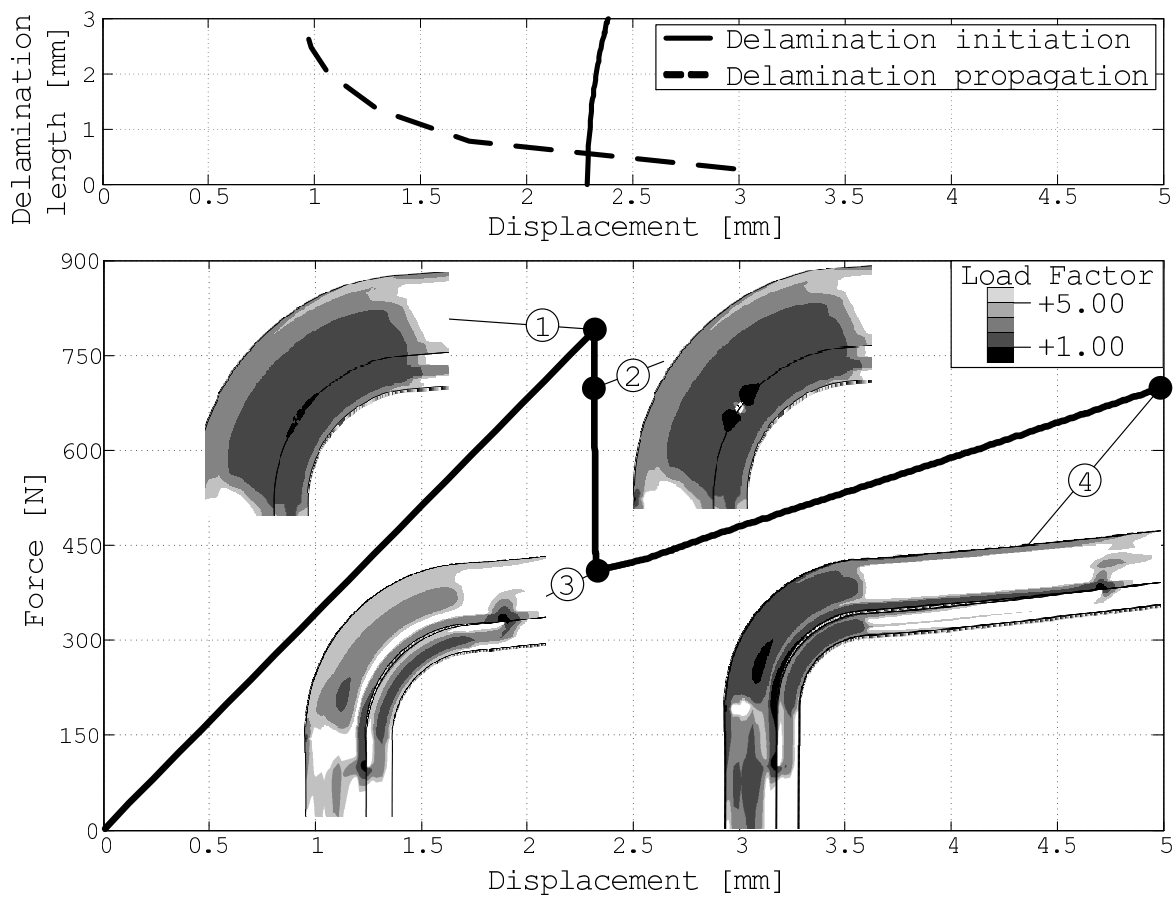

Figure 6.5: Predicted delamination process in the L–shaped laminate; delamination initiation curve and delamination propagation curve (top), structural response (bottom).

delamination growth changes from unstable to stable. Hence, the prescribed displacement has to be increased to cause further delamination growth.

Between point 2 and point 3 unstable delamination growth takes place. Such growth might accompanied by dynamic effects, but they are not considered in the present analysis and the predicted structural response beyond point 3 is, therefore, only an approximation. In point 4 a load factor smaller than unity is predicted in the outer part of the curved section and the analysis is stopped. Delamination is predicted to occur there and the proposed strength/energy approach can be used, of course, to predict the emergence of a second delamination.

Growth of Existing Delaminations

So far, emergence of delaminations in an initially flawless structure was discussed, now the structural response of specimens with initial through–the–width delaminations is predicted using the semi–analytical approach presented in Chapter 4. Specimens with an initial delamination in the interface between plies nine and ten are considered; this interface is chosen as it is the critical one in the flawless case. The FEM model described above is parametrized in the delamination coordinates and the compliance as well as the mode mix are computed for the entire parameter field of delamination coordinates. Based on the data generated equilibrium delamination growth and its stability is predicted. Three initial delaminations are selected as examples and for each one the structural response is shown in terms of the force–displacement curve in Fig. 6.6. The delaminations are placed within the interface at their most detrimental positions, i.e. positions where the load required to propagate the delamination is smallest. For the small initial delamination with a length of 1 mm the structural response is linear until the delamination growth load (u= 1.75 mm) is reached. Then unstable equilibrium delamination growth takes place, the equilibrium load decreases as the delamination size increases. As soon as a certain delamination size is reached growth becomes stable and a load increase is required to propagate the delami-

nation further. Such pronounced snap back behavior can only be realized theoretically, in displacement–controlled experiments unstable delamination growth would take place as indicated by the thin dashed line. For the intermediate initial delamination (3 mm) growth is stable under displacement controlled loading but would be unstable under force controlled loading. For the large delamination (5 mm) growth is stable for all loading conditions.

Crack Kinking

Kinking of the 3 mm initial delamination is investigated. In Fig. 6.7 the shear stresses which are relevant for delamination kinking, i.e. σ_{ln} of the 0° ply and σ_{qn} of the 90° ply, are shown. At the top delamination front the shear stresses are negative, thus the delamination will kink with a positive angle and grow into the 90° ply. At the bottom delamination front the shear stresses are positive and the delamination will kink with a negative angle and grow again into the 90° ply. These predictions are based on criteria for kinking of a crack in an
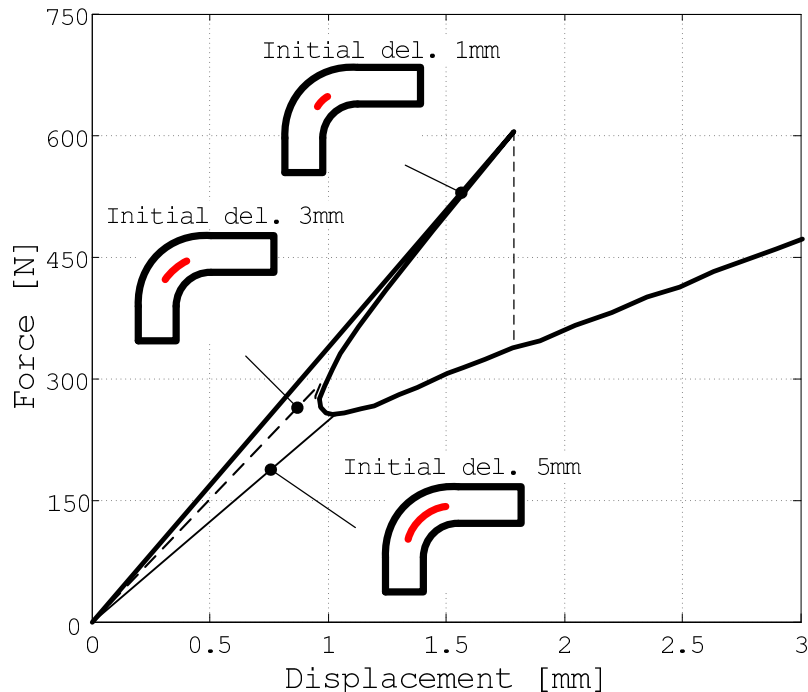

Figure 6.6: Predicted structural response caused by equilibrium delamination growth in the L–shaped laminate; three sizes of initial delaminations considered.

isotropic material. Furthermore, it is assumed that the critical energy release rate of the ply and the interface are the same and that the delamination front is parallel to the fibers of the 90° ply.

Note, that delamination kinking is not considered in the strength/energy approach and in the semi–analytical approach. These approaches are based on the assumption that the delamination will grow along the interface.

6.4.2   Experimental Testing

Based on the computational predictions two sets of test specimens are selected for experimental testing. First, test specimens without initial delaminations are tested and unstable delamination growth as predicted in Fig. 6.5 (bottom) is expected to occur. Second, test specimens with an initial delamination are tested. An initial delamination length of 3 mm, centered in the curvature of the specimen, is selected and a structural response similar to the predictions in Fig. 6.6 (intermediate initial delamination) is expected to occur.
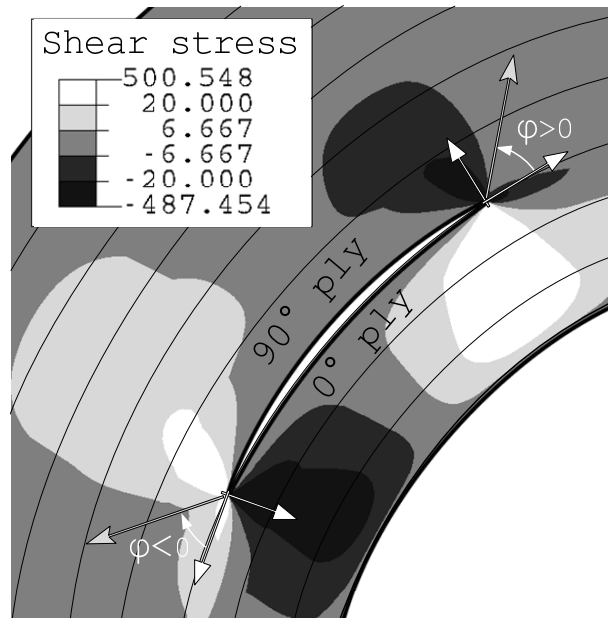

Figure 6.7: Predicted delamination growth direction for a 3 mm initial delamination in the L–shaped laminate.

Three specimens without initial delamination are tested; a picture of one of the specimens is shown together with the measured force–displacement (machine displacement) curves in Fig. 6.8. At first the structural response is approximately linear. At a force level of about 670 N an initial delamination is formed and unstable delamination growth starts, which changes to stable growth as soon as a certain delamination size is reached. The scatter in the measured data can be explained by two main reasons. On the one hand, there is some geometrical variation and the thickness of the laminate varies within each specimen and among the specimens (variation of the thickness shown for one specimen in Fig. 6.8). On the other hand, some problems when clamping the specimens occur due to the wedge form of the vertical leg of the specimen. Some slipping of the specimen in the loading device takes place during the entire loading process and at an applied displacement load of about 3.7 mm specimen #1 and specimen #2 slip out of the loading device. In Fig. 6.9 (right) the maximum principal in–plane strains measured at the free surface of the specimen with the digital image correlation system are shown for specimen #1 for an applied displacement load of about 2.5 mm. The picture shows that the strains are highest in the curvature of
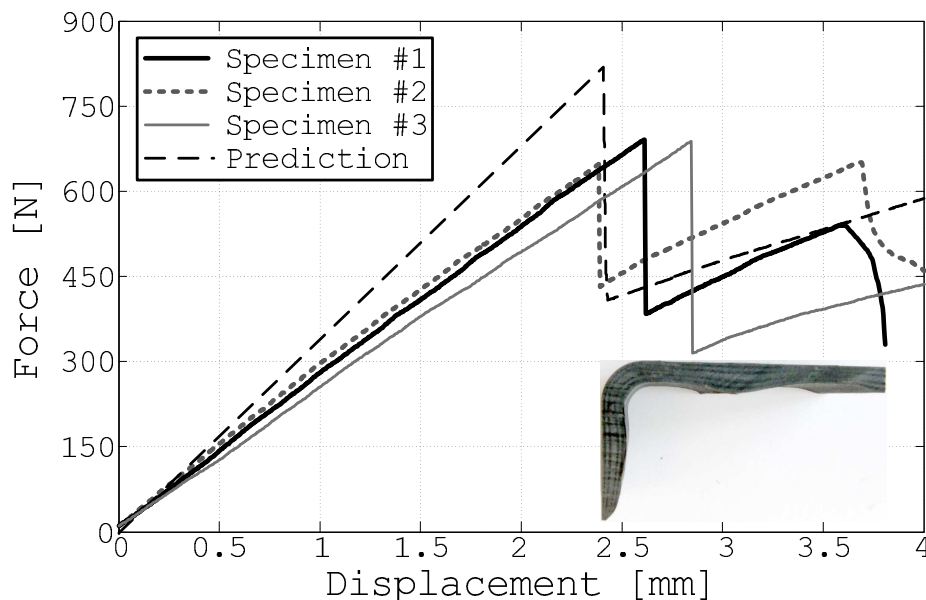

Figure 6.8: Measured and predicted structural response for L–shaped laminates without initial delaminations.

the laminate. At this location an initial delamination is formed at higher loads.

In the second run three specimens with a 3 mm wide Teflon strip inserted between plies nine and ten are tested. The Teflon strip is assumed not to be bonded to the adjacent plies and, hence, forms a flaw between the plies that acts like an initial delamination. The relevant force–displacement curves are shown in Fig. 6.10 togeher with a picture of one of the specimens. This picture shows that the specimens with initial delaminations posses an almost constant laminate thickness, especially in the region where the specimen is clamped in the loading device. As a consequence, for most of the specimens with initial delamination hardly any problems occurred when clamping. Detailed analysis of the results obtained by the image correlation photogrammetry system shows that in specimen #4 and #5 the Teflon strip inserted between the plies acts like an open initial delamination which propagated at a force of about 280 N in a stable manner. The non–linearity in specimen #4 at lower loads may have been caused by slipping of the specimen in the loading device. For specimen #5 and #6 no such clamping problems occurred. In specimen #6 the force increases up to 350 N, then unstable delamination growth takes place followed by stable growth. For this specimen the analysis of the results obtained by the image correlation photogrammetry system shows that the Teflon strip does not act as an open delamination. The Teflon strip is sticking on the adjacent plies and holds them together.
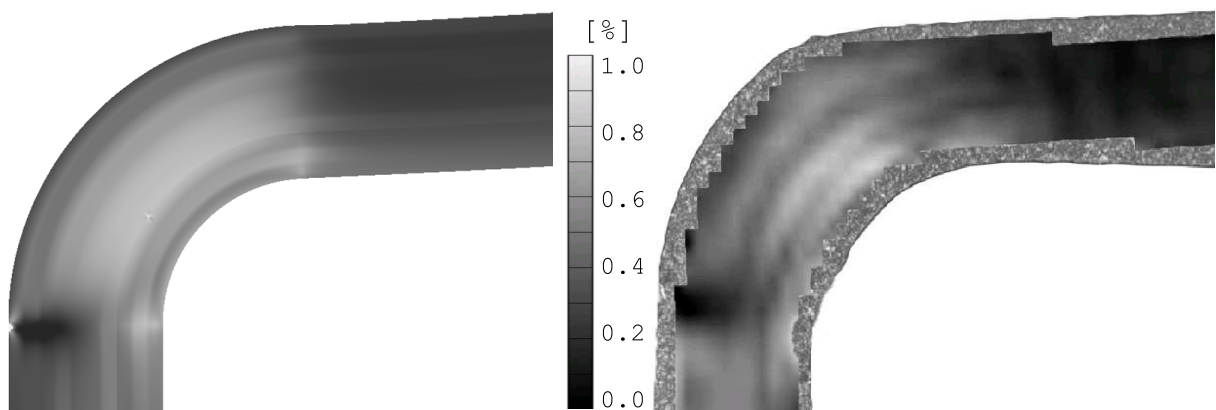

Figure 6.9: Computed (left)and measured (right) maximum in–plane strains for the L–shaped laminate at load level of about 2.36 mm.

In Fig. 6.11 (left) a picture of specimen #5 at an applied displacement load of about 2 mm is shown. The picture illustrates that kinking of the delamination takes place. Starting from the initial delamination the delamination grows across the 90° plies and then grows along its opposite 0°/90° interface (i.e. the interface between ply 12 and 13). The delaminations in specimen #4 and #6 kinked the same way. In Fig. 6.11 (right) the final state of specimen #5 is shown, corresponding to an applied displacement load of about 7 mm. The picture shows further delaminations in the curvature of the laminate which were formed at higher loads.

6.4.3   Comparison

The measured force–displacement curves shown in Figs. 6.8 and 6.10 are now compared to the computational predictions (dashed lines). For the specimens without initial delaminations (Fig. 6.8) differences concerning the predicted and the measured initial stiffnesses are observed. As such differences cannot be observed for test specimens with initial delamina-
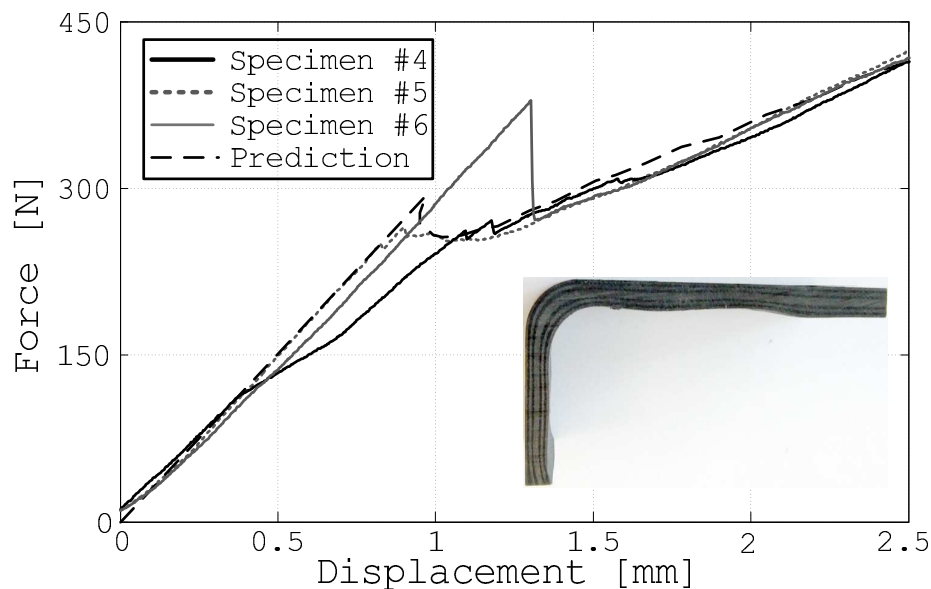

Figure 6.10: Measured and predicted structural response of L–shaped laminates with 3 mm initial delaminations.

tions (Fig. 6.10) it is assumed that they are partly caused by the non–constant thickness of specimen #1, #2, and #3 and the problems that occurred when clamping these specimens in the loading device. Detailed investigation of the results of the image correlation photogrammetry system shows further that the loading device deformed slightly at high loads. Hence, the measured machine displacement is higher than the predicted displacement and the initial stiffness is overestimated in the predictions. Concerning the delamination growth load and the growth stability the results agree reasonably good; an initial delamination is formed at the predicted load and grows in an unstable way in the first part and in a stable way in the second part.

For the specimens with initial delaminations (Fig. 6.10) the predicted and the measured initial stiffnesses are in good agreement. For specimen #5 also the prediction and the measured delamination growth load and the growth stability agree well. For specimen #4 some additional non–linearity is observed, for specimen #6 a load higher than the predicted one is required to cause delamination propagation. However, the qualitative structural response agrees well for all three specimens.

Comparing the delaminations in Figs. 6.7 and 6.11 (left) shows that the delamination has kinked in the roughly predicted direction. Note, that delamination kinking is not consid-
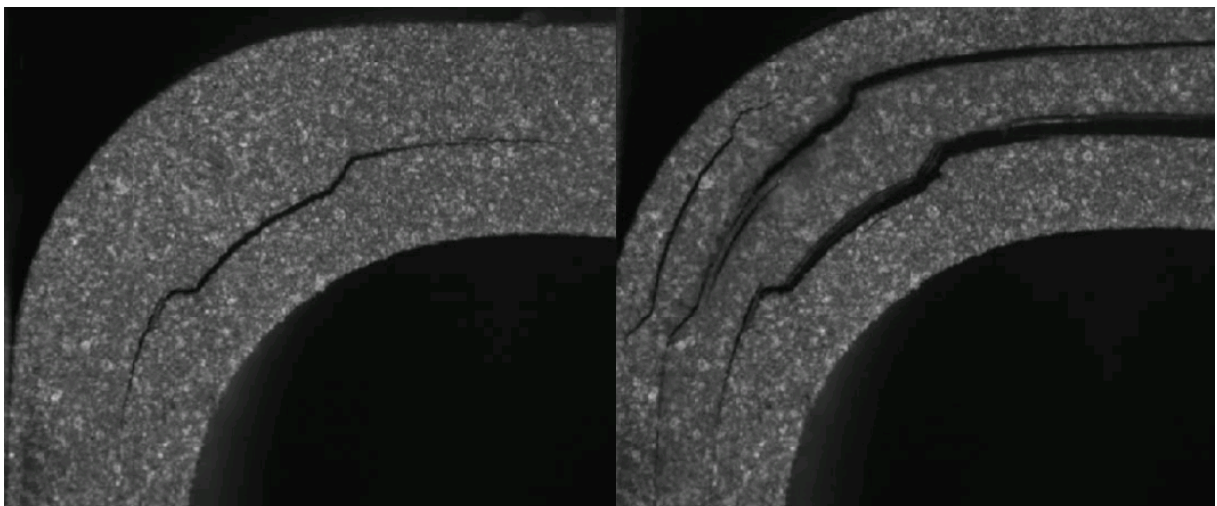

Figure 6.11: Observed delamination in an L–shaped specimen with a 3 mm initial delamination; delamination at a load level of 2 mm (left) and at a load level of 7 mm (right).

ered in the strength/energy approach and in the semi–analytical approach. Consequently, the predictions shown in Figs. 6.8 and 6.10 are based on the assumption that the delamination is growing strictly along the interface. The final configuration, Fig. 6.11 (right), reveals that additional delaminations are formed in the outer part of the laminate, which is in agreement with the predictions of the strength/energy approach, Fig. 6.5 (point 4). The maximum principal in–plane strains measured at the free surface, Fig. 6.9 (right), coincide with the strains computed by the generalized plane strain FEM model, Fig. 6.9 (left). In both cases high strains are found in the curvature of the laminate and low strains are found in the region close to the point where the specimen is in contact with the steel loading device. Note that the computed values correspond to the strain state inside the specimen remote from the free edge. However, the considered principal strains are almost the same inside the structure and at the free surface.

6.5 Summary

Numerically efficient methods for the prediction of emergence and growth of delaminations are employed to analyze emergence and growth of delaminations in a curved laminate made of plies of a unidirectional carbon fiber reinforced epoxy resin. Based on the computational predictions a test design is developed and two sets of specimens are produced by *FACC AG* and tested experimentally at the *Polymer Competence Center Leoben GmbH*. First, test specimens without any initial delaminations are tested and emergence of delaminations in the curvature of the specimens is found. For these specimens differences concerning the predicted and the measured initial stiffnesses are observed which can be explained by the non–constant laminate thickness of these specimens. The measured and the predicted delamination growth load and the growth stability agree reasonably good. Second, test specimens with an initial delamination of $3\,\text{mm}$ length are tested and stable delamination growth is observed. For these specimens the delamination behavior and the measured force–displacement curve agree well with the computational predictions. The experimental

results show further that delamination kinking takes place, such effects are not considered in the proposed approaches.

Chapter 7

Summary

Numerically efficient and robust approaches for prediction of emergence and consecutive growth of delaminations in structures made of FRP laminates are developed. For verification of the predictions a comparison with results from experimental testing is carried out. For prediction of emergence of delaminations a strength/energy approach is proposed. This approach bridges the gap between strength criteria and linear elastic fracture mechanics in a way that yields conservative results. It allows to predict critical initial delaminations and the load carring capacity of a structure. Delaminations emerging in the curvature of an L–shaped laminate and delaminations emerging from a sharp notch of a DLS test specimen are predicted successfully. For both examples it turns out that the predicted load carring capacity is more sensitive to changes in the interface strength than to changes in the critical energy release rate of the interface. Part of these predictions are verified by non–linear FEM analyses employing CZE.

For prediction of consecutive growth of delaminations with straight fronts a semi–analytical approach is proposed. This approach can handle arbitrary combinations of mechanical, displacement, temperature, and moisture loads. Quasi–static load cases can be treated as well as as load cases where some load components are constant and some load components are cyclic. The semi–analytical approach offers systematic understanding of the influence of

size and position of a delamination on the structural response. Furthermore, it allows to predict the most detrimental position of delaminations of given size but unknown location. Hence, it can be used for a fast interpretation of the results from non–destructive testing. Two examples, an L–shaped laminate and a T–joint, are investigated in detail. For the L–shaped laminate a pronounced structural snap–back behavior is found and for the T–joint a structural snap–through behavior is predicted.

For prediction of consecutive growth of delaminations with curved fronts a total delamination front criterion is proposed. The delamination is assumed to advance from its current shape to a predefined advanced shape. Growth of a delamination in a laminated plate and growth of a delamination at the free edge of an L–shaped laminate are investigated. For the plate delamination growth is predicted to be stable and for the L–shaped laminate a pronounced structural snap–back behavior is found. Comparison of these findings to results obtained by other methods shows that the total delamination front criterion is more accurate and numerically more efficient. Furthermore, it turns out that it is essential to take the actual fracture mode mix into account.

For verification of the predictions, emergence and consecutive growth of delaminations in an L–shaped laminate is predicted by the proposed approaches and tested experimentally at the *Polymer Competence Center Leoben GmbH* (*PCCL*, Austria). The specimens tested are produced by *FACC AG* (Ried, Austria). Test specimens without initial delaminations and test specimens with initial delaminations, created by a Teflon strip, are investigated and good agreement among the predicted and the measured delamination growth load and the growth stability is obtained.

Bibliography

[1] ABAQUS. *VCCT for ABAQUS, User's Manual, Version 1.1.*

[2] D. F. Adams. *Comprehensive Composite Materials*, Vol: Test Methods, Nondestructive Evaluation, and Smart Materials, Cha: Test Methods for Mechanical Properties, pages 113–146. Elsevier Science Ltd, Oxford, UK, 2000.

[3] G. Alfano and M. Crisfield. Finite element interface models for the delamination analysis of laminated composites: mechanical and computational issues. *International Journal for Numerical Methods in Engineering*, 50:1701–1736, 2001.

[4] O. Allix. *Interface damage mechanics: application to delamination.* Elsevier Science Ltd, Oxford, UK, 2002.

[5] J. Anderson and M. Koenig. Dependence of fracture toughness of composite laminates on interface ply orientation and delamination growth direction. *Composite Science and Technology*, 64:2139–2152, 2004.

[6] J. Andersons, M. Hojo, and S. Ochiai. Model of delamination propagation in brittle-matrix composites under cyclic loading. *Journal of Reinforced Plastics and Composites*, 20:431–450, 2001.

[7] ASTM. *D6415/D6415M Standard Test Method for Measuring the Curved Beam Strength of a Fiber–Reinforced Polymer–Matrix Composite.*

[8] G. I. Barenblatt. The mathematical theory of equilibrium cracks in brittle fracture. *Advances in Applied Mechanics*, 7:55–129, 1962.

[9] V. V. Bolotin. *Prediction of Service Life for Machines and Structures*. ASME PRESS, New York, 1989.

[10] V. V. Bolotin. Delamination in composite structures: its origin, buckling, growth and stability. *Composites Part B*, 27B:129–145, 1996.

[11] J. C. Brewer and P. A. Lagace. Quadratic stress criterion for initiation of delamination. *Journal of Composite Materials*, 22:1141–1155, 1988.

[12] A. J. Brunner. *Mechanics of Composite Materials and Structures*, chapter Towards Standardised Interlaminar Fracture Tests for Unidirectional Fiber–Reinforced Polymer–Matrix Composites, pages 279–287. Kluwer Academic Publishers, Netherlands, 1999.

[13] P. Camanho and C. Davila. Mixed mode decohesion finite elements for the simulation of delamination in composite materials. *NASA*, NASA/TM-2002-211737:1–42, 2002.

[14] P. Camanho, C. Davila, and D. R. Ambur. Numerical simulation of delamination growth in composite materials. *NASA*, NASA/TM-2001-211041:1–24, 2001.

[15] C. Dahlen and G. S. Springer. Delamination growth in composites under cyclic loads. *Journal of Composite Materials*, 28:732–781, 1994.

[16] B. D. Davidson. An analytical investigation of delamination front curvature in double cantilever beam specimens. *Journal of Composite Materials*, 24:1124–1139, 1990.

[17] B. D. Davidson, H. Hu, and R. A. Schapery. An analytical crack–tip element for layered elastic structures. *Journal of Applied Mechanics*, 62:294–305, 1995.

[18] G. A. O. Davies, D. Hitchings, and J. Ankersen. Predicting delamination and debonding in modern aerospace composite structures. *Composite Science and Technology*, 66:846–854, 2006.

[19] D. S. Dugdale. Yielding of steel sheets containing slits. *Journal of the Mechanics and Physics of Solids*, 8:100–104, 1960.

[20] D. Evans, I. Johnson, H. Jones, and D. D. Hughes. Shear testing of composite structures at low temperatures. *Advances in Cryogenic Engineering*, 36:819–826, 1962.

[21] F. Fosdick and L. Truskinovsky. About Clapeyrons's theroem in linear elasticity. *Journal of Elasticity*, 72:145–172, 2003.

[22] A. C. Garg. Delamination - a damage mode in composite structures. *Engineering Fracture Mechanics*, 29:557–584, 1988.

[23] A. A. Griffith. The phenomena of rupture and flow in solids. *Philosophical Transactions of the Royal Society of London. Series A*, 221:163–198, 1921.

[24] D. Gross and T. Seelig. *Bruchmechanik mit einer Einführung in die Mikromechanik*. Springer Verlag Berlin Heidelberg New York, Germany, 2001.

[25] C. G. Gustafson and M. Hojo. Delamination fatigue crack growth in unidirectional graphite/epoxy laminates. *Journal of Reinforced Plastics and Composites*, 6:36–52, 1987.

[26] H. G. Hahn. *Bruchmechanik*. Teubner, Stuttgart, Germany, 1976.

[27] Z. Hashin. Failure criteria for unidirectional fiber composites. *Journal of Applied mechanics*, 47:329–334, 1980.

[28] T. K. Hellen. On the method of the virtual crack closure extension. *International Journal for Numerical Methods in Engineering*, 9:187–207, 1975.

[29] D. Hemanth, K. S. Shivakumar Aradhya, T. S. Rama Murthy, and N. Govinda Raju. Strain energy release rates for an interface crack in orthotropic mediaa finite element investigation. *Engineering Fracture Mechanics*, 72:759–772, 2005.

[30] F. Hild. *Discrete versus continuum damage mechanics: a probabilistic perspective.* Elsevier Science Ltd, Oxford, UK, 2002.

[31] C. Hwu and J. S. Hu. Stress intensity factors and energy release rates of delaminations in composite laminates. *Engineering Fracture Mechanics*, 42:977–988, 1992.

[32] G. R. Irwin. Analysis of stresses and strains near the end of a crack transvering a plate. *Journal of Applied Mechanics*, 24:361–264, 1957.

[33] G. R. Irwin. *Fracture.* Handbuch der Physik, Band 6, Springer Verlag Berlin, 1958.

[34] W. C. Jackson and R. H. Martin. An interlaminar tension strength specimen. *NASA*, NASA/TM-1992-107623:1 – 50, 1992.

[35] R. Krueger. Virtual crack closure technique: History, approach, and applications. *Applied Mechanics Reviews*, 57:109–143, 2004.

[36] R. Krueger and P. J. Minguet. Skin–stiffener debond prediction based on computational fracture analysis. *NASA*, NASA/CR-2005-213915:1–42, 2005.

[37] R. Krueger, P. J. Minguet, and T. K. O'Brien. A method for calculating strain energy release rates in preliminary design. *NASA*, NASA/TM-1999-209365:1–33, 1999.

[38] R. Krueger, S. Rinderknecht, and M. Koenig. Two– and three–dimensional finite element analyses of crack fronts in a multidirectional composite enf specimen. *ISD–Report*, 97:1–34, 1997.

[39] M. Kuna. *Numerische Beanspruchungsanalyse von Rissen.* Vieweg+Teubner, Wiesbaden, Germany, 2008.

[40] P. Ladevéze and G. Lubineau. On a damage mesomodel for laminates: micro-meso relationships, possibilities and limits. *Composite Science and Technology*, 61:2149–2159, 2001.

[41] P. A. Lagace and N. V. Bhat. On the prediction of delamination initiation. In *Proceedings of the International Conference on Advanced Composites, Wollongong, Australia, February, 1993*, pages 335–341, 1993.

[42] Y. J. Lee, C. H. Lee, and W. S. Fu. Study on the compressive strength of laminated composite with through-the-width delamination. *Composite Structures*, 41:229–241, 1998.

[43] R. H. Martin. Delamination failure in a unidirectional curved composite laminate. *NASA*, NASA/CR-1990-182018:1–46, 1990.

[44] P. Middendorf. Auslegung und Simulation von Composite Strukturen in der Luftfahrt: Stand der Technik, zukünftige Anforderungen und Forschungsschwerpunkte. *NAFEMS Magazin*, 1:34–42, 2008.

[45] S. H. Narayan and J. L. Beuth. Designation of mode mix in orthotropic composite delamination problems. *International Journal of Fracture*, 90:383–400, 1998.

[46] A. Needleman. A continuum model for void nucleation by inclusion debonding. *Journal of Applied Mechanics*, 54:525–531, 1987.

[47] T. K. O'Brien. Composite interlaminar shear fracture thoughness, G_{IIc}: Shear measurement or sheer myth. *NASA TM*, 110280:1–18, 1997.

[48] T. K. O'Brien. Interlaminar fracture toughness:the long andwinding road to standardization. *Composites Part B*, 29:57–62, 1998.

[49] N. J. Pagano and G. A. Schoeppner. *Comprehensive Composite Materials*, Vol: Polymer Matrix Composites, Cha: Delamintion of Polymer Matrix Composites: Problems and Assessment, pages 433–528. Elsevier Science Ltd, Oxford, UK, 2000.

[50] D. H. Pahr. *Experimental and Numerical Investigations of Perforated FRP–Laminates*. PhD thesis, Institute of Lightweight Design and Structural Biomechanics, Vienna University of Technology, Vienna, Austria, 2003.

[51] D. H. Pahr, F. G. Rammerstorfer, P. Rosenkranz, K. Humer, and H. W. Weber. A study of short-beam-shear and double-lap-shear specimens of glass fabric/epoxy composites. *Composites Part B*, 33:125–132, 2002.

[52] A. Puck. *Festigkeitsanalyse von Faser-Matrix-Laminaten*. Carl Hanser Verlag, München Wien, Germany, 1996.

[53] A. Puck, J. Kopp, and M. Knops. Guidelines for the determination of the parameters in Puck's action plane strength criterion. *Composite Science and Technology*, 62:371–378, 2002.

[54] A. Puck and H. Schürmann. Failure analysis of FRP laminates by means of physically based phenomenological models. *Composite Science and Technology*, 58:1045–1067, 1998.

[55] I. S. Raju. Calculation of strain-energy release rates with higher order and singular finite elements. *Engineering Fracture Mechanics*, 28:251–274, 1987.

[56] I. S. Raju, J. H. Crews, and M. A. Aminpour. Convergence of strain release rate components for edge-delaminated composite laminates. *Engineering Fracture Mechanics*, 30:383–396, 1988.

[57] I. S. Raju, R. Sistla, and T. Krishnamurthy. Fracture mechanics analysis for skin–stiffener debonding. *Engineering Fracture Mechanics*, 54:371–385, 1996.

[58] J. R. Rice. A path independent integral and the approximate analysis of strain concentration by notches and cracks. *Engineering Fracture Mechanics*, 35:379–386, 1968.

[59] J. R. Rice. Elastic fracture mechanics concepts for interfacial cracks. *Transactions of the ASME*, 55, 1988.

[60] S. Rinderknecht and B. Kröplin. A computational method for the analysis of delamination growth in composite plates. *Computers and Structures*, 64:359–374, 1997.

[61] A. J. Russell and K. N. Street. Predicting interlaminar fatigue crack growth rates in compressively loaded laminates. *ASTM STP*, 1012:162–178, 1989.

[62] E. F. Rybicki and M. F. Kanninen. A finite element calculation of stress intensity factors by a modified crack closure integral. *Engineering Fracture Mechanics*, 9:931–938, 1977.

[63] C. Schuecker. *Mechanism based modeling of damage and failure in fiber reinforced polymer laminates*. PhD thesis, Institute of Lightweight Design and Structural Biomechanics, Vienna University of Technology, Vienna, Austria, 2005.

[64] C. Schuecker and B. Davidson. Evaluation of the accuracy of the four-point bend end-notched flexure test for mode II delamination toughness determination. *Composite Science and Technology*, 60:2137–2146, 2000.

[65] C. Schuecker, D. H. Pahr, and H. E. Pettermann. Accounting for residual stresses in FEM analyses of laminated structures using the Puck criterion for three-axial stress states. *Composite Science and Technology*, 66:2054–2062, 2006.

[66] H. Schürmann. *Konstruieren mit Faser-Kunststoff-Verbunden*. Springer Verlag Berlin Heidelberg New York, Germany, 2005.

[67] D. J. Shim, R. C. Alderliesten, S. M. Spearing, and D. A. Burianek. Fatigue crack growth prediction in GLARE hybrid laminates. *Composites Science and Technology*, 63:1759 – 1767, 2003.

[68] P. A. Smith. *Comprehensive Composite Materials*, Vol: Polymer Matrix Composites, Cha: Carbon Fiber Reinforced Plastics – Properties, pages 107–150. Elsevier Science Ltd, Oxford, UK, 2000.

[69] L. N. Sneddon and M. Lowengrub. *Crack problems in the classical theory of elasticity.* John Wiley Sons, New York, 1969.

[70] C. T. Sun and M. G. Manoharan. Strain energy release rates of an interfacial crack between two orthotropic solids. *Journal of Composite Materials*, 23:460–480, 1989.

[71] Z. Suo. Singularities, interfaces and cracks in dissimilar anisotropic media. *Proceedings of the Royal Society of London*, A 427:331–358, 1990.

[72] J. Teßmer. *Theoretische und algorithmische Beiträge zur Berechnung von Faserverbundschalen*. PhD thesis, Institut für Baumechanik und Numerische Mechanik, Universität Hannover, Germany, 2000.

[73] A. Turon, P. Camanho, J. Costa, and C. Davila. An interface damage model for the simulation of delamination under variable-mode ratio in composite materials. *NASA*, NASA/TM-2004-213277:1–26, 2004.

[74] A. Turon, J. Costa, P. Camanho, and C. Davila. Simulation of delamination in composites under high-cycle fatigue. *Composites Part A*, 38:2270 – 2282, 2007.

[75] A. Turon, C. Davila, P. Camanho, and J. Costa. An engineering solution for using coarse meshes in the simulation of delamination with cohesive zone elements. *NASA*, NASA/TM-2005-213547:1–26, 2005.

[76] H. Westergaard. Bearing pressures and cracks. *Journal of Applied Mechanics*, 6:49–43, 1939.

[77] G. Wimmer, W. Kitzmüller, G. Pinter, T. Wettemann, and H. E. Pettermann. Computational and experimental investigation of delamination in L–shaped laminated composite components. *Engineering Fracture Mechanics*, 2008. (submitted).

[78] G. Wimmer and H. E. Pettermann. A semi–analytical model for the simulation of delamination in laminated composites. *Composites Science and Technology*, 68:2332–2339, 2007.

[79] G. Wimmer and H. E. Pettermann. Simulation of delamination in laminated composite components – a fracture mechanics based method. In *Proc. of the ECCOMAS Conference on Mechanical Response of Composites*, 2007.

[80] G. Wimmer and H. E. Pettermann. A semi–analytical approach for the simulation of delamination growth under quasi–static and cyclic loading. In *Proceedings of the 13th European Conference on Composite Materials*, 2008.

[81] G. Wimmer and H. E. Pettermann. A semi-analytical approach for the prediction of delamination growth in laminated structures loaded by quasistatic and cyclic loads. *Journal of Composite Materials*, 2008. (submitted).

[82] G. Wimmer and H. E. Pettermann. Numerical simulation of consecutive growth of delaminations with curved fronts. In *Proc. of the 2nd ECCOMAS Conference on Mechanical Response of Composites*, 2009.

[83] G. Wimmer, C. Schuecker, and H. E. Pettermann. Numerical simulation of delamination onset and growth in laminated composites. *e-Journal of Nondestructive Testing*, 11:1–10, 2006.

[84] G. Wimmer, C. Schuecker, and H. E. Pettermann. Numerical simulation of delamination in laminated composite components - a combination of a strength criterion and fracture mechanics. *Composites Part B*, 2008. (accepted).

[85] D. Xie and S. B. Biggers. Strain energy release rate calculation for a moving delamination front of arbitrary shape based on the virtual crack closure technique. Part I: Formulation and validation. *Engineering Fracture Mechanics*, 73:771 –785, 2006.

[86] D. Xie and S. B. Biggers. Strain energy release rate calculation for a moving delamination front of arbitrary shape based on the virtual crack closure technique. Part II: Sensitivity study on modeling details. *Engineering Fracture Mechanics*, 73:786–801, 2006.